CRYSTALLIZATION OF NANOCOMPOSITE GLASSES MADE BY THE SSG PROCESS

FINAL TECHNICAL REPORT

to

AIR FORCE OFFICE OF SCIENTIFIC RESEARCH
Bolling Air Force Base, DC 20332

Award No. AFOSR-89-0446

Period Covered:

November 15, 1989 – December 31, 1992
which includes the no-cost extension period from
November 15 – December 31, 1992

Submitted by:

Rustum Roy and Sridhar Komarneni
Materials Research Laboratory
The Pennsylvania State University
University Park, PA 16802

SECURITY CLASSIFICATION OF THIS PAGE

REPORT DOCUMENTATION PAGE

Form Approved OMB No. 0704-0188

1a. REPORT SECURITY CLASSIFICATION: Unclassified	1b. RESTRICTIVE MARKINGS
2a. SECURITY CLASSIFICATION AUTHORITY	3. DISTRIBUTION/AVAILABILITY OF REPORT: Approved for public release; Distribution is unlimited.
2b. DECLASSIFICATION/DOWNGRADING SCHEDULE	
4. PERFORMING ORGANIZATION REPORT NUMBER(S): Final Technical Report	5. MONITORING ORGANIZATION REPORT NUMBER(S): Final Technical Report
6a. NAME OF PERFORMING ORGANIZATION: Pennsylvania State University; 6b. OFFICE SYMBOL (If applicable):	7a. NAME OF MONITORING ORGANIZATION: AFOSR/NC
6c. ADDRESS (City, State, and ZIP Code): Materials Research Laboratory, University Park, PA 16802	7b. ADDRESS (City, State, and ZIP Code): 110 Duncan Avenue, Suite 100, Bolling Air Force Base, D.C. 20332-0001
8a. NAME OF FUNDING/SPONSORING ORGANIZATION: AFOSR; 8b. OFFICE SYMBOL (If applicable): NC	9. PROCUREMENT INSTRUMENT IDENTIFICATION NUMBER: AFOSR-89-0446
8c. ADDRESS (City, State, and ZIP Code): 110 Duncan Avenue, Suite 100, Bolling Air Force Base, D.C. 20332-0001	10. SOURCE OF FUNDING NUMBERS

PROGRAM ELEMENT NO.	PROJECT NO.	TASK NO	WORK UNIT ACCESSION NO.
61102F	2303	A3	

11. TITLE (Include Security Classification)

(U) Crystallization of Nanocomposite Glasses Made by the SSG Process

12. PERSONAL AUTHOR(S)

Rustum Roy and Sridhar Komarneni

13a. TYPE OF REPORT	13b. TIME COVERED	14. DATE OF REPORT (Year, Month, Day)	15. PAGE COUNT
Final Technical Report	FROM 11/15/91 TO 12/31/92	January 12, 1993	62

16. SUPPLEMENTARY NOTATION

17. COSATI CODES			18. SUBJECT TERMS (Continue on reverse if necessary and identify by block number)
FIELD	GROUP	SUB-GROUP	

19. ABSTRACT (Continue on reverse if necessary and identify by block number)

The two main objectives of this research were: (a) to crystallize nanocomposite glasses through solid-state epitaxy and (b) to demonstrate the critical role of epitaxy in crystallization by fabricating sol-gel films on single crystal substrates of a paticular orientation. During the last three years we have been able to achieve both these goals using several compositional systems. We have been able to crystallize through seeding albite ($NaAlSi_3O_8$) glass which has been considered to be impossible to crystallize. Orthoclase ($KAlSi_3O_8$) which is extremely difficult to crystallize has also been crystallized using a compositionally multiphasic gel and crystalline seeds of $KAlSi_3O_8$, $NaAlSi_3O_8$, $CaAl_2Si_2O_8$ and $SrAl_2Si_2O_8$ feldspars. Monoclinic $BaAl_2Si_2O_8$ has been crystallized at significantly lower temperatures by seeding with monoclinic $BaAl_2Si_2O_8$ or $SrAl_2Si_2O_8$ seeds. The effect of seeding has been minor or could not be detected in other glass systems such as Li_2O-Al_2O_3-SiO_2, Rb_2O-Al_2O_3-SiO_2 and Cs_2O-Al_2O_3-SiO_2. Little or no effect of seeding was found in non-oxide glasses such as silicon oxycarbide glasses. The role of epitaxy in crystallization has been demonstrated convincingly by making dense, epitaxial $SrTiO_3$ and TiO_2 thin films on single crystals of $SrTiO_3$ and TiO_2 of a particular orientation. The nanocomposite approach which has been discovered and developed through AFOSR support to us is now a well established practice the world over.

20. DISTRIBUTION/AVAILABILITY OF ABSTRACT	21. ABSTRACT SECURITY CLASSIFICATION
☐ UNCLASSIFIED/UNLIMITED ☐ SAME AS RPT. ☐ DTIC USERS	

22a. NAME OF RESPONSIBLE INDIVIDUAL	22b. TELEPHONE (Include Area Code)	22c. OFFICE SYMBOL
Thomas E. Erstfeld	202-767-4960	AFOSR/NC

DD Form 1473, JUN 86 *Previous editions are obsolete.* SECURITY CLASSIFICATION OF THIS PAGE

TABLE OF CONTENTS

SUMMARY OF PROGRESS

Support by the U.S. Air Force Office of Scientific Research during the last several years has enabled the two co-principal investigators to make a lasting impact on ceramic materials synthesis in two areas. First it helped them develop the second generation sol-gel research which led to the discovery and development of nanocomposites. Unlike the first generation sol-gel research which was developed by one of the proposers (R.R.) in the early fifties and is presently practiced throughout the world, the goal of the second generation sol-gel research is to achieve ultraheterogeneity or nanoheterogeneity during processing, i.e., to make nanocomposites. The solution sol-gel (SSG) derived nanocomposites have led to (a) lower crystallization temperatures, (b) enhanced densification at lower sintering temperatures, and (c) phase and morphology control in some cases. Most recently we have worked with glasses and also achieved spectacular results. For example we have been able to crystallize, by using nanocomposite seeding, albite glass which has been impossible to crystallize. The "nanocomposite" theme has now been widely and accurately copied and used worldwide and developed especially in Japan which held the first international conference on the topic two years ago (see Reprints #1 and #2 for developments in nanocomposites and sol-gel).

The main objective of the present grant is to extend this concept and try to crystallize nanocomposite *glasses* through solid-state epitaxy. This approach could in principle then lead to a universal composition glass ceramic process. An additional objective is to prove the critical role of *epitaxy in crystallization by fabricating* sol-gel films on single crystal substrates of a particular orientation. During the first year of this AFOSR grant, we have made a high visibility advance by crystallizing *albite glass* which has been considered to be impossible to crystallize (please see Interim Report of December 12, 1990). During the second year of this grant, the nanocomposite approach has been extended to glasses in BaO-Al_2O_3-SiO_2 system and to ceramics of the Al_2O_3-TiO_2 system. In addition solid state epitaxy has been demonstrated on single crystals of TiO_2 and $SrTiO_3$ (please see Interim Report of November 21, 1991). During the third year this concept has been extended to other glasses and ceramic systems as described below.

1. Crystallization of Oxide Glasses and Gels Through Isostructural and Non-Isostructural Seeding

Na_2O-Al_2O_3-SiO_2 System. Albite glasses seeded with $CaAl_2Si_2O_8$ and $SrAl_2Si_2O_8$ crystallized faster than those seeded with $LiAlSi_3O_8$ or $NaAlSi_3O_8$ crystals. The results of crystallization of albite seeded glasses have been reported earlier (see Interim Report of December 12, 1990) and the results of crystallization of anorthite seeded glasses have been published recently (see Reprint #3). The albite gels seeded with different feldspars crystallized only partially unlike the glasses. However, no crystallization of albite was observed in gels and glasses which are unseeded or those seeded with non-isostructural seeds such as TiO_2, ZrO_2, etc.

K_2O-Al_2O_3-SiO_2 system. Glasses and monophasic gels of orthoclase ($KAlSi_3O_8$) could not be crystallized to feldspar by seeding with $KAlSi_3O_8$, $NaAlSi_3O_8$, $LiAlSi_3O_8$, $CaAl_2Si_2O_8$ and $SrAl_2Si_2O_8$ feldspar crystals. Both the seeded and unseeded glasses and gels remained amorphous up to about 1000°C but crystallized to leucite ($KAlSi_2O_6$) above this temperature. However, we have been able to crystallize high sanidine ($KAlSi_3O_8$) feldspar using multiphasic gels of orthoclase composition by seeding them with $NaAlSi_3O_8$, $KAlSi_3O_8$, $CaAl_2Si_2O_8$ and $SrAl_2Si_2O_8$ feldspar crystals but not with $LiAlSi_3O_8$. This approach constitutes the use of so-called both compositionally and structurally different nanocomposites. The use of these nanocomposites in this system suppressed partially or fully the formation of leucite in the temperature range of 850°-1100°C.

BaO-Al_2O_3-SiO_2 System. Several types of celsian ($BaAl_2Si_3O_8$) gels were made among which the gel from alkoxide method led to sintered samples of highest density. The unseeded gel crystallized only to hexagonal celsian above 900°C. Feldspar crystalline seeds of $NaAlSi_3O_8$, $KAlSi_3O_8$, $CaAl_2Si_2O_8$, $SrAl_2Si_2O_8$ and $BaAl_2Si_2O_8$ did not affect the transformation kinetics of hexagonal celsian formation in the temeprature range of 900°-1000°C. But monoclinic celsian started to form around 1200°C and became phase pure above 1300°C. Unseeded gels did not transform to monoclinic celsian below 1450°C. Celsian gels seeded with $LiAlSi_3O_8$ crystallized to hexagonal celsian above 850°C and phase pure monoclinic celsian above 1200°C. When these gels were seeded with rutile (TiO_2), the gels started to form hexagonal celsian at 850°C and transformed to pure monoclinic celsian at 1300°C but with much slower kinetics compared to the feldspar seeded gels. The crystallization with rutile can be explained by some epitaxial relations between rutile and the feldspar.

Li_2O-Al_2O_3-SiO_2 and CaO-Al_2O_3-SiO_2 Systems. No seeding effects have been detected in the crystallization of $LiAlSi_3O_8$ and $CaAl_2Si_2O_8$ glasses and gels. The crystallization of feldspars in these two systems is too rapid to detect the effect of solid state epitaxy by the addition of crystalline feldspar seeds.

2. Effect of Isostructural Seeding on Crystallization of Non-Oxide Glasses

We have reported earlier that isostructural seeding with SiC crystals of silicon oxycarbide glasses was found to be ineffective. High temperature stability studies of oxycarbide glasses revealed that they have a highly polymerized structure which led to their greater resistance to crystallization (see Preprint #1).

3. Demonstration of Solid State Epitaxy on Single Crystals Using Sol-Gel Films

We have thoroughly demonstrated the role of epitaxy in the crystallization of TiO_2 and $SrTiO_3$ sol-gel films deposited on single crystals of TiO_2 and $SrTiO_3$ of special orientation (see Interim Report dated November 21, 1991). We have recently prepared $Pb(Zr_{0.52}Ti_{0.48})$ thin films on platinum-coated single crystal silicon by a modified sol-gel process using lead acetylacetonate as the lead source. The

use of this new lead precursor provided more stability to the PZT precursor solution compared to the commonly used lead acetate trihydrate (see Manuscript #2 for details).

In summary, the twin goals of this research have been accomplished and several papers have been published or are in press. A Ph.D. thesis will be prepared shortly on the crystallization of glasses through solid-state epitaxy.

CUMULATIVE LIST OF PUBLICATIONS AND PRESENTATIONS SUPPORTED BY AFOSR

1. D. Hoffmann, R. Roy and S. Komarneni, "Diphasic Ceramic Composites via a Sol-Gel Method," Mat. Letters 2, 245-247 (1984).
2. D. Hoffmann, S. Komarneni and R. Roy, "Preparation of a Diphasic Photosensitive Xerogel," J. Mat. Sci. Letter 3, 439-442 (1984).
3. R. Roy, S. Komarneni and D.M. Roy, "Multiphasic Ceramic Composites Made by Sol-Gel Technique," in the Proceedings of the Symposium on Better Ceramics Through Chemistry (Eds. C.J. Brinker et al.), Elsevier, North-Holland, pp. 347-359 (1984) (jointly supported by NSF).
4. D.W. Hoffmann, R. Roy and S. Komarneni, "New Sol-Gel Strategies for Making Ceramic-Ceramic Composites," Abstracts, 1984 American Ceramic Society Meeting, Am. Ceram. Soc. Bull. 63, 459 (1984).
5. R. Roy, S. Komarneni and D.W. Hoffmann, "Sol-Gel Approach to Making Photochromic Xerogels and Glasses," Abstracts, 1984 American Ceramic Society Mtg., Am. Ceram. Soc. Bull. 63, 499 (1984).
6. R. Roy, L.J. Yang and S. Komarneni, "Controlled Microwave Sintering and Melting of Gels," Abstracts, 1984 American Ceramic Society Meeting, Am. Ceram. Soc. Bull. 63, 459 (1984).
7. S. Komarneni, L.J. Yang and R. Roy, "Hydrothermal Reaction Sintering of Single and Diphasic Xerogels," Abstracts, 1984 American Ceramic Society Mtg., Am. Ceram. Soc. Bull. 63, 459 (1984).
8. R. Roy, S. Komarneni and L.J. Yang, "Controlled Microwave Sintering and Melting of Gels," J. Am. Ceram. Soc. 68, 392 (1985).
9. S. Komarneni, R. Roy, E. Breval and Y. Suwa, "Hydrothermal Route to Ultrafine Powders Utilizing Single and Diphasic Gels," Abstracts of the Second International Symposium on Hydrothermal Reactions in University Park, p. 62.
10. S. Komarneni, R. Roy, E. Breval, M. Ollinen and Y. Suwa, "Hydrothermal Route to Ultrafine Powders Utilizing Single and Diphasic Gels," Adv. Ceramic Mats. 1, 87 (1986).
11. R. Roy, Y. Suwa and S. Komarneni, "Nucleation and Epitaxial Growth in Reactions of the Diphasic (Crystalline + Amorphous) Gels," presented at the Second Intl. Conf. on Ultrastructure Processing of Ceramics, Glasses and Composites in February 1985 (jointly supported by NSF).
12. T.C. Simonton and R. Roy, "Natural Gel Derived Ceramics: Chemistry, Microstructure and Properties of Opal, Chert, Agate, Etc.," Abstracts of the American Ceramic Society Meeting, Cincinnati, OH, 1985, p. 269.
13. R. Roy, "Seeding: A Special Approach to Diphasic Xerogels," Abstracts of the American Ceramic Society Meeting, Cincinnati, OH, 1985, p. 270.
14. R. Roy, "Microwave Melting of Ceramics and Gels," Patent applications filed via AFOSR.
15. C. Scherer and C. Pantano, "Ti-Si Glasses Using a Colloidal Sol-Gel Process," presented at the Third Intl. Workshop on Glasses and Glass Ceramics from Gels, Montpellier, France, 1985.
16. S. Komarneni and R. Roy, "Microwave Processing of Zeolites," AF Invention 17310 (1985).
17. Y. Suwa, R. Roy and S. Komarneni, "Crystallographic Effects in Seeded (Diphasic Gels): II. Microstructural and Sintering Properties," Abstracts of the American Ceramic Society Meeting, Cincinnati, OH, 1985, p. 270.
18. Y. Suwa, R. Roy and S. Komarneni, "Enhancing Densification by Solid State Epitaxy in Structurally Diphasic Al_2O_3-MgO Xerogels," Abstracts, Materials Research Society, 1985 Fall Meeting, p. 468 (1985).
19. S. Komarneni and R. Roy, "Anomalous Microwave Sintering and Melting of Zeolites," Abstracts, Materials Research Society, 1985 Fall Meeting, p. 468 (1985).
20. R. Roy, Y. Suwa and S. Komarneni, "Nucleation and Epitaxial Growth in Reactions of Diphasic (Crystalline + Amorphous) Gels," in Ultrastructure Processing of Ceramics, Glasses and Composites (Eds. L.L. Hench and D.R. Ulrich), pp. 247-258 (1986).
21. Y. Suwa, R. Roy and S. Komarneni, "Lowering Sintering Temperature and Enhancing Densification by Epitaxy in Structurally Diphasic Al_2O_3 and Al_2O_3-MgO Xerogels," Mat. Sci. Eng. 83, 151 (1986).
22. S. Komarneni and R. Roy, "Anomalous Microwave Melting of Zeolites," Mat. Lett. 4, 107 (1986).

23. S. Komarneni, G. Vilmin, Y. Suwa and R. Roy, "Enhancing Densification of Al_2O_3-MgO Xerogels by Double Seeding with a-Al_2O_3 and $MgAl_2O_4$," Abstracts, The American Ceramic Society 88th Annual Meeting, p. 92 (1986).
24. S. Komarneni, A. Kijowski, T.C. Simonton and R. Roy, "Diphasic Glass Composites," Abstracts, The American Ceramic Society 88th Annual Meeting, p. 92 (1986).
25. T.C. Simonton, S. Komarneni and R. Roy, "Diphasic Composites of Natural Gel Derived Ceramics," Abstracts, The American Ceramic Society 88th Annual Meeting, p. 117 (1986).
26. T.C. Simonton, S. Komarneni and R. Roy, "Radiation Assisted Chemical Bonding of Natural and Synthetic Gel-Derived Ceramics," Abstracts, The American Ceramic Society 88th Annual Meeting, p. 122 (1986).
27. S. Komarneni, Y. Suwa and R. Roy, "Application of Compositionally Diphasic Xerogels for Enhanced Densification: The System Al_2O_3-SiO_2," J. Am. Ceram. Soc. 69, C-155 (1986).
28. T.C. Simonton, R. Roy, S. Komarneni and E. Breval, "Microstructure and Mechanical Properties of Synthetic Opal: A Chemically Bonded Ceramic," J. Mat. Res. 1, 667 (1986).
29. S. Komarneni, Y. Suwa and R. Roy, "Enhancing Densification of 93% Al_2O_3-7% MgO Triphasic Xerogels with Crystalline a-Al_2O_3 and $MgAl_2O_4$ Seeds," J. Mat. Sci. Lett. 6, 525 (1987).
30. T.C. Simonton, S. Komarneni and R. Roy, "Ultrafine Microstructure in Synthetic Opal, A Diphasic Composite," Abstracts, Materials Research Society, 1986 Fall Meeting, p. 747 (1986).
31. W.A. Yarbrough and R. Roy, "Extraordinary Effects of Mortar-and-Pestle Grinding on Microstructure of Sintered Alumina Gel," Nature 322, 347 (1986).
32. C.P. Scherer and C.G. Pantano, "Titania-Silica Glasses Using a Colloidal Sol-Gel Process," J. Non-Cryst. Solids 82, 246 (1986).
33. W.A. Yarbrough and R. Roy, "Microstructure Evolution in Sintering of AlOOH Gels," J. Mat. Res. (in press).
34. R. Roy, "Some New Advances with SSG Derived Nanocomposites," Abstracts, Third Intl. Conf. on Ultrastructure processing of Ceramics, Glasses and Composites, p. 44 (1987).
35. R. Roy, S. Komarneni and W.A. Yarbrough, "Some New Advances with SSG Derived Nanocomposites," Third International Conference on Ultrastructure Processing of Ceramics, Glasses and Composites (Eds. J.D. MacKenzie and D.R. Ulrich), pp. 571-588 (1988).
36. D. Zaide, E. Breval and C.G. Pantano, "Colloidal Sol/Gel Processing of Ultra-low Expansion TiO_2/SiO_2 Glasses," presented at the Fourth Intl. Workshop on Glasses-Ceramics from Gels, Kyoto, Japan, 1987.
37. Y. Suwa, S. Komarneni and R. Roy, "Effect of Seeding on Crystallization and Sintering of Diphasic Al_2O_3-MgO Monolithic Gels," Proceedings of the Japanese Ceramic Society, Vol. 3, pp. 735-736 (1987).
38. Y. Suwa, R. Roy and S. Komarneni, "Effect of Epitaxial Seeding on Crystallization Process and on Densification in Diphasic Al_2O_3-MgO Xerogel," Abstracts, '87 Intl. Symposium & Exhibition on Science and Technology of Sintering, Tokyo, Japan, p. 420-421 (1987). (Also, in press.)
39. S. Komarneni, "Hydrothermal Preparation of Low-Expansion 'NZP' Family of Materials," '87 Intl. Symposium & Exhibition on Science and Technology of Sintering, Tokyo, Japan, p. 422 (1987). (Also, in press.)
40. R. Roy, "The Al_2O_3-SiO_2 Phase Diagram: Metastability and Order-Disorder," Abstracts, First Intl. Workshop on Mullite, p. 13 (1987); and submitted for publication.
41. S. Komarneni and R. Roy, "Mullite Derived From Diphasic Gels," Abstracts, 1st International Workshop on Mullite, p. 23 (1987); and submitted for publication.
42. R. Roy, "Ceramics Via the Solution-Sol-Gel Route," Science 238, 1664-1669 (1987).
43. A.K. Kijowski, S. Komarneni and R. Roy, "Multi-phasic Nanocomposite Sol-Gel Processing of Cordierite," Better Ceramics Through Chemistry, Vol. III (C.J. Brinker, D.E. Clark and D.R. Ulrich, eds.), Mat. Res. Soc. Proc., Pittsburgh, PA, pp. 245-250 (1988).
44. S. Komarneni, E. Breval and R. Roy, "Microwave Preparation of Mullite Powders," Abstracts, Materials Research Society Spring Meeting, Reno, Nevada (1988).
45. S. Komarneni, E. Breval and R. Roy, "Microwave Preparation of Mullite Powders," in Microwave Processing of Materials (M.H. Brooks, I.J. Chabinsky and W.H. Sutton, eds.), Mat. Res. Soc. Proc., Pittsburgh, PA, pp. 235-238 (1988).

46. S. Komarneni, "Nanocomposite Sol-Gel Processing," New Ceramics (invited paper in Japanese) 2, 89-94 (1989).
47. A.M. Kazakos, "Sol-Gel Processing of Cordierite," M.S. Thesis, Graduate School, The Pennsylvania State University, 115 pp. (1989).
48. R. Roy, "Synthesizing New Materials to Specification," Solid State Ionics 32/33, 3-22 (1989).
49. R. Roy, S. Komarneni and A.M. Kazakos, "Application of Sol-Gel Derived Nanocomposites to Solid State Epitaxial Growth of Oxides and Selected Semiconductors," Abstracts, Mat. Res. Soc. Fall Meeting, Boston, MA, p. 619 (1989).
50. R. Roy, "Nanocomposites—The Multifunctional Family of Materials," Abstracts, Mat. Res. Soc. Fall Meeting, Boston, MA, p. 616 (1989).
51. H. Zhang and C.G. Pantano, "Sol-Gel Processing of Si-O-C Glasses for Glass Matrix Composites," Ultra Structure Processing of Advanced Ceramics (in press).
52. A.M. Kazakos, S. Komarneni and R. Roy, "Sol-Gel Processing of Cordierite: Effect of Seeding and Optimization of Heat Treatment," J. Mat. Res. 5, 1095-1103 (1990).
53. U. Selvaraj, S. Komarneni and R. Roy, "Synthesis of Cordierite and Mullite Gels from Metal Alkoxides and Characterization by ^{27}Al and ^{29}Si MASNMR," Abstracts, 92nd Annual Meeting of the Am. Ceram. Soc., Dallas, TX. p. 362 (1990).
54. U. Selvaraj, S. Komarneni and R. Roy, "Seeding Effects on Crystallization Temepatures of Cordierite Glas Powder," Abstracts, 92nd Annual Meeting of the Am. Ceram. Soc., Dallas, TX, p. 261 (1990).
55. A. Kazakos, S. Komarneni and R. Roy, "Preparation and Densification of Forsterite (Mg_2SiO_4) by Nanocomposite Sol-Gel Processing," Mat. Lett. 9, 405-409 (1990).
56. N.J. Wlodarczyk, Nanocomposite Versus Monophasic Processing of Gels and Glasses in the Lithium Aluminosilicate System, M.S. Thesis, Solid State Science, The Pennsylvania State University, University Park, PA, 104 pp. (1990).
57. U. Selvaraj, S. Komarneni and R. Roy, "Synthesis of Glass-Like Cordierite from Metal Alkoxides and Characterization by ^{27}Al and ^{29}Si MASNMR," J. Am. Ceram. Soc. 73, 3663-3669 (1990).
58. H. Zhang and C.G. Pantano, "Synthesis and Characterization of Silicon Oxycarbide Glasses," J. Am. Ceram. Soc. 73, 958-963 (1990).
59. H. Kido and S. Komarneni, "Preparation of $La_{1-x}Sr_xCoO_3$ (x = 0, 0.3) by Two Solution Routes," in Electro-Optical Materials for Switches, Coatings, Sensor Optics and Detectors, R. Hartman, M.J. Soileau and V.K. Varadan, Eds., Proc. SPIE 1307, 129-133 (1990).
60. U. Selvaraj, S. Komarneni and R. Roy, "Seeding Effects on Crystallization Temperatures of Cordierite Glass Powders," J. Mat. Sci. 26, 3689-3692 (1991).
61. U. Selvaraj, C.L. Liu, S. Komarneni and R. Roy, "Epitaxial Crystallization of Seeded Albite Glass," J. Am. Ceram. Soc. 74, 1378-1381 (1991).
62. U. Selvaraj, A.V. Prasadarao, S. Komarneni and R. Roy, "Sol-Gel Thin Films of $SrTiO_3$ from Chemically Modified Alkoxide Precursors," Mat. Lett. 12:311-315 (1991).
63. H. Kido, S. Komarneni and R. Roy, "Preparation of $La_2Zr_2O_7$ by Sol-Gel Route," J. Am. Ceram. Soc. 74, 422-424 (1991).
64. U. Selvaraj, A.V. Prasadarao, S. Komarneni and R. Roy, "Epitaxial $SrTiO_3$ Thin Films by Sol-Gel Processing," J. Mat. Res. (in press).
65. U. Selvaraj, A.V. Prasadarao, S. Komarneni and R. Roy, "Sol-Gel Fabrication of Epitaxial and Oriented TiO_2 Thin Films," J. Am. Ceram. Soc. 75:1167-1170 (1992).
66. A.V. Prasadarao, U. Selvaraj, S. Komarneni, A.S. Bhalla and R. Roy, "Enhanced Densification by Seeding of Sol-Gel Derived Aluminum Titanate," J. Am. Ceram. Soc. 75:1529-1533 (1992).
67. U. Selvaraj, S. Komarneni and R. Roy, "Sol-Gel Derived Mullite: Structural Differences Characterized by ^{27}Al and ^{29}Si MASNMR in Mullite Xerogels from Different Precursors," J. Solid State Chem. (submitted for publication).
68. C. Liu, S. Komarneni and R. Roy, "Crystallization of Anorthite Seeded Albite Glass by Solid State Epitaxy," J. Am. Ceram. Soc. 75:2665-2670 (1992).
69. S. Komarneni, A. K. Kijowski and R. Roy, "Highly Dense Cordierite and Method of Manufacturing Same," U.S. Patent No. 5,030,592 assigned to U.S. AFOSR (1991).

70. H. Zhang and C. G. Pantano, "High Temperature Stability of Oxycarbide Glasses," MRS Proceedings, Volume 271.
71. R. Roy, "Solution-Sol-Gel Technology and Science: Past, Present and Future," in *Chemical Processing of Advanced Materials* (Eds. L. L. Hench and J. K. West), Wiley and Sons, Inc., pp. 1023-1033 (1992).
72. U. Selvaraj, K. Brooks, A. V. Prasadarao, S. Komarneni, R. Roy and L. E. Cross, "Sol-Gel Fabrication of $Pb(Zr_{0.52}Ti_{0.48})O_3$ Thin Films Using Lead Acetylacetonate as the Lead Source," J. Am. Ceram. Soc. (in press).
73. S. Komarneni, "Nanocomposites," J. Mater. Chem. 2:1219-1230 (1992).

J. MATER. CHEM., 1992, 2(12), 1219–1230

FEATURE ARTICLE

Nanocomposites

Sridhar Komarneni
Materials Research Laboratory and Department of Agronomy, The Pennsylvania State University, University Park, PA 16802, USA

The use of nanocomposites in materials processing can lead to monophasic or multiphasic ceramics, glasses or porous materials, with tailored and improved properties. This review deals with a variety of nanocomposites such as sol–gel, intercalation, entrapment, electroceramic and structural ceramic types, which exhibit superior properties when compared to the monophasic or microcomposite alternatives. The utilization of nanocomposites in materials processing is forecasted to have a major impact in catalytic, sensor, optical, electroceramic and structural ceramic materials.

Keywords: *Nanocomposite*; *Sol–gel processing*; *Catalyst*; *Sensor*; *Electroceramic*; *Feature Article*

1. Definitions

The term 'nanocomposites' was first coined by Roy, Komarneni and colleagues sometime during the period 1982–1983 to describe the major conceptual re-direction of the sol–gel process, *i.e.* using the solution sol–gel (SSG) process to create maximally heterogeneous rather than homogeneous materials.[1–4] Di- and multi-phasic nanoheterogeneous sol–gel materials were prepared and documented in 1984.[1–4] Nanocomposites should be clearly differentiated from 'nanocrystalline' and 'nanophase' materials, which refer to single phases in the nanometre range. 'Nanocomposites' refers to composites of more than one Gibbsian solid phase where at least one dimension is in the nanometre range and typically all solid phases are in the 1–20 nm range. The solid phases can be amorphous, semicrystalline or crystalline or combinations thereof. They can be inorganic or organic, or both, and essentially of any composition. The 'nanocomposite' theme has now been widely and accurately adopted, used worldwide, and developed especially in Japan. Although the term 'nanocomposites' was coined only recently, nanocomposites are pervasive throughout the biological systems (*e.g.* plants and bones). Only very few man-made materials, such as intercalation compounds (*e.g.* graphite intercalation compounds, pillared clays and clay–organic complexes) and entrapment-type compounds (*e.g.* zeolite–organic complexes) have dealt with this size of material. In the biological world, plants form nanocomposites with the accumulation of significant amounts of inorganic components such as Si, Ca, Al, *etc.* at the tissue and cellular level to deal with the mechanical and biophysical demands of their survival. In the animal world, bones, teeth and shells consist of nanocomposites of inorganic and organic materials to achieve several key properties. The objective of this article, however, is to review the work on man-made nanocomposite materials and to identify areas where further developments are likely to occur.

2. Different Families of Nanocomposites

Although nanocomposites can be classified as other composites based on connectivity,[5] here I have identified several major families of nanocomposites based on their material function, physical and chemical differences, temperature of formation, *etc.* There are five major groups of nanocomposites at present: (1) sol–gel nanocomposites, which are composites made at low temperatures (<100); these nanocomposite precursors can lead to homogeneous single-crystalline phase ceramics or multiphasic crystalline ceramics upon high-temperature heating; (2) intercalation-type nanocomposites, which can be prepared at low temperatures (<200 °C) and lead to useful materials upon heating to modest temperatures (<500 °C); (3) entrapment-type nanocomposites, which can be prepared from three-dimensionally linked network structures such as zeolites which can also be synthesized at low temperatures (<250 °C); (4) electroceramic nanocomposites, which can be prepared by mixing nanophases of ferroelectric, dielectric, superconducting and ferroic materials in a polymer matrix at low temperatures (<200 °C); (5) structural ceramic nanocomposites, which are prepared by traditional ceramic processing at very high temperatures (1000–1800 °C). These five major categories can be subdivided further and are described below in detail.

2.1 Sol–Gel Nanocomposites

The worldwide goal of all SSG work has been ultrahomogeneity, while our goal in this area has been switched in the early 1980s to the preparation of nanocomposites that exhibit ultraheterogeneity or nanoheterogeneity. This conceptual innovation of nanocomposite materials was a new direction for sol–gel research. The concept of diphasic ceramic–ceramic gels as a new class of materials with interesting potential was first introduced by Roy.[2] This new direction for the sol–gel processing science is now well established in our laboratory and elsewhere.[3–37] The goal of ceramic materials processing *via* the nanocomposite ceramic gels is to exploit the thermodynamics of metastable materials and, in particular, to utilize the heat of reaction of the discrete phases and the advantages offered by epitaxy. Here the concepts are illustrated with the processing of densification of different types of sol–gel nanocomposite leading to the crystallization and densification of mullite, alumina, and zircon ceramics which have numerous technological applications such as infrared transmitting materials, refractory materials, substrate materials and high-temperature structural materials. The readers are requested to refer to the numerous publications cited above for a thorough understanding of these concepts. In addition to the above exploitation of the thermodynamics of sol–gel materials, one can also process sol–gel materials into various shapes

such as films, fibres and monoliths with pore sizes in which organic and inorganic second phases can be incorporated.

Sol–gel nanocomposites are further subdivided into six categories: (1) compositionally different nanocomposites; (2) structurally different nanocomposites; (3) both compositionally and structurally different nanocomposites; (4) nanocomposites of gels with precipitated phases; (5) nanocomposites of xerogels with metal phases; (6) nanocomposites of inorganic gels and organic molecules.

2.1.1 *Compositionally Different Sol–Gel Nanocomposites*

These are very intimate mixtures composed of two or more solid phases that differ in composition and each with particle size of the order of 10–20 nm. Solid phases of these dimensions produce 'sols' when dispersed in a liquid. Two or more sols of different composition can be uniformly mixed and gelled to obtain compositionally different nanocomposites. Fig. 1 shows the transmission electron microscope (TEM) picture of a sol–gel nanocomposite of mullite composition consisting of spherical silica particles (20 nm) and rod-like alumina (boehmite) particles (*ca.* 7 nm). Such a uniform physical mixture can be distinguished from a homogeneous sol–gel material which does not show any non-uniformity because it is mixed on an atomic scale [Fig. 1(*b*)].[8,32] The compositionally different sol–gel nanocomposites have been shown to sinter to crystalline products in several compositional systems[8,23,26,27,37] with close to theoretical density at much lower temperatures than the homogeneous gels.[23,27] Fig. 2 compares the scanning electron micrographs of sintered bodies of cordierite made from nanocomposites and homogeneous gels. This example clearly shows that the compositionally different sol–gel nanocomposites densify much better than the homogeneous gels.

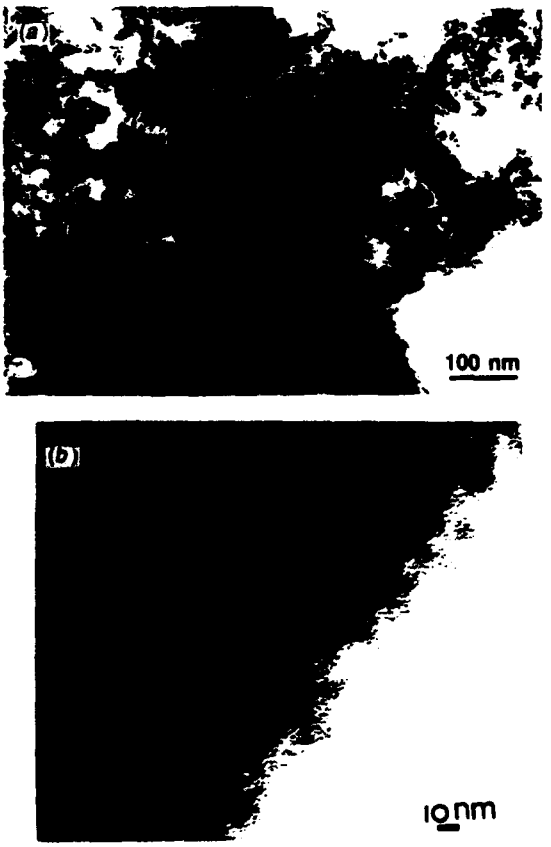

Fig. 1 Transmission electron micrographs of mullite composition gels: (*a*) nanocomposite and (*b*) homogeneous (single phase)

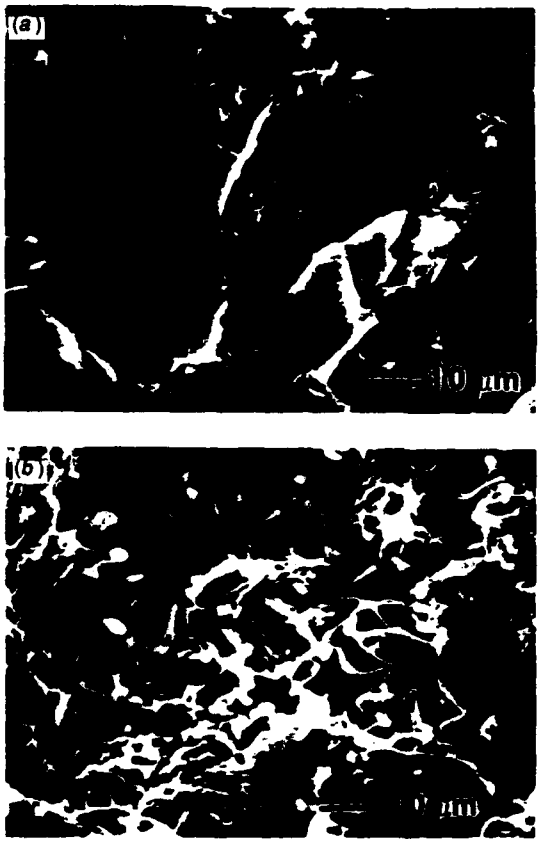

Fig. 2 Scanning electron micrographs of fracture surfaces of cordierite composition gels sintered at 1300°C for 2 h: (*a*) nanocomposite and (*b*) homogeneous (single phase). Reprinted by permission from ref. 27

Similar results have been obtained in other compositional systems such as Al_2O_3–SiO_2, SiO_2–MgO, Al_2O_3–TiO_2, *etc.*[8,30,37] The enhanced densification of the nanocomposite gels made from two or more sols or nanophases may be attributed to the heat of reaction among the sols or nanophases. The nanocomposite gels store much higher metastable energy than the single-phase gels (Fig. 3)[4] and thus the enhanced densification of the nanocomposites may be attributed to the additional energy provided during the exothermic heat of reaction. Another reason for enhanced densification in the nanocomposites appears to be due to the simultaneous densification and crystallization, unlike the homogeneous gels where crystallization precedes densification because of atomic-scale mixing. Once the crystallization of the equilibrium phase takes place, it is difficult to densify unless very high temperatures are used. The above concept of compositionally different sol–gel nanocomposites is generalizable and applicable to all oxide ceramics which can be used as structural or electroceramic materials. The lower processing temperatures are not only useful in conserving energy but also advantageous in preparing electroceramics and multilayer capacitors, which contain volatile elements and therefore need to be processed at low temperatures.

2.1.2 *Structurally Different Sol–Gel Nanocomposites*

These nanocomposites consist of two or more solid phases with the same composition but different structure. Examples include mixtures of ultrafine crystalline seeds in amorphous or semicrystalline xerogels. The gel materials are highly amenable for uniformly distributing the ultrafine crystalline seeds. Using the system Al_2O_3, the effects of α-Al_2O_3 seeds in

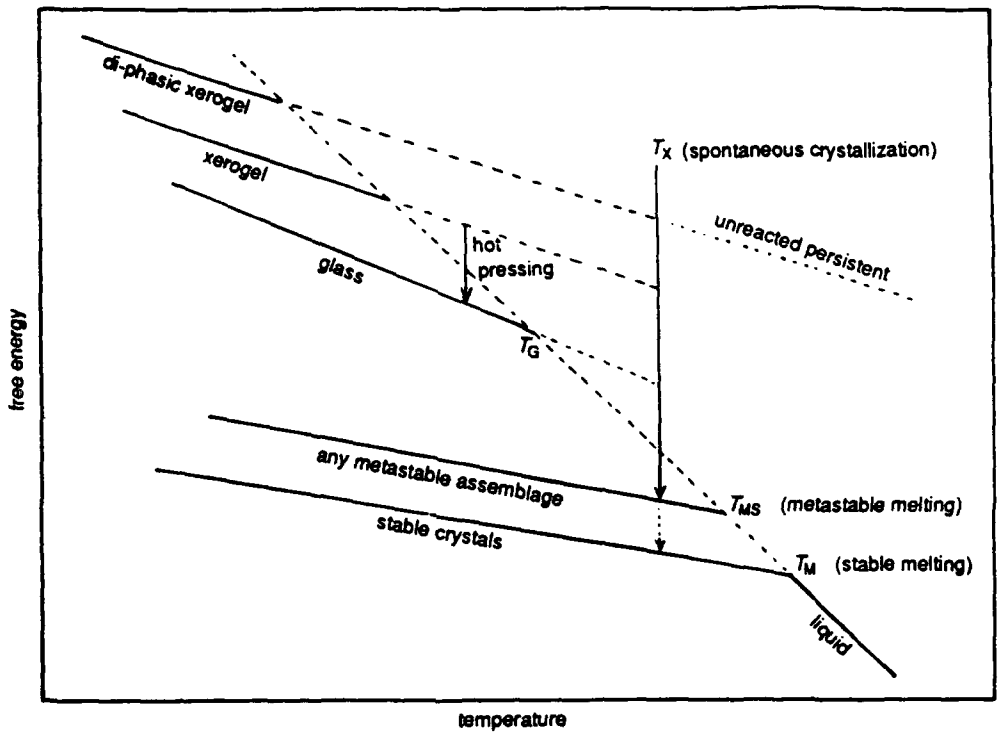

Fig. 3 Representation of $G-T$ relations among isoplethal phases. Reprinted by permission of the American Ceramic Society (*J. Am. Ceram. Soc.*, 1984, 67 468)

lowering crystallization temperature through epitaxy[10-16,20,24,25] have been clearly demonstrated. Further evidence for epitaxy has been thoroughly demonstrated with sol–gel films on single-crystal substrates[31,35,36] where the gel crystallized into a single-crystal-like film with the same orientation as the substrate. Fig. 4 shows an X-ray diffractogram of a TiO_2 film on a TiO_2 single-crystal (110) substrate with the same orientation; the film is indistinguishable from the substrate below.[36] The role of solid-state epitaxy in lowering the crystallization temperature is now well established in numerous compositional systems including electroceramics. The resultant effects of this structural epitaxy on microstructure and sintering of alumina and other gels have already been reported. Using the structurally different nanocomposite sol–gels, it is now possible to crystallize some feldspar gels (and glasses, see below) which have been found previously to be impossible to crystallize. The effect of solid-state epitaxy in compositional systems which have high energy barriers is significant and can be exploited in the making of all types of ceramic. Further developments are likely to occur in electroceramics where there are some useful phases such as lead zinc niobate, which cannot be crystallized under ordinary pressures.

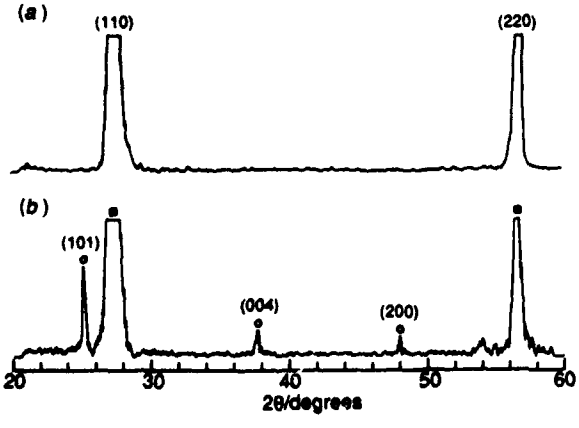

Fig. 4 X-Ray diffractogram of a TiO_2 film on rutile single crystal (110) substrate (*a*) After 6 h at 900 °C; (*b*) after 1 h at 650 °C. ○ = anatase. ■ = rutile. Reprinted by permission of the American Ceramic Society (Sol-Gel Fabrication of Epitaxial and Oriented TiO_2 Thin Films, U. Selvary, A.V. Prasadarao, S. Kamarneni and R. Roy, *J. Am. Ceram. Soc.*, 1992, 75, 1167)

2.1.3 *Both Compositionally and Structurally Different Sol–Gel Nanocomposites*

These nanocomposites are a combination of the above two types of nanocomposite and consist of compositionally discrete phases with crystalline seeds of the equilibrium phase. This combination utilizes the heat of reaction of the compositionally discrete phases and the lowering of the energy barrier through epitaxial growth on the crystalline seeds. Using zircon[17] as the prototype model, we have shown that both the compositionally and structurally different sol–gel nanocomposites crystallize at a lower sintering temperature than either the compositionally or structurally different sol–gel nanocomposites. Table 1 shows the lowest temperatures at which zircon formed for different types of nanocomposite. It

Table 1 Lowest temperature at which zircon formed in different mono- and nano-composite precursors[17]

structural diphasicity	compositional diphasicity	
	no	yes
no	1325 °C	1175 °C
yes	1100 °C	1075 °C

Reprinted by permission of Chapman and Hall.

is obvious from Table 1 that both the compositionally and structurally different nanocomposite gels yielded zircon at the lowest temperature. Similar results were obtained for ThO_2–SiO_2 and Al_2O_3–MgO systems.[18,19] In the latter case, densification and microstructural studies of Al_2O_3 (93%)–MgO (7%) (abrasive grain composition by 3M Co.) gels seeded with both α-Al_2O_3 and $MgAl_2O_4$ seeds revealed that the double seeding has led to complete densification with very fine microstructure.[19]

2.1.4 *Nanocomposites of Gels with Precipitated Phases*

These are one type of ceramic–ceramic nanocomposite which are prepared by the growth of extremely fine crystalline or non-crystalline phases inside the pores of a pre-made gel (*e.g.* SiO_2) structure.[1,6,7] The growth of fine phases is accomplished by soaking the gel in metal salt solution and subsequent precipitation of the metal with selected anions. Such a precipitation presents a vastly more versatile (with respect to composition of the matrix) approach to such nanocomposite materials than is possible with, say, precipitation out of a glass. The gel pores can be modified by liquid- and gas-deposition techniques.[38] This leads to modification of the chemical character and the effective pore size and gives rise to nanophases well below the size of the pores.[38] The nanocomposite materials made by this method extend the processing options for photochromic glasses and catalytic materials with interesting and improved transport, catalytic and mechanical properties.

2.1.5 *Nanocomposites of Xerogels with Metal Phases*

The sol–gel process has been extended to the preparation of new diphasic xerogels leading to new ceramic–metal nanocomposite materials.[3] These nanocomposites have been prepared by two methods (Fig. 5). Xerogels of Al_2O_3, SiO_2 and ZrO_2 have been prepared as the matrices with Cu, Pt and Ni (5–50 nm) as the dispersed metal phases. Very finely dispersed metal particles (2–4 nm) have been deposited by liquid- and gas-deposition techniques in sol–gel membranes.[38] These materials are obviously important as catalysts and they can be optimized by manipulating the process parameters of the sol–gel methods. Iron/silica or alumina gel nanocomposites have been prepared, and properties such as spin-glass magnetic behaviour, change in magnetic state with ammonia treatment and iron magnetic moments[39–43] have been investigated. Sol–gel-derived glass–metal nanocomposites involving Fe, Ni and Cu in a silica glass matrix have been prepared and electrical and optical properties have been studied.[44–46] Although the use of these nanocomposites in electrical, magnetic and optical devices is a long shot, their future in catalysis appears to be bright.

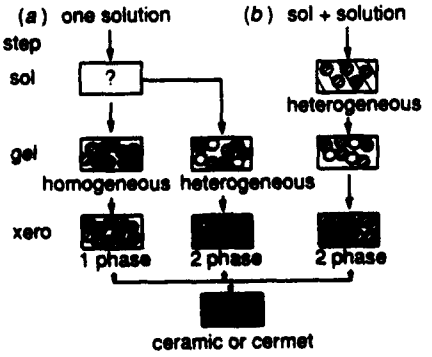

Fig. 5 Two preparation routes used in making ceramic–metal nanocomposites. Method (*a*), solution mixing of all components simultaneously. Method (*b*) uses a pre-made sol to which a further solution is added before gelation. Reprinted by permission from ref. 3

2.1.6 *Nanocomposites of Inorganic Gels and Organic Molecules (Dyes)*

The sol–gel process is highly amenable to incorporating optically active organic molecules such as laser dyes in porous gel or glass-like matrices because the gels can be prepared at room temperature and the porosity can be controlled. One can incorporate the organic species including polymers during gelation[47] or the organic molecules can be introduced into the pre-made sol–gel matrices through diffusion. Various laser dyes, conducting and conjugated polymers, polymers that contain hydrogen-bond acceptor groups and photochromic molecules have been successfully incorporated into silica gels[47,48] and these nanocomposites may have interesting optical, non-linear optical, conducting and photochromic properties with potential applications in optical devices, laser materials and chemical sensors. Preliminary studies of the last 5 years or so have demonstrated that the activity of the different molecules is not impaired by their incorporation in sol–gel matrices. Further studies in this area include the interactions between the sol–gel matrix and the guest molecules for optimizing the properties of the resulting nanocomposites for various applications and the engineering of the gel pore structure to incorporate selectively chemical molecules which will lead to the development of optically based chemical sensors. Further details about these nanocomposites can be obtained from an excellent review by Dunn and Zink.[48]

2.2 Intercalation-type Nanocomposites

Naturally occurring or synthetic crystals of layer structure, such as graphite and clays, can be intercalated with inorganic and organic species to generate bi-dimensional nanocomposites. The layered crystals are of two types: (1) with an unbalanced charge on the layers and (2) neutral layers. The 2:1 clay minerals and hydrotalcites (anionic clays) belong to the first group while the 1:1 clay minerals and graphite are examples of the second type. Table 2 gives numerous examples of the layered crystals[49] which can be utilized in the prep-

Table 2 Layered crystals[49]

molecular layered crystals	cation exchangeable layered crystals
element	silicates
graphite	Montmorillonite
chalcogenides	vermiculite
MX_2 (TiS_2, $NbSe_2$, MoS_2)	hectorite
MPX_3 ($MnPS_3$, $FePSe_3$)	phosphates
Ta_2S_2C	$Zr(HPO_4)_2 \cdot nH_2O$
oxides	$Ti(HPO_4)_2 \cdot nH_2O$
MoO_3, V_2O_5	$Na(UO_2PO_4) \cdot nH_2O$
oxyhalides	titanates
FeOCl, VOCl, CrOCl	$Na_2Ti_3O_-$
ZrNCl	$KTiNbO_5$
hydroxides	$Rb_xMn_xTi_{2-x}O_4$
$Zn(OH)_2$, $Cu(OH)_2$	vanadates
silicates	KV_3O_8
kaolinite, halloysite	$K_2V_8O_{14}$
$H_2Si_2O_5$	$CaV_6O_{16} \cdot nH_2O$
$H_2Si_{14}O_{29} \cdot 5H_2O$	$Na(UO_2V_3O_8) \cdot nH_2O$
miscellaneous	niobates
$Ni(CN)_2$	$K_4Nb_6O_{1-}$
$VOSO_4$, $VOPO_4$	KNb_3O_8
WO_2Cl_2	miscellaneous
	$Na_2W_4O_{13}$
	$Na_2U_2O_-$
	$Mg_2Mo_2O_-$
	hydrotalcites

aration of nanocomposites. Although there are numerous layered crystals, only a few, such as clays and graphite, have been extensively studied as intercalation compounds. There is a large amount of literature on the graphite intercalation compounds[50] and this subject will not be covered here. The main intercalation-type composites which will be described in detail are (*a*) pillared clays; (*b*) metal-intercalated clays, and, (*c*) clay–organic composites.

2.2.1 *Pillared Clays*

Swelling clay minerals such as montmorillonite, hectorite, saponite, nontronite and biedellite of the smectite family can be pillared in the interlayers by exchanging their interlayer cations with polymeric hydroxy cations followed by dehydration, which leads to ceramic oxide pillars (Fig. 6). The silicate layers are permanently propped apart by the oxide pillars and zeolitic micropores are formed between the silicate layers. Pillared clays are the perfect example of a nanocomposite because the clay layer is *ca.* 1 nm and the oxide pillars are *ca.* 1–2 nm. Vaughan *et al.*[51] were the first to synthesize pillared clays with alumina and subsequently, several other oxides such as ZrO_2, Cr_2O_3, TiO_2, Fe_2O_3, Bi_2O_3 *etc.*[52–57] and mixed oxides such as Al_2O_3–SiO_2, SiO_2–TiO_2 and SiO_2–Fe_2O_3[58–60] have been introduced as pillars between the clay layers. Pillared clays are versatile microporous materials because the dimensions and the surface characteristics of the micropores can be designed by changing the size and composition of the pillaring species. In addition, they have high surface areas and high thermal stabilities. Therefore, these have potential applications as catalysts, catalyst substrates, selective adsorbents[60–66] and desiccants.[67–69] We have determined the water adsorption and desorption isotherms of several pillared clays for determining their suitability as desiccants for gas-*fired cooling and dehumidification equipment*. Fig. 7 shows the adsorption isotherms of several pillared clays and the data show that these can serve as good desiccants.[69] Although there is a great deal of research on the pillared clays, the pore-size distribution is not well understood. One can estimate the pillar sizes from the basal spacings (Table 3) by subtracting 9.6 Å for the thickness of the clay layer but the size of the pores along the *a*–*b* directions is mostly unknown. It is imperative that more research is needed to determine the pore sizes of these samples before they can find wide-ranging applications. The pore size along the *a*–*b* directions is expected to depend upon the charge density, the uniformity of charge distribution, the size and type of polymeric cations used, *etc.* The pore structures are usually characterized by nitrogen or water adsorption measurements. Techniques such as neutron and X-ray scattering and nuclear magnetic resonance may help unravel the pore structure of these nanocomposite porous materials and this information will be useful in the future design of chemical sensors from these nanocomposites.

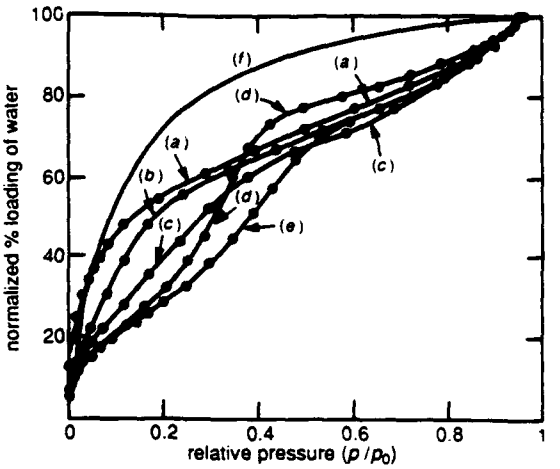

Fig. 7 Water adsorption isotherms of different smectites with alumina pillars (*a*) nontronite treated with NH_3 and exchanged with Cu^{2+}, (*b*) original pillared nontronite, (*c*) original pillared saponite, (*d*) original pillared montmorillonite (kunimine), (*e*) original pillared hectorite (hectabrite AW), and (*f*) ideal isotherm shape for use in dehumidification and cooling equipment[69]

Table 3 Precursor cations used in pillaring the clay and the resulting basal spacings[63]

pillar oxide	precursor	basal spacing Å
Al_2O_3	$[Al_{13}O_4(OH)_{24}]^{7+}$	17–19
ZrO_2	$[ZR_4(OH)_{14}]^{2+}$	17–20
Fe_2O_3	$[Fe_3O(OCOCH_3)_6]^+$	17
Cr_2O_3	$[Cr_n(OH)_m]^{(3n-m)+}$	21–17
Bi_2O_3	$[Bi_6(OH)_{12}]^{6+}$	16
Al_2O_3–SiO_2	$[Al_{13}O_4(OH)_{24-n}]$–$[OSi(OH)_3]_n^-$	17–19
TiO_2	sol solution	24–27
SiO_2–TiO_2	sol solution	40–50
SiO_2–Fe_2O_3	sol solution	40–100

In addition to the above cationic clays, anionic clays of the hydrotalcite group, $[Mg_2Al(OH)_6]^+Cl^-\cdot xH_2O$, $[Al_2Li(OH)_6]^+Cl^-\cdot xH_2O$ are potential layered compounds which can be utilized in the making of porous nanocomposites. The anionic species in the interlayers can be exchanged with bulkier inorganic or organic anions.[70–78] Hydrotalcite group of materials containing Cl^-, NO_3^-, SO_4^{2-} or CrO_4^{2-} have interlayer spacings in the range of 3.0–4.0 Å.[72–74] Substitution of CO_3^{2-} gives the smallest interlayer spacing, *i.e.* 2.8 Å.

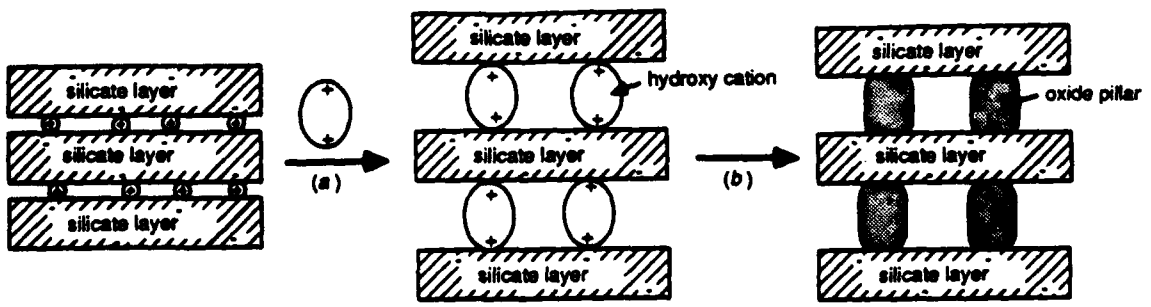

Fig. 6 Schematic illustration of the pillaring process in bidimensional clay: (*a*) ion exchange with precursor cations and (*b*) conversion to oxide by calcination. Reprinted by permission of the American Ceramic Society (Design and Synthesis of Functional Layered Nanocomposites, S. Yamanaka, *Am. Ceram. Soc. Bull.* 1991, **70**, 1056)

whereas substitution with $Fe(CN)_6^{3-}$ or $Fe(CN)_6^{4-}$ gives a spacing of 6.1 Å.[74] An interlayer spacing of 8.1 Å was obtained by the intercalation of naphthol yellow S^{2-} in hydrotalcite.[78] Thus, one can design porous nanocomposites for potential applications as adsorbents. For example, a $Co(CN)_6^{3-}$-exchanged sample shows[78] the following order of adsorption for several hydrocarbons: hexane ≈ 2-methylpentane ≫ cyclohexane > methylcyclohexane. In addition to the pore size, the surface properties can be modified through numerous substitutions.[70-79] Because these materials are not stable above *ca.* 300 °C, all the applications are restricted to temperatures below this. Although the anionic species in the interlayers of these nanocomposites are not dehydrated, unlike pillared clays, because of their poor thermal stability, it should not be impossible to create pillared anionic clays with low-temperature dehydration of the anionic species through future molecular engineering.

2.2.2 *Metal-intercalated Clays*

Expandable layer silicates such as montmorillonite can be converted to efficient heterogeneous catalysts by introducing catalytically active sites or guest species between the layers or on the external surfaces. Previous attempts to produce intercalated zero-valent transition-metal particles in layer silicates, by hydrogen reduction for example, have, however, failed: the layers tend to collapse, sometimes followed by deposition of metal particles on the external surfaces. Recently Malla *et al.*,[79,80] have described the successful intercalation of copper metal clusters of 4–5 Å in montmorillonite by *in situ* reduction of Cu^{2+} ions using ethylene glycol. These metal-cluster intercalates were stable up to at least 500 °C. The clusters prop the silicate layers apart, much as metal oxides do in pillared clays, and may thus be able to introduce unique catalytic product selectivity through a molecular sieving effect similar to that in cluster-loaded zeolites. As metal clusters of these dimensions behave very differently from the bulk metal, intercalates of this sort may prove to be versatile catalysts.

2.2.3 *Clay–Organic Nanocomposites*

These are often referred to as clay–organic complexes and have been around since at least biblical times.[81] During this period, clays have been used to decolourize edible oils and clarify alcoholic beverages utilizing clay–organic reaction or complexation.[81] The interaction of clays with organic species has been implicated in the origin of life.[82] The structure of swelling clays, especially of the smectite group is amenable to forming clay–organic nanocomposites because of the weak bonding (van der Waals and electrostatic) between the layers. The clay–organic intercalation compounds can be grouped into two main types: (*a*) those that are formed by ion exchange of interlayer exchangeable cations, and (*b*) those that are formed by adsorption of polar organic molecules. Clay–organic complexes have been utilized in the past for surface-area measurements, layer-charge determination, soil stabilization, *etc.* Recently, clay–organic nanocomposites have been proposed for several new applications in the materials field. Because of the nanoscale mixing of inorganic and organic components in the clay–organic nanocomposites, they can be utilized as precursors in the preparation of structural non-oxide ceramic materials such as Si_3N_4, SiC, AlN, Sialon, *etc.*[83-91] When the clay–organic nanocomposites are heated in an inert atmosphere, carbothermal reduction reactions take place leading to the formation of non-oxide structural ceramic materials as follows:

$$3SiO_2 + 6C + 2N_2 \rightarrow Si_3N_4 + 6CO \quad (1)$$

$$SiO_2 + 3C \rightarrow SiC + 2CO \quad (2)$$

Several naturally occurring clay minerals such as montmorillonite, kaolinite, pyrophyllite and illite have been studied as raw materials in the synthesis of non-oxide ceramic materials[83-91] but montmorillonite–polyacrylonitrile complex was found to be the best because of the intimate mixing. An alumina pillared clay has been found to be a suitable precursor to mix with carbon in the synthesis of β-sialon by carbothermal reduction.[92] Sugahara *et al.*,[84] used a magadiite ($Na_2Si_{14}O_{29}\cdot nH_2O$)–$C_{12}H_{25}N(CH_3)_3^+$ nanocomposite and a physical mixture of magadiite with carbon in their carbothermal reduction reactions and found that the former yielded β-SiC while the latter yielded SiO_2. Thus the reaction process in the nanocomposite is quite different because of the intimate mixing achieved on a nanoscale.

Clay–organic nanocomposites have also been proposed as low relative permittivity substrates.[93-96] These nanocomposites consist of a quasi-two-dimensional layered structure (fluorohectorite or other swelling clay) and an organic compound such as polyaniline, n-$C_6H_5NH_2$ intercalated between the layers by ion exchange. The ceramic (clay) layer imparts good mechanical and thermal stabilities while the organic compound gives low relative permittivity and good processability to the nanocomposite material. The present disadvantage with these nanocomposites is that they are hydrophilic, *i.e.* they adsorb water, which can increase the relative permittivity. To alleviate this problem, future work needs to deal with the incorporation of hydrophobic polymers in the interlayers. With other applications in mind, clay–organic nanocomposites having hydrophobic characteristics have already been prepared by exchanging aminosilane or organic chrome complex for Li^+ or Na^+ from swollen clay gels.[97] These nanocomposite gels can be processed to form paper, board, film, fibre and coatings and the dried gel powders can be hot-pressed to give a body of crosslinked organic polycation–mica derivatives.

Intercalation of electroactive polymers such as polyaniline and polypyrrole in mica-type layered silicates leads to metal–insulator nanocomposites.[98,99] The conductivity of these nanocomposites in the form of films is highly anisotropic with the in-plane conductivity 10^3–10^5 times higher than the conductivity in the direction perpendicular to the film. Conductive polymer–oxide bronze nanocomposites have been prepared by intercalating polythiophene in V_2O_5 layered phase which is analogous to clays.[100] Studies of these composites are expected not only to provide fundamental understanding of the conduction mechanism in the polymers but also to lead to diverse electrical and optical properties.

Intercalation of ethylenediamine functionalized buckminsterfullerene in fluorohectorite clay has been achieved[101] and these nanocomposites may lead to microporous materials analogous to pillared clays upon the elimination of the ligands by suitable heat treatment in oxygen. A new microporous tubular silicate-layered silicate (TSLS) nanocomposite has been synthesized by selective hydrolysis of γ-aminopropyl triethoxysilane from the external surfaces of imogolite, which led to its intercalation into layered silicate.[102] The N adsorption and *t*-plot analysis of this porous nanocomposite showed a bimodal pore structure which is attributed to intratube and intertube adsorption environments.[103] The TSLS nanocomposite has been found to be active for the acid-catalysed dealkylation of cumene at 350 °C, but this composite has been found to be less reactive than a conventional Al_2O_3 pillared montmorillonite.[103] High-surface-area (*ca.* 900 $m^2\,g^{-1}$) microporous materials have been prepared[104,105] by calcining nanocomposites of alkyltrimethylammonium–kanemite ($NaHSi_2O_5\cdot 3H_2O$), the latter being a layered polysilicate. During the organic intercalation, the SiO_2 layers in the complexes condense to form three-dimensional SiO_2 networks.

The calcined products of the complexes have micropores in the range 2–4 nm (Fig. 8) and such materials are expected to find applications in catalysis.

Clay–fluorescence dye nanocomposites have been prepared by ion exchange and the fluorescence properties of different dyes, as affected by the inorganic crystal field of the clay, have been investigated extensively.[106–110] Such confinement can lead not only to high thermal stability but also to higher luminescence efficiency.[109, 110]

2.3 Entrapment-type Nanocomposites

The entrapment-type nanocomposites can be prepared from zeolites and are of two types: (1) zeolite–inorganic, and (2) zeolite–organic. Zeolite crystals are three-dimensionally linked network structures of aluminosilicate, aluminophosphate (ALPO) and silicoaluminophosphate (SAPO) composition and are porous, the pores being in the range 2.8–10 Å. Many of the highly siliceous, ALPO and SAPO zeolites have been synthesized using organic templates such as tetrapropylammonium, tetramethylammonium, di-*n*-propylamine, *etc.*[111,112] After the synthesis, the organics are removed by different techniques, the main one being combustion, to get access to all the pore space.

2.3.1. *Zeolite–Inorganic Nanocomposites*

Fine metal clusters supported in zeolites are a good example of this type of nanocomposite and they possess unique catalytic properties, molecular selectivity and polyfunctional activity.[113–115] A large volume of literature exists on the preparation and the catalytic properties of metal clusters or aggregates dispersed in zeolites.[116,117] Various methods, such as ion-exchange, evaporation, irradiation, thermal decomposition, particle-beam method, impregnation, adsorption or deposition and coprecipitation, have been used to introduce metal ions or complexes which are then reduced to zerovalent metal forms by molecular or atomic hydrogen, ammonia, metal vapours and various organic compounds. We have recently used[118] a new approach, *i.e.* polyol process to entrap Ni and Cu metal clusters in zeolites. The interface chemistry associated with nanophase confinement and packaging and some features of three-dimensional surface confinement using zeolites and molecular sieves has recently been reviewed,[119] and silver sodalites have been touted as novel optically responsive nanocomposites.[120] Future studies may exploit the zeolite–inorganic nanocomposites for materials applications other than catalysis because of the great potential for nanodesigning.

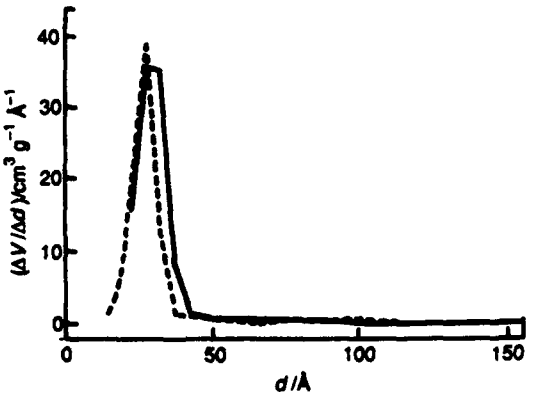

Fig. 8 Pore-size distributions of (—) Calcined product obtained from hexadecyltrimethylammonium–kanemite complex and (- - -) calcined product obtained from trimethylsilylated derivative. Reprinted by permission from ref. 105

2.3.2 *Zeolite–Organic Nanocomposites*

There has not been a great deal of work utilizing the zeolite–organic nanocomposites directly in materials applications. Recently, pyridine ($C_5H_{11}N$) incorporated ZSM-39 and Dodecasil-3C zeolites have been synthesized[121] and these nanocomposites show an optical memory effect and interesting domain structure. The ability to rotate polar groups within unusual symmetries gives rise to field response in the molecular nanocomposite properties.[121] Future work in this area needs to emphasize the growth of large single crystals of zeolites with organic molecules incorporated in them for optical and other applications.

2.4 Electroceramic Nanocomposites

Newnham and co-workers have developed a large family of microcomposite materials with properties superior to those obtainable from single phases for use as electrochemical transducers, PTC and NTC thermistors, piezoresistors, and chemical sensors during the past decade and recently they have turned their attention to nanocomposites for electronic applications.[122,123] Recent advances in both information and charge storage in the electronics industry may be attributed to electroceramic nanocomposites and especially those that are based on ferroic materials because both the presence of domain walls and the ferroic transition are affected by the crystallite size. The size dependence of ferroic properties is shown in Fig. 9.[122] Multidomain effects accompanied by hysteresis take place in large crystallites. Reductions in size (Fig. 9) led to single domain particles, and yet smaller sizes to destabilized ferroics with large property coefficients, and finally, to normal behaviour as the particle size approaches the nano or atomic scale.[122] Because of the nanoscale, there are different quantum effects leading to variation of energy states and electronic structure of their components. Other basic features of these nanocomposites are the remarkable modification of the electronic structure by widespread interface interaction at the electronic level and the great variety of nanostructures ranging from high-level ordered three-dimensional periodic structures to stoichiometrically dispersed medium of nano-particles.[124] Electroceramic nanocomposites can be further classified into (*a*) magnetic (*b*) ferroelectric and (*c*) superconducting, ferroelectric, (*d*) dielectric and (*e*) conducting, semiconducting and insulating types of materials. Two excellent reviews have been

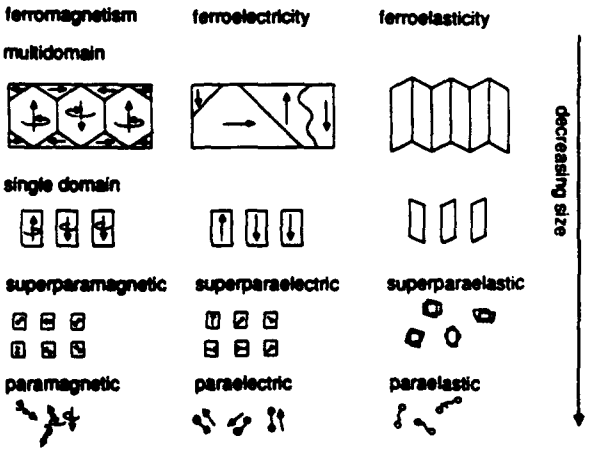

Fig. 9 Changes in the domain configurations of ferroics as a function of size. Reprinted by permission from ref. 122

published on magnetic, ferroelectric and ferroelastic nanocomposites[122,123] and the readers are advised to refer to these for more details.

Among the electroceramic nanocomposites, the magnetic nanocomposites consisting of small particles or ultrathin films have been investigated extensively. The use of nanoparticles in magnetic recording media can lead to smaller storage units where the information is stored at a higher density.[122] Nanoparticles are also used in ferrofluids where the size of the crystallites is small enough to prevent settling in the fluid. Ferrofluids can be construed as solid–fluid nanocomposites and they have applications in non-contaminating seals, loudspeakers, ink-jet printers, levitation systems for separating materials of different density, vibration dampers, engines for converting low-grade heat to usable energy and devices to measure very small inclination angles.[122,125–128] A novel fabrication of a Co–Cr nanocomposite by r.f. sputtering has led to very-high storage density with the perpendicular recording technique.[129,130] Another innovative example is the processing of a 1–3 nanocomposite for uniform, high-density magnetic components.[130] In this work, an aluminium alloy substrate is first oxidized to achieve a regular network of honeycomb cells on the surface. The columnar pores which are formed during the oxidation are etched and then back-filled with iron to create a high density of magnetic elements with practical values for the coercive force.[122,125]

2.4.1 *Ferroelectric Nanocomposites*

These nanocomposites have not yet been explored to a significant extent because research is concentrated on microcomposites, which have been found to be extremely useful as pressure transducers, vibration dampers and transducers. The need for optical transparency or low driving voltages may lead to the development of ferroelectric nanocomposites in the future.[122] A solid 0–3 ferroelectric nanocomposite has been prepared recently using ultrafine (*ca.* 20 nm) $PbTiO_3$ powders dispersed in a polymeric matrix. This type of composite may be useful in optical applications. Single-phase relaxor ferroelectrics exhibit compositional and order–disorder inhomogeneities on a nanometre scale.[122–136] These single phases on a macroscopic scale can be construed as 'nanocomposites' if the definition of the nanocomposite term can be extended to include materials which show inhomogeneities in structure, composition or properties on a nanoscale. For example, the $A(B'_{1/2}, B''_{1/2})O_3$ and $A(B'_{2/3}, B''_{1/3})O_3$ perovskites have been found to display microdomains (*ca.* 2–3 nm in size) of 1:1 ordering on the B sublattice dispersed in a disordered matrix.[134–136] Other types of ferroelectric nanocomposites can be prepared by mixing two or more nanophases. By mixing nanoparticles of a ferroelectric in an organic liquid, one can design ferroelectric fluids which are analogous to ferromagnetic fluids discussed above. A ferromagnetic fluid prepared from ultrafine $BaTiO_3$ particles and an organic carrier liquid showed a maximum in the dielectric constant at the tetragonal–cubic phase transition of the perovskite phase.[122,137] By dispersing 10 nm particles of $BaTiO_3$ in a mixture of heptane and oleic acid, Bachman and Barner[138] have shown that the nanoparticles show permanent polar moments. These types of ferroelectric fluids may be useful as an alternative to liquid crystals in display panels.[122] Future research in the ferroelectric nanocomposites may lead to applications in optical devices.

2.4.2 *Superconducting Ferroelectric Nanocomposites*

Thin-film heterostructures of $Bi_4Ti_3O_{12}$ $Bi_2Sr_2CuO_{6-x}$ have been grown on single crystals of $SrTiO_3$, $LaAlO_3$ and $MgAl_2O_4$ by pulsed-laser deposition.[139] These films have been found to be ferroelectric and the thickness of the layers can be in the nanometre range if so desired. These thin films look promising for use as novel, lattice-matched, epitaxial ferroelectric film electrode heterostructures in non-volatile memory applications.

2.4.3 *Dielectric Nanocomposites*

There is a need for substrates with very low relative permittivity (<3) in very-large-scale integration (VLSI) devices so that acceptable limits of cross-talk, signal-line impedance and transmission delay are maintained.[140] Ceramic–polymer nanocomposites using fumed silica and polydimethylsiloxane have been fabricated to achieve low relative permittivity substrates.[141] Clay–organic nanocomposites are also proposed as low-permittivity substrates (see above). Future studies in this area can try to take advantage of highly microporous, hydrophobic zeolites mixed in an organic or inorganic matrix to achieve very-low-permittivity substrates for electronic packaging.

2.4.4 *Conducting–Semiconducting–Insulating Nanocomposites*

Nanocomposites in the form of superlattice structures have been fabricated with metallic,[142] semiconductor,[143] and ceramic[144] materials for semiconductor-based devices.[145] The material is abruptly modulated with respect to composition and or structure. Semiconductor superlattice devices are usually multiple quantum structures, in which nanometre-scale layers of a lower bandgap material such as GaAs are sandwiched between layers of a larger bandgap material such as GaAlAs.[145] Quantum effects such as enhanced carrier mobility (two-dimensional electron gas) and bound states in the optical absorption spectrum, and non-linear optical effects, such as intensity-dependent refractive indices, have been observed in nanomodulated semiconductor multiple quantum wells.[146] Examples of devices based on these structures include fast optical switches, high-electron-mobility transistors, and quantum-well lasers.[146] Room-temperature electrochemical deposition of nanomodulated (5–10 nm) ceramic superlattice thin films of $Tl_aPb_bO_c$ $Tl_dPb_eO_f$ has been reported recently.[146] The electrochemical method offers several advantages over vapour deposition methods such as molecular-beam epitaxy for depositing nanomodulated materials with nearly square-wave modulation of composition and structure, because the low processing temperatures minimize interdiffusion.[146] These structures are hoped to show quantum electronic, optical or optoelectronic effects as the modulation wavelength approaches the electron mean path.[146]

Other methods such as sputtering, electrodeposition and chemical techniques[147–153] have also been used to prepare nanocomposites. Nanocomposites of Mo in Al matrix were prepared by sputtering techniques. Nanoscale particles of Mo were first produced by high-pressure sputtering at >100 mTorr in a thermal gradient and then they were embedded in an Al matrix by normal sputtering.[148] A new class of diamond-like nanocomposite materials was synthesized,[149] consisting of Si—O and transition-metal networks imbedded in a diamond-like C matrix. In metal-containing nanocomposites, the conductivity can be varied continuously over 18 orders of magnitude by varying the concentration of metal atoms. Conductivities as high as 104 S cm^{-1} have been achieved with W-containing films.[149] Clusters of metallic silver have been formed by electrodeposition within the surface of an oxide glass which was subjected to a silver-ion exchange process.[150] The clusters have a fractal structure and the fractal growth within the glass results in the formation of a glass–metal nanocomposite with particle diameter of *ca.* 12 nm. A new approach in nanocomposite synthesis has been developed and it involves rapid condensation of metallic and non-metallic species produced by laser-induced reactions.[151] These composite surface layers form by codeposition of fine amorph-

ous silica fibres of 25–120 nm diameter and a metal matrix where the fibres exist in the form of a random-weave structure. A chemical technique has been used to produce metal–polymer nanocomposites.[152] In this method, poly(vinylpyridine)s were heated with copper formate in MeOH to 125 °C and the resulting thermal decomposition of the complex initiated a redox reaction which reduced the Cu^{2+} to Cu metal and oxidized the formate to CO_2 and H_2, leading to solid Cu–polymer nanocomposites containing up to 23 wt.% Cu. A review article by Hirai and Sasaki[153] deals with the *in situ* preparation methods such as chemical vapour deposition for different nanocomposites.

2.5 Structural Ceramic Nanocomposites

Glass ceramics, which are well known materials constitute a type of ceramic nanocomposite with nanocrystals being embedded in the glassy phase. These will not be treated here. However, one recent breakthrough in glass ceramics is worth mentioning.[154] Albite glass, which has been thought to be impossible to crystallize, has been crystallized by seeding both gels and glasses with fine albite seeds, *i.e.* the nanocomposite approach.[154] Recently, Niihara and his colleagues[155–173] developed ceramic nanocomposites from oxide–non-oxide and non-oxide–non-oxide mixtures and they have classified these into four categories: (*a*) intragranular, (*b*) intergranular, (*c*) both intra- and inter-granular and (*d*) nano/nanocomposites (Fig. 10). In the intra- and inter-granular nanocomposites, the nano-size particles are dispersed mainly within the matrix grains or at the grain boundaries of the matrix, respectively (Fig. 10). The intragranular and intergranular nanocomposites or their combination showed tremendous improvement in mechanical properties such as hardness, strength and creep and fatigue fracture resistances even at high temperatures compared to those of monophasic and microcomposites. The nano/nanocomposites were found to offer advantages in machinability and superplasticity.[173] Ceramic nanocomposites can be fabricated by chemical vapour deposition,[174–177] pressureless sintering, HIPing and hot pressing.[155–173] The fabrication process of oxide-based nanocomposites is shown in Fig. 11. Niihara and co-workers succeeded in preparing numerous ceramic nanocomposites such as Al_2O_3 SiC, Al_2O_3 Si_3N_4, Al_2O_3 TiC, mullite SiC, B_4C SiC, B_4C TiB_2, SiC amorphous SiC, Si_3N_4 SiC and others. Table 4 shows the significant improvements in mechanical properties which can be achieved by the nanocomposite route for various compositional systems.[173] The improvement in mechanical properties is attributed to the nano-size dispersions.[173] Niihara and Nakahira[173] have also made hybrid composites with nanocomposites and microcomposites and found significant improvements in not only toughness but also strength. Low-temperature methods have been used to fabricate ceramic nanocomposites, in addition to the above solid-state method. A gel-based method has been used to prepare SiC Al_2O_3 nanocomposites, which also exhibited enhanced mechanical properties.[178] A novel epitaxial growth of nickel(II) hydroxide on layer silicate followed by sintering led to metal–ceramic nanocomposites.[179] A proprietary, apparently low-temperature process, has been used to produce synthetic opal which is a nanocomposite of amorphous silica and crystalline zirconia.[180] The synthetic opal invented by Gilson, is commercially available from Nakazumi Chemicals.[181] Unlike natural opal, synthetic opal revealed the presence of separate crystalline ZrO_2 balls that were nearly spherical and ranged in diameter 7–50 nm among the 200 nm non-crystalline SiO_2 balls. The ZrO_2 balls were arranged in basically two patterns: hexagonal rings and nearly square grids [Fig. 12(*a*),(*b*)]. This nanocomposite also showed significantly higher fracture toughness compared to the monophasic natural opal.[180] The above studies demonstrate that the nanocomposites are clearly superior to the monophasic or microcomposite alternatives in ceramic processing.

3. Summary and Conclusions

The nanocomposite approach in sol–gel, catalytic, optical, sensor, electroceramic and structural ceramic materials is now well established. Sol–gel nanocomposites have been shown to lower crystallization temperatures and enhance densification of ceramic materials, in general. Tailoring of nanocomposites

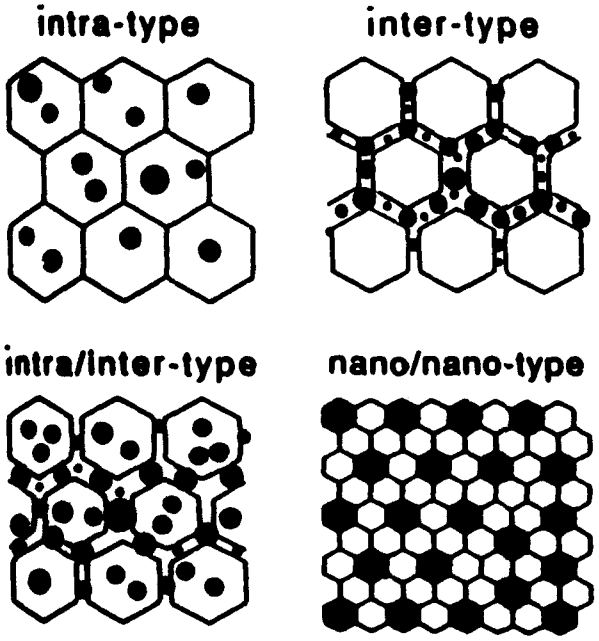

Fig. 10 Schematic illustration of ceramic nanocomposites. Reprinted by permission from ref. 173

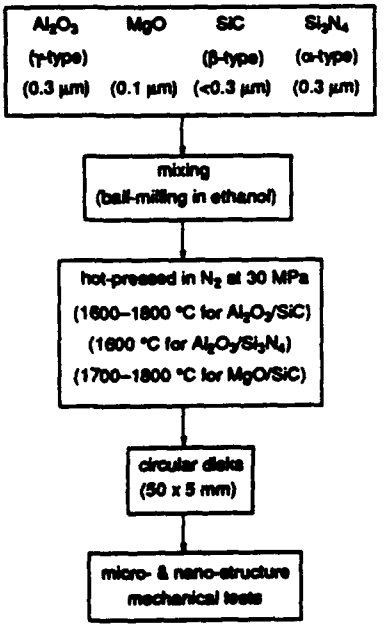

Fig. 11 The fabrication process of nanocomposites. Reprinted by permission from ref. 173

Table 4 Improvement of mechanical properties observed for the ceramic nanocomposites. (Reprinted by permission from ref. 173)

composite system	toughness MPa $m^{1/2}$	strength MPa	max. operating temperature[a] °C
Al_2O_3-SiC	3.5→4.8	350→1520	800→1200
Al_2O_3-Si_3N_4	3.5→4.7	350→850	800→1300
MgO-SiC	1.2→4.5	340→700	600→1400
Si_3N_4-SiC	4.5→7.5	850→1550	1200→1400

[a] Maximum operating temperature at the high loads.

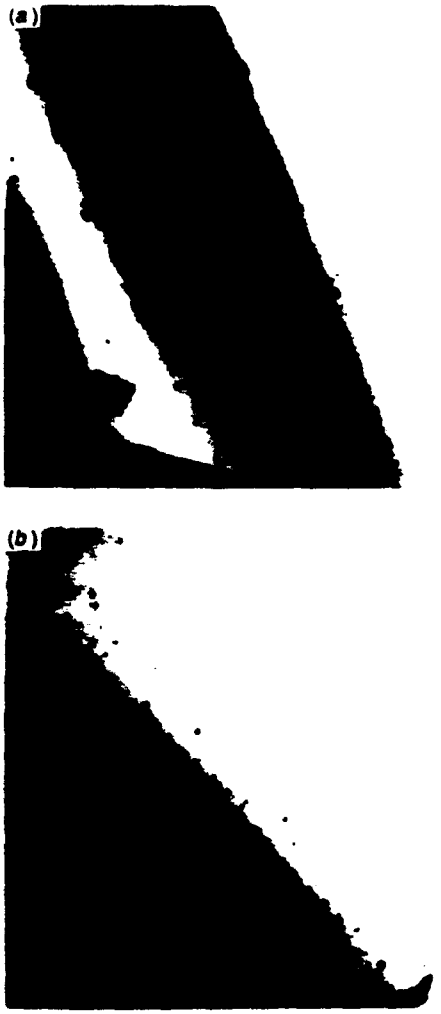

Fig. 12 Transmission electron micrographs of synthetic nanocomposite opal showing two different arrays of nano-sized (7–50 nm) ZrO_2 balls in the void spaces of silica balls. Reprinted by permission from ref. 180

with low-dimensional solids such as clays have led to novel microporous materials, which may find application in catalytic, sensor and laser materials. Nano-designing in the electroceramics area has yielded improved dielectric, optical, optoelectronic, magnetic, quantum electronic and superconducting properties. Structural ceramic processing through nanocomposites has resulted in significant improvement in mechanical properties such as hardness, strength, creep and fatigue fracture resistances, machinability and superplasticity. Dramatic improvements in materials functions are expected in the future through judicious processing of nanocomposites.

The author is grateful for the support of this work by the Air Force Office of Scientific Research under Grant No. AFOSR-89-0446. I thank Professor Rustum Roy for his valuable comments on the manuscript.

References

1 R. Roy, S. Komarneni and D. M. Roy, *Mater. Res. Soc. Symp. Proc.*, 1984, **32**, 347.
2 R. Roy, *Mater. Res. Soc. Annu. Mtg., Abstr.*, Boston, MA, 1982, p. 370.
3 R. A. Roy and R. Roy, *Mater. Res. Bull.*, 1984, **19**, 169.
4 D. W. Hoffman, R. Roy and S. Komarneni, *J. Am. Ceram. Soc.*, 1984, **67**, 468.
5 R. E. Newnham, D. P. Skinner and L. E. Cross, *Mater. Res. Bull.*, 1978, **13**, 525.
6 D. W. Hoffman, R. Roy and S. Komarneni, *Mater. Lett.*, 1984, **2**, 245.
7 D. W. Hoffman, S. Komarneni and R. Roy, *J. Mater. Sci. Lett.*, 1984, **3**, 439.
8 S. Komarneni, Y. Suwa and R. Roy, *J. Am. Ceram. Soc.*, 1986, **69**, C-155.
9 Y. Suwa, R. Roy and S. Komarneni, *J. Am. Ceram. Soc.*, 1985, **68**, C-238.
10 R. Roy, Y. Suwa and S. Komarneni, in *Science of Ceramic Chemical Processing*, ed. L. L. Hench and D. R. Ulrich, Wiley, New York, 1986, p. 247.
11 Y. Suwa, S. Komarneni and R. Roy, *J. Mater. Sci. Lett.*, 1986, **5**, 21.
12 Y. Suwa, R. Roy and S. Komarneni, *Mater. Sci. Eng.*, 1986, **83**, 151.
13 M. Kumagai and G. L. Messing, *J. Am. Ceram. Soc.*, 1984, **67**, C-230.
14 M. Kumagai and G. L. Messing, *J. Am. Ceram. Soc.*, 1985, **68**, 500.
15 G. L. Messing, J. L. McArdle and R. A. Shelleman, *Mater. Res. Soc. Symp. Proc.*, 1986, **73**, 471.
16 R. A. Shelleman, G. L. Messing and M. Kumagai, *J. Non-Cryst. Solids*, 1986, **82**, 277.
17 G. Vilmin, S. Komarneni and R. Roy, *J. Mater. Sci.*, 1987, **22**, 3556.
18 G. Vilmin, S. Komarneni and R. Roy, *J. Mater. Res.*, 1987, **2**, 489.
19 S. Komarneni, Y. Suwa and R. Roy, *J. Mater. Sci. Lett.*, 1987, **6**, 525.
20 W. Yarbrough and R. Roy, *J. Mater. Res.*, 1987, **2**, 494.
21 R. Roy, R. A. Roy and D. M. Roy, *Mater. Lett.*, 1986, **4**, 323.
22 R. Roy, *Science*, 1987, **238**, 1664.
23 A. Kazakos-Kijowski, S. Komarneni and R. Roy, *Mater. Res. Soc. Symp. Proc.*, 1988, **121**, 245.
24 J. L. McArdle and G. L. Messing, L. A. Tietz and C. B. Carter, *J. Am. Ceram. Soc.*, 1989, **72**, 864.
25 J. C. Huling and G. L. Messing, *J. Am. Ceram. Soc.*, 1989, **72**, 1725.
26 R. Roy and S. Komarneni, *U.S. Pat.*, 4828031, 1989.
27 A. M. Kazakos, S. Komarneni and R. Roy, *J. Mater. Res.*, 1990, **5**, 1095.
28 P. Ravindranathan, S. Komarneni and R. Roy, *J. Am. Ceram. Soc.*, 1990, **73**, 1024.
29 L. Pach, R. Roy and S. Komarneni, *J. Mater. Res.*, 1990, **5**, 278.
30 A. Kazakos, S. Komarneni and R. Roy, *Mater. Lett.*, 1990, **9**, 405.
31 A. Kazakos, S. Komarneni and R. Roy, *Mater. Lett.*, 1990, **10**, 75.
32 S. Komarneni and R. Roy, *Ceram. Trans.*, 1990, **6**, 209.
33 R. Roy, *Mater. Res. Soc. Symp. Proc.*, 1990, **175**, 15.
34 S. Komarneni, A. M. Kazakos and R. Roy, *U.S. Pat.*, 5030592, 1991.

35 U. Selvaraj, A. V. Prasadarao, S. Komarneni and R. Roy, *J. Mater. Res.*, 1992, in the press.
36 U. Selvaraj, A. V. Prasadarao, S. Komarneni and R. Roy, *J. Am. Ceram. Soc.*, 1992, **75**, 1167.
37 A. V. Prasadarao, U. Selvaraj, S. Komarneni, A. S. Bhalla and R. Roy, *J. Am. Ceram. Soc.*, 1992, **75**, in the press.
38 A. J. Burggraaf, K. Keizer and B. A. Van Hassel, *Solid State Ionics*, 1989, **32–33**, 771.
39 R. D. Shull and J. J. Ritter, *Mater. Res. Soc. Symp. Proc.*, 1990, **195**, 435.
40 R. D. Shull, J. J. Ritter and L. J. Swartzendruber, *J. Appl. Phys.*, 1991, **69**, 5144.
41 R. D. Shull, J. J. Ritter, A. J. Shapiro and L. J. Swartzendruber, *J. Appl. Phys.*, 1990, **67**, 4490.
42 R. D. Shull, J. J. Ritter, A. J. Shapiro, L. J. Swartzendruber and L. H. Bennett, *Mater. Res. Soc. Symp. Proc.*, 1988, **132**, 179.
43 R. D. Shull, J. J. Ritter, A. J. Shapiro, L. J. Swartzendruber and L. H. Bennett, *Mater. Res. Soc. Symp. Proc.*, 1991, **206**, 455.
44 A. Chatterjee and D. Chakravorty, *J. Phys. D*, 1990, **23**, 1097.
45 A. Chatterjee and D. Chakravorty, *J. Phys. D*, 1989, **22**, 1386.
46 G. C. Das and D. Chakravorty, *Bull. Mater. Sci.*, 1989, **12**, 449.
47 P. N. Prasad, *Mater. Res. Soc. Symp. Proc.*, 1990, **180**, 741.
48 B. Dunn and J. I. Zink, *J. Mater. Chem.*, 1991, **1**, 903.
49 S. Yamanaka, *Proceedings of the Seventh Seminar on Frontier Technology-Nano-Hybridization and Creation of New Functions*, Feb. 7–10, 1989, Oiso, Japan.
50 *Intercalation Chemistry*, ed. M. S. Whittingham and A. J. Jacobsen, Academic Press, New York, 1982.
51 D. W. E. Vaughan, R. J. Lussier and J. S. Magee, *U.S. Pat.*, 4176090, 1974.
52 S. Yamanaka and G. W. Brindley, *Clays Clay Miner.*, 1979, **27**, 119.
53 G. W. Brindley and S. Yamanaka, *Am. Mineral.*, 1979, **64**, 830.
54 T. J. Pinnavaia, M. S. Tzou and S. D. Landau, *J. Am. Chem. Soc.*, 1985, **107**, 4783.
55 S. Sterte, *Clays Clay Miner.*, 1986, **34**, 658.
56 S. Yamanaka, T. Doi, S. Sako and M. Hattori, *Mater. Res. Bull.*, 1984, **19**, 161.
57 S. Yamanaka, G. Yamashita and M. Hattori, *Clays Clay Miner.*, 1980, **28**, 281.
58 J. Sterte and J. Shabtai, *Clays Clay Miner.*, 1987, **35**, 429.
59 S. Yamanaka, T. Nishihara and M. Hattori, *Mater. Res. Soc. Symp. Proc.*, 1988, **111**, 283.
60 S. Yamanaka, H. Matsumoto, F. Okumura, M. Yoshikawa and M. Hattori, *Abstracts of the 28th Annual Meeting of the Basic Science Division of the Ceramic Society of Japan*, Tokyo, 1990, p. 43.
61 T. J. Pinnavaia, *Science*, 1983, **220**, 365.
62 H. Yoneyama, S. Haga and S. Yamanaka, *J. Phys. Chem.*, 1989, **93**, 4833.
63 S. Yamanaka, *Am. Ceram. Soc. Bull.*, 1991, **70**, 1056.
64 R. C. Zielke and T. J. Pinnavaia, *Clays Clay Miner.*, 1988, **36**, 403.
65 T. Nolan, K. R. Srinivasan and H. S. Fogler, 1989, **37**, 487.
66 K. R. Srinivasan, H. S. Fogler, E. Gulari, T. Nolan and J. S. Schultz, *Environ. Prog.*, 1985, **4**, 239.
67 P. B. Malla, S. Yamanaka and S. Komarneni, *Solid State Ionics*, 1989, **32/33**, 354.
68 S. Yamanaka, P. B. Malla and S. Komarneni, *J. Colloid Interface Sci.*, 1990, **134**, 51.
69 P. Malla and S. Komarneni, *Sci. Geol. Mem.*, 1990, **86**, 59.
70 S. Miyata, *Clays Clay Miner.*, 1975, **23**, 396.
71 S. Miyata and T. Kumura, *Chem. Lett.*, 1973, **843**.
72 S. Miyata and A. Okada, *Clays Clay Miner.*, 1977, **25**, 14.
73 S. Kikkawa and M. Koizumi, *Mater. Res. Bull.*, 1982, **17**, 191.
74 F. A. P. Cavalcanti, A. Schutz and P. Biloen, in *Preparation of Catalysts IV*, ed. B. Delmon, P. Grange, P. A. Jacobs and G. Poncelet, Elsevier, Amsterdam, pp. 165–174.
75 S. Miyata and A. Okada, *Clays Clay Miner.*, 1977, **25**, 14.
76 A. Schutz and P. Biloen, *J. Solid State Chem.*, 1987, **68**, 360.
77 S. Idemura, E. Suzuki and Y. Ono, *Clays Clay Miner.*, 1989, **37**, 553.
78 E. Suzuki, S. Idemura and Y. Ono, *Clays Clay Miner.*, 1989, **37**, 173.
79 P. B. Malla, P. Ravindranathan, S. Komarneni and R. Roy, *Nature (London)*, 1991, **351**, 555.
80 P. B. Malla, P. Ravindranathan, S. Komarneni, E. Breval and R. Roy, *J. Mater. Chem.*, 1992, **2**, 559.
81 B. K. G. Theng, *The Chemistry of Clay-Organic Reactions*, Wiley, 1974, pp. 343.
82 G. V. Jacks, *Soils Fertilizers*, 1973, **26**, 147.
83 Y. Sugahara, K. Kuroda and C. Kato, *J. Am. Ceram. Soc.*, 1984, **67**, C-247.
84 Y. Sugahara, K. I. Sugimoto, T. Yanagisawa, Y. Nomizu, K. Kuroda and C. Kato, *Yogyo-Kyokai-Shi*, 1987, **95**, 1.
85 Y. Sugahara, K. Kuroda and C. Kato, *Clay Sci.*, 1987, **7**, 17.
86 Y. Sugahara, K. Kuroda and C. Kato, *J. Mater. Sci.*, 1988, **23**, 3572.
87 Y. Sugahara, K. Kuroda and C. Kato, *Ceram. Int.*, 1988, **14**, 1.
88 Y. Sugahara, K. I. Sugimoto, K. Kuroda and C. Kato, *J. Am. Ceram. Soc.*, 1988, **71**, C-325.
89 Y. Sugahara, J. Miyamoto, K. Kuroda and C. Kato, *Appl. Clay Sci.*, 1989, **4**, 11.
90 H. Mostaghaci, F. L. Riley and J. P. Torre, *Int. J. High Technol. Ceram.*, 1988, **4**, 51.
91 Y. Sugahara, J. Miyamoto, K. Kuroda and C. Kato, *Ceram. Int.*, 1988, **14**, 163.
92 Z. Hrabe, S. Komarneni, P. B. Malla, V. Srikanth and R. Roy, *J. Mater. Sci.*, in the press.
93 V. Mehrotra and E. P. Giannelis, *Mater. Res. Soc. Symp. Proc.*, 1990, 171.
94 V. Mehrotra, T. Kwon and E. P. Giannelis, *Mater. Res. Soc. Symp. Proc.*, 1990, 167.
95 E. P. Giannelis, V. Mehrotra and M. W. Russell, *Mater. Res. Soc. Symp. Proc.*, 1990, 180.
96 V. Mehrotra and E. P. Giannelis, *Solid State Commun.*, 1991, **77**, 155.
97 S. N. Hoda and A. R. Olszewski, *U.S. Pat.*, 4454237, 1984.
98 V. Mehrotra and E. P. Giannelis, *Solid State Commun.*, 1991, **77**, 155.
99 V. Mehrotra and E. P. Giannelis, *Solid State Ionics*, 1992, **51**, 1.
100 M. G. Kanatzidis, C. G. Wu, H. O. Marcy, D. C. DeGroot and C. R. Kannewurf, *Chem. Mater.*, 1990, **2**, 222.
101 V. Mehrotra, E. P. Giannelis, R. F. Ziolo and P. Rogalskyj, *Chem. Mater.*, 1992, **4**, 20.
102 L. M. Johnson and T. J. Pinnavaia, *Langmuir*, 1991, **7**, 2636.
103 T. A. Werpy, L. J. Michot and T. J. Pinnavaia, *ACS Symp. Ser.*, 1990, **437**, 119.
104 T. Yanagisawa, T. Shimizu, K. Kuroda and C. Kato, *Bull. Chem. Soc. Jpn.*, 1990, **63**, 988.
105 T. Yanagisawa, T. Shimizu, K. Kuroda and C. Kato, *Bull. Chem. Soc. Jpn.*, 1990, **63**, 1535.
106 T. Endo, T. Sato and M. Shimada, *J. Phys. Chem. Solids*, 1986, **47**, 799.
107 T. Endo, N. Nakada, T. Sato and M. Shimada, *J. Phys. Chem. Solids*, 1988, **49**, 1423.
108 M. Shimada, *Proceedings of the Seventh Seminar on Frontier Technology-Nano-Hybridization and Creation of New Functions*, Feb. 7–10, 1989, Oiso, Japan.
109 T. Endo, N. Nakada, T. Sato and M. Shimada, *J. Phys. Chem. Solids*, 1989, **50**, 133.
110 J. M. Thomas, in *Intercalation Chemistry*, ed. M. S. Whittingham and A. J. Jacobson, Academic Press, New York, 1982, pp. 55–99.
111 S. T. Wilson, B. M. Lok, C. A. Messina, T. R. Cannan and E. M. Flanigen, *Adv. Chem. Ser.*, 1982, **101**, 1146.
112 R. M. Barrer, *Hydrothermal Chemistry of Zeolites*, Academic Press, London, 1982, p. 360.
113 C. P. Nicolaides and M. S. Scurrell, in *Keynotes in Energy Related Catalysis*, Elsevier, New York, 1988, pp. 319–379.
114 W. M. Minachev and I. Ya. Isakov, *Am. Chem. Soc. Monogr.*, 1976, **171**, 552.
115 P. A. Jacobs, in *Metal Clusters in Catalysis*, Elsevier, New York, 1986.
116 P. Gallezot and G. Bergeret, in *Metal Microstructures in Zeolites*, ed. P. A. Jacobs, N. I. Jaeger, P. Jiru and G. Schulz-Ekloff, Elsevier, Amsterdam, 1982, p. 162.
117 N. I. Jaeger, P. Ryder and G. Schulz-Ekloff in *Structure and Reactivity of Modified Zeolites*, ed. P. A. Jacobs, N. I. Jaeger, P. Jiru, V. B. Kazansky and G. Schulz-Ekloff, Elsevier, Amsterdam, 1984, p. 299.
118 P. B. Malla, P. Ravindranathan, S. Komarneni, E. Breval and R. Roy, *Mater. Res. Soc. Symp. Proc.*, 1991, **233**, 207.
119 G. D. Stucky, *Mater. Res. Soc. Symp. Proc.*, 1991, **206**, 507.
120 G. A. Ozin, A. Stein, J. P. Godber and G. D. Stucky, Report No. AD-A208208, NTIS, 1988, pp. 29.
121 H. K. Chae, W. G. Klemperer, D. A. Payne and C. T. A. Suchicital, *Abstracts, Advanced Materials Science and Engineering Society Symposium on Hydrothermal Reactions*, Tokyo, Japan, 1989, p. 16.

122 R. E. Newnham, S. E. McKinstry and H. Ikawa, *Mater. Res. Soc. Symp. Proc.*, 1990, **175**, 161.
123 R. E. Newnham and S. E. Trolier-McKinstry, *Ceram. Trans.*, 1990, **8**, 235.
124 L. Wen and R. Huang, *C-MRS Int. Symp. Proc.*, 1991, **1**, 117.
125 N. Tsuya, Y. Saito, H. Nakamura, S. Hayano, A. Furugohri, K. Ohta, Y. Wakui and T. Tokushima, *J. Mag. Mag. Mater.*, 1986, **54–57**, 1681.
126 J-C. Bacri, R. Perzynski and D. Salin, *Endeavor, New Series*, 1988, **12**, 76.
127 R. E. Rosenweig, *Sci. Am.*, October 1982, 136.
128 R. V. Mehta, in *Thermomechanics of Magnetic Fluids*, ed. B. Berkovsky, Hemisphere, Washington, 1978.
129 M. Camras, *Magnetic Recording Handbook*, Van Nostrand Reinhold, New York, 1988.
130 R. M. White, *Sci. Am.*, 1980, **243**, 138.
131 M. Lee, A. Halliyal and R. E. Newnham, *Ferroelectrics*, 1988, **87**, 71.
132 L. E. Cross, *Ferroelectrics*, 1987, **76**, 241.
133 G. A. Smolensky, *J. Phys. Soc. Jpn.*, 1970, **28** (Suppl. 26).
134 J. Chen, H. M. Chan and M. P. Harmer, *J. Am. Ceram. Soc.*, 1989, **72**, 593.
135 C. A. Randall, D. J. Barber, P. Groves and R. W. Whatmore, *J. Mater. Sci.*, 1988, **23**, 3678.
136 C. A. Randall, A. S. Bhalla and L. E. Cross, *Jpn. J. Appl. Phys.*, 1990, **29**, 327.
137 D. V. Miller, Ph.D. Thesis, Pennsylvania State University, University Park, PA, 1991.
138 R. Bachmann and K. Barner, *Solid State Commun.*, 1988, **68**, 865.
139 R. Ramesh, A. Inam, W. K. Chan, B. Wilkens, K. Myers, K. Remschnig, D. L. Hart and J. M. Tarascon, *Science*, 1991, **252**, 944.
140 A. Das, Ph.D. Thesis, Pennsylvania State University, 1988.
141 A. Das, T. T. Srinivasan and R. E. Newnham, *Mater. Res. Soc. Symp. Proc.*, 1990, **167**, 165.
142 C. M. Falco and I. K. Schuller, in *Synthetic Modulated Structures*, ed. L. L. Chang and B. C. Giessen, Academic Press, Orlando, 1985, pp. 339–362.
143 *Interfaces, Quantum Wells, and Superlattices NATO Ser. B: Physics*, **179**, ed. C. R. Leavens and R. Taylor, Plenum, New York, 1988.
144 T. Terashima and Y. Bando, *J. Appl. Phys.*, 1984, **56**, 3445.
145 *Physics and Applications of Quantum Wells and Superlattices NATO Ser. B: Physics*, **170**, ed. E. E. Mendez and K. von Klitzing, Plenum, New York, 1987.
146 J. A. Switzer, M. J. Shane and R. J. Phillips, *Science*, 1990, **247**, 444.
147 G. M. Chow, A. Patnaik, T. E. Schlesinger, R. C. Cammarata, M. E. Twigg and A. S. Edelstein, *J. Mater. Res.*, 1991, **6**, 737.
148 G. M. Chow, R. L. Holtz, C. L. Chien and A. S. Edelstein, *Mater. Res. Soc. Symp. Proc.*, 1990, **195**, 623.
149 V. F. Dorfmann, T. A. Skotheim and B. N. Pypkin, *Proc. Electrochem. Soc.*, 1991, **91–8**, 393.
150 S. Roy and D. Chakravorty, *Appl. Phys. Lett.*, 1991, **59**, 1415.
151 G. M. Chow and P. R. Strutt, *High Temp. Sci.*, 1990, **27**, 311.
152 A. M. Lyons, S. Nakahara and E. M. Pearce, *Mater. Res. Soc. Symp. Proc.*, 1988, **132**, 37.
153 T. Hirai and M. Sasaki, *Mater. Sci. Monogr.*, 1991, **68**, 541.
154 U. Selvaraj, C. L. Liu, S. Komarneni and R. Roy, *J. Am. Ceram Soc.*, 1991, **74**, 1378.
155 T. Uchiyama, S. Inoue and K. Niihara, *Silicon Carbide Ceramics*, ed. S. Somiya and K. Inomata, Uchida Rokakuho, Tokyo, 1989, pp. 193–200.
156 K. Niihara, *J. Ceram. Soc. Jpn.*, 1991, **99**, in the press.
157 K. Niihara and A. Nakahira, *Proceeding of MRS Meeting on Advanced Composites*, Plenum, New York, 1988, pp. 129–134.
158 K. Niihara, *J. Jpn. Soc. Powder Powder Metal.*, 1990, **37**, 348.
159 K. Niihara, A. Nakahira, H. Ueda and H. Sasaki, *Proc. 1st Jpn Int. SAMPE Symp.*, 1989, pp. 1120–1125.
160 K. Niihara, T. Hirano, A. Nakahira and K. Izaki, *Proc. MRS Meeting Adv. Mater.*, Tokyo, 1988, pp. 107–112.
161 K. Niihara, T. Hirano, A. Nakahira, K. Suganuma, K. Izaki and T. Kawakami, *J. Jpn. Soc. Powder Powder Metal.*, 1989, **36**, 243.
162 K. Niihara, K. Izaki and T. Kawakami, *J. Mater. Sci. Lett.*, 1990, **9**, 598.
163 K. Niihara, K. Suganuma and K. Izaki, *J. Mater. Sci.*, 1990, **9**, 112.
164 K. Niihara, K. Izaki and A. Nakahira, *J. Jpn. Soc. Powder Powder Metal.*, 1990, **37**, 352.
165 K. Suganuma, G. Sasaki, T. Fujita and K. Niihara, *J. Jpn Soc. Powder Powder Metal.*, 1991, **38**, 374.
166 K. Izaki, A. Nakahira and K. Niihara, *J. Jpn. Soc. Powder Powder Metal.*, 1991, **38**, 357.
167 F. Wakai, Y. Kodama, S. Sakaguti, N. Murayama, K. Izaki and K. Niihara, *Nature (London)*, 1990, **344**, 421.
168 K. Niihara and A. Nakahira, *Advanced Structural Inorganic Composite*, ed. P. Vincenzini, Elsevier, Amsterdam, 1990, pp. 637–664.
169 K. Niihara and A. Nakahira, *Ann. Chim.*, 1991, **16**, 479.
170 K. Niihara and A. Nakahira, *Mater. Sci. Monogr.*, 1991, **68**, 637.
171 A. Sawaguchi, K. Toda and K. Niihara, *J. Am. Ceram. Soc.*, 1991, **74**, 1142.
172 K. Niihara, K. Izaki and T. Kawakami, *J. Mater. Sci. Lett.*, 1991, **10**, 112.
173 K. Niihara and A. Nakahira, in *Ceramics: Toward the 21st Century*, ed. N. Soga and A. Kato, Ceram. Soc. Jpn., Tokyo, 1991, pp. 404–417.
174 K. Niihara and T. Hirai, *Ceramics*, 1986, **26**, 598.
175 Y. Wang, M. Sasaki and T. Hirai, *J. Mater. Sci.*, 1991, **26**, 6618.
176 L. Wen, J. Gong, B. Yu, R. Huang and L. Guo, 1991, *C-MRS Int. Symp. Proc.*, 1990, **4**, 219.
177 Y. Wang, M. Sasaki and T. Hirai, *J. Mater. Sci.*, 1991, **26**, 5495.
178 R. S. Haaland, B. I. Lee and S. Y. Park, *Ceram. Eng. Sci. Proc.*, 1987, **8**, 872.
179 K. Ohtsuka, J. Koga, M. Tsunoda, M. Suda and M. Ono, *J. Am. Ceram. Soc.*, 1990, **73**, 1719.
180 T. C. Simonton, R. Roy, S. Komarneni and E. Breval, *J. Mater. Res.*, 1986, **1**, 667.
181 Y. Nakazumi, in *27th Symposium on Synthetic Minerals*, 1982, paper no. S-2.

Paper 2 03256B; *Received* 22*nd June*, 1992

91

SOLUTION–SOL–GEL TECHNOLOGY AND SCIENCE: PAST, PRESENT, AND FUTURE

RUSTUM ROY

INTRODUCTION

My colleague at Penn State, the social historian, Professor Ivan Illich, wrote last year that "the present is the future of the past," and it is the only future worth studying and knowable for sure. My curve describing the progress of scientific knowledge (Fig. 91.1) tells us why we cannot expect to be able to predict what will be happening in solution–sol–gel (SSG) research with any degree of assurance for more than a few years. The serendipitous step functions obviously cannot be predicted. Yet they can have a profound effect on the conduct of science. Think of the hundreds of ceramists working today on superconductors and the dozens who have abandoned cold fusion. The difference is obviously not connected with the intrinsic need to know the answer to a burning scientific question, nor to the technological pull, nor to the societal need. A $100 million government *program* decided the "future" of ceramic superconductor research activity. Had a $50 million program in cold fusion been started, there would no doubt be a thousand more scientists doing something or other in cold fusion. Conferences would proliferate, papers would be written by the hundreds, very few would ever be read, and even fewer cited. *Sic transit gloria scientiae.*

Chemical Processing of Advanced Materials,
Edited by Larry L. Hench and Jon K. West.
ISBN 0-471-54201-6

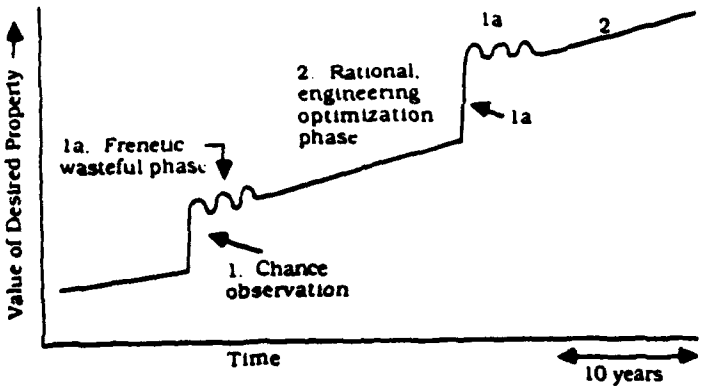

Figure 91.1. New materials synthesis often consists of two steps: (1) A chance observation by an experienced observer; (1a) after a postdiscovery frenetic phase, there is (2) the rational "engineering" optimization phase. The advances in desired property achieved by phase 2 are often as large as the advance in phase [1].

I begin with this particular observation because I believe the future may hold a very different method of funding science from the past. The fact is that somewhere between 50 and 90% of the research on sol–gel science would probably not have been done except that the money was there. The self-test is simple. If you had been given the same amount of money *before you ever started SSG research* and told to do whatever you please, would you have started in SSG? The future may hold a time when we will see a higher percentage of idea-pulled science by the relatively small number of those who have such ideas. The future will also no doubt hold more technological target-driven science, in which the optimization and detailed backup are studied and done in areas where there is a national need (Fig. 91.1).

Figures 91.2 and 91.3 provide a different approach to predicting the future. The two figures plot the numbers† of papers listed in *Chemical Abstracts* as a function of time under two sets of key words: *quasicrystals* and *sol–gel*. In spite of the rosy rhetoric with which *Nature's* editor announced the first papers on quasicrystals, no technological value whatsoever has been found for this curiosity—as expected, as I pointed out at that time. Yet the numbers of papers skyrocketed for 2–3 years but now have peaked and have started to decline. One can predict that the numbers will trail off soon roughly symmetrically. The SSG processing led to many valuable products: window coatings, nuclear fuel pellets, ceramic fibers, abrasive grains, and so on, *before* the steep rise in papers, indeed 15–30 years ago. During that period the numbers of papers on SSG were very

†I am fully aware of the limitations of these crude measures due to the key words chosen, or not, in the title. Indeed my original first SSG review, *J. Am. Ceram. Soc.* (1956), which is the first citation classic in all of ceramics and the first in that Journal, would not have been picked up by this search. The data, however, are quite appropriate for the present purposes.

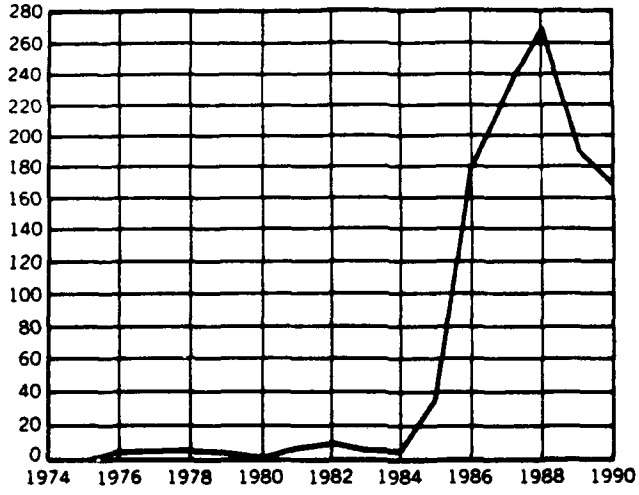

Figure 91.2. Number of papers on quasicrystals abstracted by *Chemical Abstracts* as a function of time.

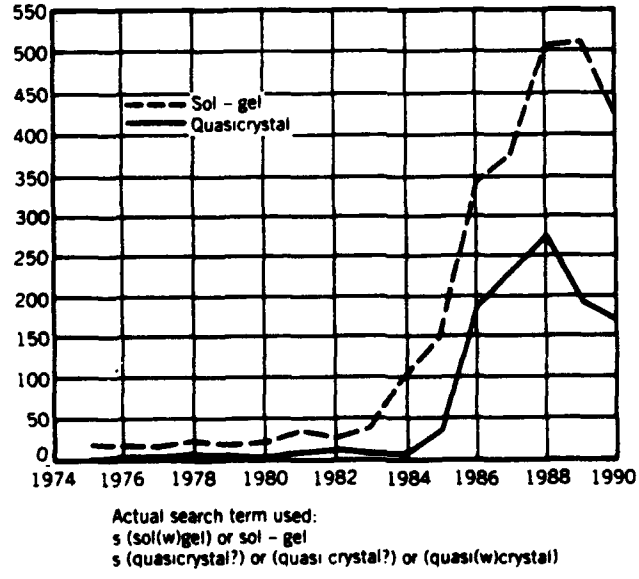

Figure 91.3. Number of papers on sol–gel in *Chemical Abstracts* over time (quasicrystal data repeated for comparison).

modest. Indeed I recall that after 1948 when we presented papers on "solution-ceramics" and sol–gel preparation of ceramic powders and glasses, virtually no other groups worked in the field for 10–15 years. The recent activity in SSG has paralleled the development of some rather modest new technologies such as silica optics, transparent aerogels, and so on. But these will not likely be justification enough to sustain a continued large basic science effort much longer. The past history of SSG itself compared to the recent history of other processing discoveries such as Lanxide's directed oxidation process prove that technological opportunity is not what drives academic and government scientific research. In the latter field of the most innovative high-tech structural composites one corporation has filed over 2500 patents in 5 years (over 500 have issued, 100 in the United States), announcing its results in dozens of papers, and new products appear regularly. Yet less than 5 papers appear to have been written by scientists outside the company in 5 years. Comparisons of the superconductors, diamond films, and Lanxide inventions have been presented elsewhere [2]. So much for innovation driving scientists.

WHAT THE PAST CAN TEACH US

In spite of my theory that step function advances in the discovery of new *materials* happen largely by chance events, we also recognize that in new *processes*, the innovation is done quite deliberately. Examples abound in ceramics research: Glass-ceramics at Corning, although advanced by the double accident in Stookey's laboratory†, was very much a targeted effort. So also was float glass at Pilkington. Likewise, in July 1948, I was very clearly focused on making homogeneous reactive ceramic powders and homogeneous glasses starting with all the components in solution. The use of organic precursors—some of which I had to make—was simply the only way to mix all components in solution. Compositionally we started with simple systems: Al_2O_3, Ga_2O_3, and Al_2O_3–SiO_2 (and are still doing work in this system), but in the next 5 years we moved in the direction of making homogeneous gels of four- and five-component systems and involving a very wide range of oxides. The titanates and niobates did not present difficulties, but the alkali ions did. Gels corresponding to synthetic micas and beidellite-clays such as $KNi_3GaSi_3O_{10}(OH)_2$ or $Na_xAl_2Al_xSi_{4-x}O_{10}(OH)_2 \cdot nH_2O$ pose a real challenge for retaining homogeneity on a nanoscale. The solutions we arrived at in those early days were effective, albeit primitive, but they were adequate for the task.

The future of SSG in general will, I am sure, as it has already started to do in the superconductors and ferroelectrics, move in the direction of dealing with complexification toward multicomponent systems. Whenever the gels are heated to temperatures greater than $\approx 1000°C$, it has not been established that greater sophistication in processing at the precursor level offers much benefit.

†The furnace controller malfunctioned, but the glass body did not melt. Then on pulling the sample out it dropped on the floor and did not break—indicating its remarkable strength.

THE PRESENT

The fine review article by Don Ulrich is really an admirable snapshot [3], while the Brinker and Scherer book *Sol–Gel Science* is a veritable album [4] of the present (1990) state of play. I admire it for its scope and thoroughness especially with reference to the *science* of SSG. Perhaps the state of play in the present overall SSG research is most evident in the book in the ratio of pages devoted to "science" (835 pages) and its "applications" (31 pages). Moreover, what is most significant is that a closer examination of the application chapter shows that in most cases the application had preceded the science and that hardly any connections could be made, even retrospectively, between the two. In other words, the two-tree theory of S&T (Shapley and Roy [5]) is alive and well in SSG. We have two independently developing fields: SSG technology and SSG science. The former will no doubt use bits and pieces of the enormous body of science that had been generated and are available to all, but they are probably of marginal significance to technological advances on the horizon or further in the future.

However, in order to be able usefully to extrapolate into the future, one needs to examine the early hints in the *present* and to make a judgment as to which will produce significant science or technology. I have selected a few areas of research I believe will yield significant new technology and derivatively new science.

Maximum Heterogeneity via SSG: Nanocomposites

In 1982–1983 I presented four papers [6–9] outlining the rationale behind my reversal of the original and still universal goal of SSG processing—making *homogeneous* ceramics. I do not believe that the significance of the idea of maximizing heterogeneity has been understood or appreciated by many in the community. First, of course, SSG is valuable in attaining this goal because as we are dealing with charged colloids it becomes possible to mix very easily and efficiently two sols, so that one gets nominally perfect mixing of two different phases in the Gibbsian meaning—hence "diphasic gels of maximum heterogeneity." Moreover as Fig. 91.4 shows, one can have heterogeneity of structure and of composition or of both.

These di-, or more generally, multiphasic gels are really a whole new class of *materials of controllable reactivity*. We have demonstrated beyond any doubt the following remarkable properties of these materials and in some cases of these materials alone.

1. The phase to be formed by heat treatment can be completely controlled by the use of the proper second phase. Vilmin, Komarneni, and Roy [10] could form either huttonite or thorite (10% less dense) from $ThSiO_4$ just by changing 1% of the second phase (example of Fig. 91.4c).
2. Reaction temperatures can be lowered by as much as 250–350°C due to the compositional heterogeneity (Fig. 91.4b) or solid-state epitaxy (Fig.

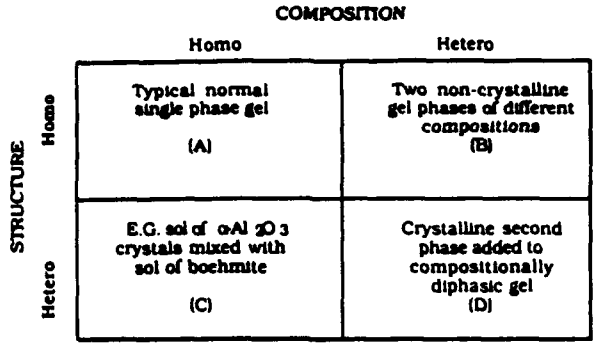

Figure 91.4. Different types of maximum heterogeneity accessed via SSG.

91.4c) due to structural heterogeneity. Thus we showed that mullite and later cordierite could be formed at the lowest temperatures and greatest speeds by using the heterogeneity strategy. This is hardly an academic exercise, although we have again found very few science papers on *compositional heterogeneity*. Yet the Chichibu Cement Company in Japan is making *compositionally* diphasic mullite powders for the ceramic industry in the amounts of some 6 tons/month. Crystallographic seeding *of gels* (structural heterogeneity), which we had used with very mixed success *at low temperatures* in the early 1950s, has caught on in industry and to some extent in academia [11–13].

3. Proper use of heterogeneity as in Fig. 91.4d can also be used to control the morphology of crystals.
4. Properties of nanocomposites can be created outside the range of properties of the end members.

Thus my first generalization for the near-term future is that the exploitation of gel-derived nanocomposites is likely to increase substantially. Moreover, it is very likely that the applications for such SSG-derived nanocomposites are much more likely to be in magnetic, optical, or "chemical," not "structural" applications. Thus Komarneni et al. [15] have created new nanocomposite desiccants with optimized thermodynamic efficiency.

(Epitaxial) Thin Films for Electroceramics

As a direct consequence of Fig. 91.4c it has become possible to grow highly oriented (nearly single-crystal) films of a wide variety of electroceramic compositions including the ferroelectrics and superconductors (e.g., at the University of Illinois, Westinghouse, and Penn State). In a review by Roy, Etzold, and Cuomo [14] these SSG-derived crystalline films have been compared with films

made by CVD, PVD, and laser ablation techniques and found to be equal or superior to the others. This is an area that is certain to be studied more extensively in the near future.

Microwave Processing of Ceramics

When Yang, Komarneni, and Roy [16] discovered the anomalous heating and melting of ordinary white ceramics in a home microwave oven, it was in a gel, as was also true of the Oak Ridge work on UO_2 [17]. Microwave processing of ceramics in general appears to be on a fast track. However, the role of the gel as a key element, especially in ceramic joining and welding (16), is not fully appreciated. Varadan (17) analyzed the absorption process and attributed the intense absorption to the size and concentration of the phase discontinuities inherent in the gel structure.

Complexification of Compositions: Addition of Organics in Final Products

It was noted above that inevitably there will be a drift away from the simplification of Al_2O_3 and SiO_2, and there will be extensive exploration of more complex inorganic compositions.

In the next phase one can also expect that useful organic–inorganic hybrid materials will be created. Hints of this appear in the work of Shimada [18] who encapsulated luminescent materials such as rhodamine B in clays and showed an order-of-magnitude increase in the luminescence under ultraviolet stimulation and an increase in thermal stability.

Crystal Growth in Gels is Not Biomimesis

For nearly 100 years the phenomenon of precipitation of inorganic phases in organic (and inorganic) gels has been studied intensively. The Liesegang phenomenon of rhythmic precipitation has not yet been explained fully even in the post-Prigogine era. In the 1950s and 1960s we had an extensive research program in the field, and much of the results were summarized by Henisch [19] and McCauley and Roy [20]. Much later, Hoffman, Roy, and Roy [21] applied these principles to create *one* set of nanocomposites precipitating extremely small ($\sim$ 1-nm) size crystals of $BaSO_4$, $CrPO_4$, AgCl, and Cds, in SiO_2 gels. It is an example of totally unscientific exaggeration to claim that the identical process applied to the precipitation of CdS in an organic gel [22, 23] (without any reference to the extensive earlier work of crystal growth in gels) is in some unspecified way connected to biomimesis, to which we now turn. I do not see much crystal growth in gels in the future.

"Biomimesis" (or Just Plain Hype-Mimesis)

Materials scientists have recently been subjected to a new onslaught of media stories and symposia on what I will call "biomimetic synthesis." This term and others used to cover this amorphous field trade on the vague idea that one can use either biological processes or biological structures as patterns for the creation of new families of materials. Unfortunately agencies and managers even a little distance removed from the field get caught up in the "excitement" of the supposedly new concept: imitate nature and life and create startling new materials. The idea unfortunately is neither new nor, so far, successful.

The idea is *at least* 20 years old, and its great future may be largely behind us. Indeed, the study of natural "hard tissue" in animals can hardly be new. After all, human bones and teeth are of major interest to us all, and the detailed chemistry, macrostructure, and microstructure of all such animal tissues have been studied so as to produce volumes, that fill shelves. In the technological world it has proved much easier to use substitutes for human hard tissue than to mimic them. The real biomaterials range from gold and sapphire in teeth to titanium and glassy carbon in bone prostheses. Here one mimics only the shape nature gave us. The interesting detailed structure of, say, tooth enamel, with its very slender fibrils of hydroxyapatite embedded in collagen, has been known for decades but has not led us to any insights on mimicking the process of growing teeth in vivo or in vitro—that would indeed be biomimesis. In fact, the process leading to egg shells probably is better understood than any other.

Our own work in the area of biomimetic materials was first reported in 1969. We were trying to understand a much stronger biological hard tissue—sea urchin spines (see Weber et al. [24, 25]). Weber was intrigued by the different microstructures of sea urchins and corals that although he could not swim, he scoured the South Sea Islands for different species in his scuba gear at depths up to 20 m. Out of this came our own successful effort at genuine biomimesis.

Excellent starting points for studying the biological structures and their value to materials science may be found in the reviews by Currey [26] and Birchall [27] and Birchall and Thomas [28]. What is to be noted from this work is that we do know and have known for a long time about the microstructure and micromechanics of biological materials. Furthermore, even these leaders of the field have not been able to use either the process or the material as a template to make any materials. Indeed, Birchall's brilliant analysis of the strength of the cuttlefish bone has not provided utilizable guidance yet to designers of structural ceramics. Yet Birchall correctly states that biomineralization has a lot to teach us in the realm of *ideas.*

Some 15 years before the major Currey and Birchall reviews, Weber, White, and Roy [24, 25] had found that the microstructure of the hard tissue of different species of corals, sea urchins, consisted of an intriguing 3 : 3 composite structure (see Newnham [29] for composite terminology) with intergrown polymeric proteins and $CaCO_3$ either as *single-crystal calcite* or polycrystalline aragonite. Moreover, different coral microstructures were very different, and some matched

human bone rather closely. White, Weber, and White [25] then developed what was called the "replamine form" process: the dissolution of either the inorganic or the organic fraction of the 3 : 3 composite and replacement with a wide variety of ceramics, metals, and so on. In a final step of double biomimesis, D. M. Roy [30] took the mimetic microstructure of Porites coral—aragonite with the polymer leached out—and imitated the composition of human bone by in situ hydrothermal transformation of aragonite to hydroxyapatite. This stellar example (the only one known to us) of a biomimetic material is commercially manufactured by Interpore International, still based on corals imported from the South Sea Islands. A nonbiomimetic example of the formation of a microstructure that resembled that of a mollusc shell appeared unexpectedly recently [31] on the precipitation of vaterite from viscous organic solutions. The visual observations and SEM photos of the assemblage of $CaCO_3$–vaterite crystals did in fact resemble many natural shells. This obviously had nothing whatever to do with biomimesis; moreover, we did not feel we had established even a crystallographic relationship between the hydroxy-ethyl-cellulose and the $CaCO_3$, although its concentration clearly affected the morphology.

An Emerging New Material Family: Aerogels

In contrast to some of the sections above in which no real "new material" is involved stands the recent work on aerogels. Although the discovery goes back to Kistler in 1931 [32], it was the recent demand for thermal insulation use and the use of CO_2-supercritical method (see Tewari [33]) that helped reopen this field.

Thus, the study of aerogels, in contrast to other subfields of SSG, is likely to become significant. [Fricke (Chapter 1) has a detailed review in these proceedings.]

From Future to Present

In summary, in the very near term we shall see a change in the accountability demanded of publicly funded science. The questions that will be (and, in my opinion, should have been) asked about sol–gel research should include:

- How does this science contribute to the national well-being? (This does not imply that all such science should directly do so, but it requires that we think, with data and analysis, about such issues.)
- What *evidence* is there that the author has read the literature?
- Can one convince a body of normally skeptical peers that there is a new idea behind the proposed research?
- If the work was totally successful, what would result besides some papers?

In the light of these observations, all SSG researchers should be open to new

ideas. They should then follow through on these ideas and perhaps a new step function increase in innovation will occur in SSG.

ACKNOWLEDGMENT

Our research in sol-gel work is supported by the Air Force Office of Scientific Research, Chemistry Division.

REFERENCES

1. R. Roy, Rational and Irrational Strategies for the Synthesis of New Materials, Presented at the American Ceramic Society, 1989 Fall Meeting (in press).
2. R. Roy, HTSC: Restoring Scientific and Policy Perspective, in: C. G. Burnham and R. D. Kane, Eds., *Proceedings of World Congress on Superconductivity*, pp. 27-41; World Scientific, Singapore (1988).
3. D. R. Ulrich, Chemical Processing of Ceramics, *Chem. Eng. News*, 28-40 (Jan. 1, 1990).
4. C. J. Brinker and G. W. Scherer, *Sol-Gel Science*, Academic Press (1990).
5. D. Shapley and R. Roy, *Lost at the Frontier*, ISI Press (1985).
6. New Hybrid Materials Made by Sol-Gel Technique, *Bull. Am. Ceram. Soc.*, 61, 374 (1982).
7. Ceramics from Solutions: Retrospect and Prospect, *Mater. Res. Soc. Annual Meeting Abs.*, 370 (1982).
8. New Metal-Ceramic Hybrid Xerogels, *Mater. Res. Soc., Annual Meeting Abs.* 377 (1982).
9. Thermal and Structural Properties of Xerogels near the Mullite Compositions, *Bull. Am. Ceram. Soc.*, 62, 375 (1983).
10. G. Vilmin, S. Komameni, and R. Roy, Crystallization of $ThSiO_4$ from Structurally and/or Compositionally Diphasic Gels. *J. Mater. Res.*, 2(4), 489-493 (1987).
11. Y. Suwa, S. Komarneni, and R. Roy, Solid-State Epitaxy Demonstrated by Thermal Reactions of Structurally Diphasic Xerogels: The System Al_2O_3, *J. Mater. Sci. Lett.*, 5, 21-24 (1986).
12. W. A. Yarbrough and R. Roy, Extraordinary Effects of Mortar-and-Pestle Grinding on Microstructure of Sintered Alumina Gel, *Nature*, 322(6077) 347-349 (24 July 1986).
13. M. Kumagai and G. I. Messing, *J. Am. Ceram. Soc.*, 67, C230 (1984).
14. R. A. Roy, K. F. Etzold, and J. J. Cuomo, Ferroelectric Film Synthesis: Past and Present, *Mater. Res. Soc. Symp. Proc.*, 200, 141-152 (1990).
15. H. Kido, P. B. Malla, and S. Komarneni, Designing Pore Size in Silica Gels: [H_2O-TMOS] System.
16. V. J. Varadan and V. V. Varadan, Microwave Joining and Repair of Composite Materials, *Polym. Eng. Sci.*, SPE-1990 Autec Issue (1991).
17. V. J. Varadan, personal communication.
18. M. Shimada, Preparation and Fluorescence Properties of Clay-Dye Composites, Proceedings, Seventh Seminar on Frontier Technology, Oiso, Japan Feb. 7-10, 1989.
19. H. K. Henisch, *Crystal Growth in Gels*, PSU Press, University Park, PA (1970).
20. J. W. McCauley and R. Roy, Controlled Nucleation and Crystal Growth of Various $CaCO_3$ Phases by the Silica Gel Technique, *Am. Mineral.*, 59, 947-963 (1974).
21. D. Hoffman, R. Roy, and S. Komarneni, Diphasic Ceramic Composites via a Sol-Gel Method, *Mater. Lett.*, 2(3), 245-247 (1984).

22. S. Mann, Flattery by Imitation, *Nature*, **349**, 285 (1991).

23. P. A. Bianconi, J. Lin, and A. R. Strzelecki, Crystallization of an Inorganic Phase Controlled by a Polymer Matrix, *Nature*, **349** 315 (1991).

24. J. W. Weber, R. Greer, B. Voight, E. W. White, and R. Roy, Unusual Strength Properties of Echinoderm Calcite Related to Structure, *J. Ultrastruct. Res.*, **26**, 355–366 (1969).

25. E. W. White, R. A. White, and J. N. Weber, Implant Casting Method, U.S. patent 3,890,107 (1975).

26. J. D. Currey, Biological Composites, in: *Fabrication of Composites*, Chapter 1, Elsevier, New York (1983); *J. Mater. Educ.*, **9**, 119 (1987).

27. J. D. Birchall, The Importance of the Study of Biomaterials to Materials Technology, in: R. J. P. Williams and S. Mann, Eds., *Biomineralization*, YCH, London (1989).

28. J. D. Birchall and H. L. Thomas, On the Architecture and Function of Cuttlefish Bone, *J. Mater. Sci.*, **18**, 2081 (1983).

29. R. E. Newnham, Composite Electroceramics, *J. Mater. Educ.*, **7**, 601 (1985).

30. D. Roy, Porous Biomaterials and Method of Making Same, U.S. patent 39,929,971 (1975).

31. L. Pach, Z. Hrabe, S. Komarneni, and R. Roy, Controlled Crystallization of Vaterite from Viscous Solution of Organic Colloids, *J. Mater. Res.*, **5**, 2928 (1990).

32. S. S. Kistler, Coherent Expanded Aerogels, *J. Phys. Chem.*, **36**, 52–64 (1932).

33. P. H. Tewari, A. J. Hunt, and K. D. Lofftus, Ambient-Temperature Supercritical Drying of Transparent Silica Aerogels, *Mater. Lett.*, **3**, 363–367 (1985).

Crystallization of Anorthite-Seeded Albite Glass by Solid-State Epitaxy

Chunling Liu,* Sridhar Komarneni,*,† and Rustum Roy*

Materials Research Laboratory, The Pennsylvania State University, University Park, Pennsylvania 16802

Stoichiometric albite glass ($NaAlSi_3O_8$) was seeded with 5 wt% crystalline anorthite ($CaAl_2Si_2O_8$) to make albite glass-ceramics. The epitaxial crystallization of the albite glass to the glass-ceramics was investigated by X-ray diffraction (XRD), scanning electron microscopy (SEM), and energy dispersive spectrometry (EDS). High albite was observed as the major crystallization product over the temperature range of 800–1200°C. No crystalline albite could be crystallized from *pure* albite glass without seeds. Small amounts of nepheline ($NaAlSiO_4$), however, crystallized along with albite after heat treatments at temperatures lower than 1000°C. The platelike microstructure of albite crystals was revealed in the seeded glasses. The albite blades grew epitaxially from the anorthite seeds, and the Ca content decreased in the direction away from the seeds. The degree of crystallization and the grain size were dependent upon the heat treatment conditions. By increasing the particle size of the seed, the crystallization process was retarded and the resultant microstructure was degraded. The seeding efficiency was also lowered by adding nonisostructural hexagonal anorthite seeds which produced less albite but more nepheline crystals. Crystallization of albite glass by seeding with 5 wt% anorthite is much greater than with the surface nucleation which takes place in a homogeneous 95 wt% albite + 5 wt% anorthite glass.

I. Introduction

Albite glass is extremely difficult to crystallize, and compositions which form albite are naturally avoided in making glass-ceramics.[1] Yet the high stability of albite glass may result from its structure. Because albite glass is a sodium aluminosilicate glass ($NaAlSi_3O_8$) with equal content of Al_2O_3 and Na_2O, the sodium only charge compensates aluminate tetrahedra and no nonbridging oxygen exists theoretically. Thus the activation energy for electrical conductivity reaches a minimum and the viscosity a maximum.[2] Taylor and Brown[3] found that the experimental radial distribution function of $NaAlSi_3O_8$ glass was inconsistent with the four-membered rings of tetrahedra associated with crystalline albite, but was, instead, consistent with interconnected six-membered rings. This structural difference between glass and crystalline phase helped explain the slow crystallization kinetics of albite glass. Schairer and Bowen[4] could not crystallize albite glass at temperatures 100°C below the melting point, but they obtained 1% albite crystals within a few hours after an "acclimating" treatment involving cooling, crushing, and reheating *for several months*. They believed that during the acclimation treatment, the glass structure is more closely related to the strucutre of crystalline albite. Uhlmann *et al.* published several studies[5–7] on the viscosity and crystallization of glasses containing albite and anorthite. They suggested that albite glass is a random network of SiO_4 and AlO_4 tetrahedra, that crystallization takes place by a surface nucleation mechanism, and that the growth rate is decreased by increasing albite content.

In the latter stage of formation of a glass-ceramic, epitaxial growth from nucleating agents occurs and is supported by the fact that the lattice spacing of growing crystals is similar to that of nucleants.[1] The first direct proof of epitaxial growth in glass-ceramics was obtained in a modified Li_2O–Al_2O_3–SiO_2 glass containing P_2O_5 nucleating agent.[8] Since 1982, this laboratory has developed a new concept of using solid-state epitaxy to make a variety of nanocomposite materials.[9] It has been shown that seeding can lower the crystallization temperature, modify the microstructure, and enhance densification in gels and glasses.[10–14] The most recent work[15] in our laboratory succeeded in further crystallizing albite glass epitaxially by adding 5 wt% of very fine albite crystals, while no crystalline albite was obtained in unseeded and ZrO_2-seeded glasses. This implies that by solid-state epitaxy, many highly stable glasses like albite can be reconsidered as starting materials for glass-ceramics. This study is a followup of the above investigation and focuses on the effects of crystalline anorthite on crystallization of albite glass. There are at least four reasons for choosing anorthite as a seed: (1) anorthite and albite have similar crystalline structures and they form complete solid solutions in the whole compositional region at high temperatures,[16] though subsequent exsolution can occur in the subsolidus region;[17] (2) amorphous anorthite crystallizes much faster than albite; (3) fine anorthite seed can be made more easily; and (4) by using a seed which has a composition different from the matrix, the seeding effect can be studied in more detail by EDS. Since crystallization in albite–anorthite glasses takes place via a surface nucleation mechanism,[6] a glass with 95 wt% albite and 5 wt% anorthite ($Ab_{95}An_5$) was also studied to distinguish this effect from epitaxial growth.

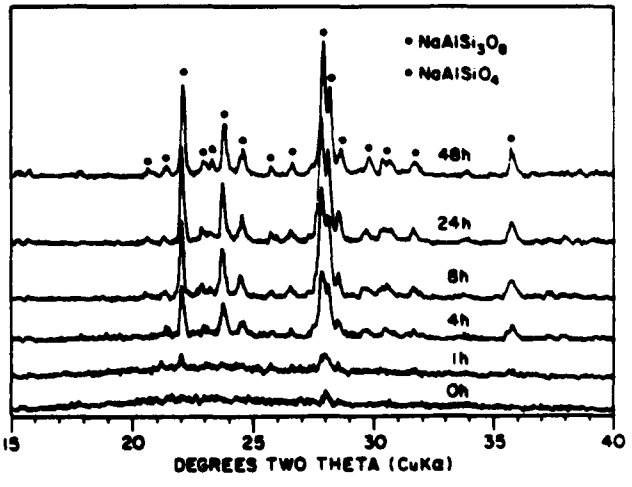

Fig. 1. Powder XRD patterns of albite glass seeded with fine, triclinic anorthite and crystallized at 950°C for various holding times.

G. H. Beall—contributing editor

Manuscript No. 196011. Received February 3, 1992; approved June 3, 1992.
Supported by the U.S. Air Force Office of Scientific Research under Grant No. AFOSR-89-0446.
*Member, American Ceramic Society.
†Also with the Department of Agronomy.

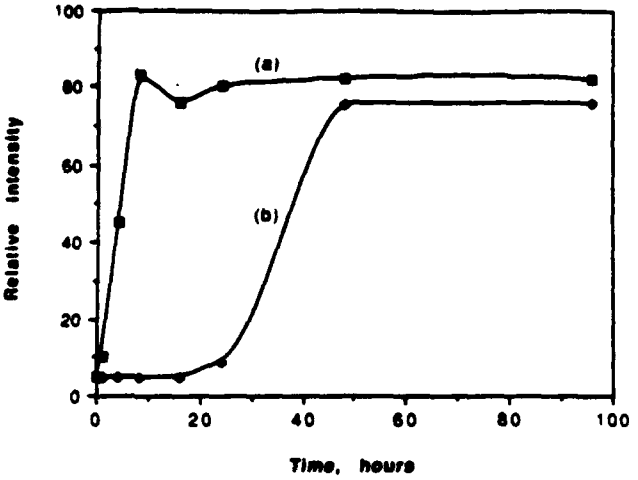

Fig. 2. Quantitative XRD analysis of albite glass seeded with fine, triclinic anorthite and heated for various times at different temperatures: (A) 950° and (B) 850°C.

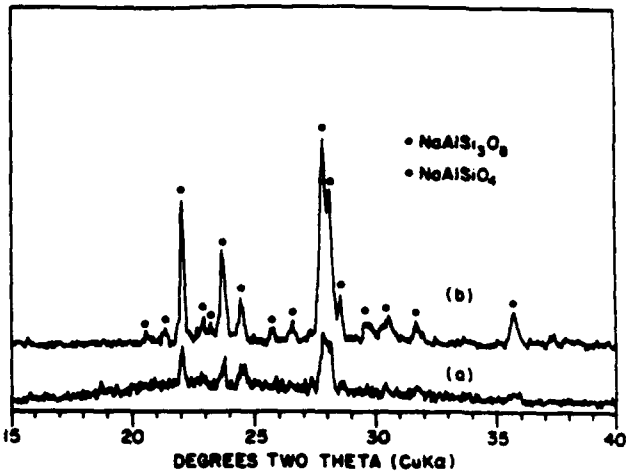

Fig. 4. XRD patterns of albite glass seeded with triclinic anorthite seeds of different sizes: (a) coarse and (b) fine, and heat-treated at 950°C for 8 h.

II. Experimental Procedure

The preparation of albite glass was described in our previous study.[15] $Ab_{95}An_5$ glass was prepared by mixing 95 wt% albite glass and 5 wt% anorthite glass with an agate mortar and pestle. The mixture was melted in a platinum crucible at 1550°C for 12 h followed by quenching into cold water, and the resultant glass was ground and sieved to obtain 325 mesh. Fine hexagonal anorthite seed (<2 μm) was made hydrothermally by heating a mixture of 1 g of anorthite glass and 8 mL of water in a 25-mL Parr bomb (Parr Instrument Co., Moline, IL) at 245°C for 1 day. The hexagonal phase was transformed to the stable triclinic phase without significant coarsening by heating at 850°C for 1 day. The triclinic powder was then dispersed in alcohol under ultrasonic vibration for several hours until an agglomerate-free suspension was obtained. Coarse triclinic anorthite seeds were obtained by a sol–gel route as follows: tetraethyl orthosilicate, aluminum nitrate nonahydrate, and calcium nitrate (molar ratio 2:2:1) were mixed completely and gelled slowly in an oven at 60°C, and then fired at 700°C to form a xerogel. The xerogel was then heated at 1350°C to achieve the highest crystallization rate[4] which led to large crystals. The crystals were powdered and sieved to <200 mesh but >325 mesh. The hexagonal anorthite and xerogel were also used directly to study the effect of phase transformation of seeds on the epitaxial growth.

The seeded powders were prepared by mixing the glass powders with 5 wt% seeds in alcohol for several hours using an agate mortar and pestle. The seeded and unseeded glass powders were dry-pressed at 5000 kg to form 0.5- and 0.75-in.-diameter disk samples. To determine the crystallization behavior, a portion of each sample was ground for X-ray diffraction analysis (XRD) and quantitative XRD measurement. For quantitative determination, α-Al_2O_3 was used as an internal standard. A 0.4-g sample was mixed with an equal amount of the internal standard and used to fill a 1-cm^2 cavity of a glass slide. A part of the sintered pellet was polished to 0.5 μm with diamond paste and then etched in 2 vol% hydrofluoric acid prior to SEM and EDS analyses. In most cases, the sample was carbon coated, but gold coating was also used for obtaining better SEM pictures.

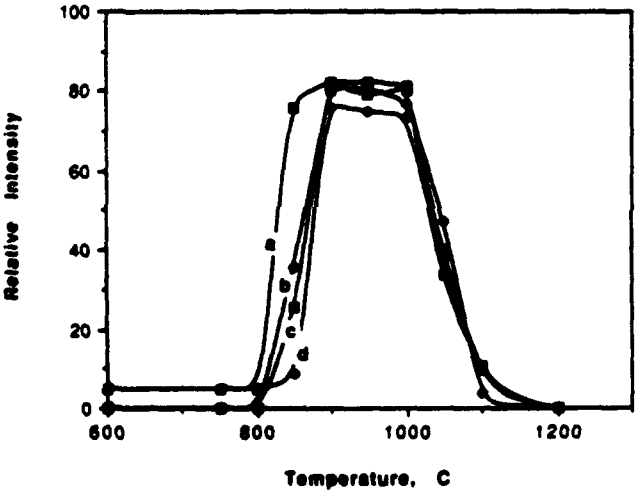

Fig. 3. Degree of crystallization in albite glass samples seeded with four different phases as a function of heating temperature: (a) fine, triclinic anorthite; (b) anorthite xerogel; (c) fine, hexagonal anorthite; and (d) coarse, triclinic anorthite.

III. Results and Discussion

(1) Crystallization Characteristics

The albite glass mixed with 5 wt% fine, triclinic anorthite seed and the unseeded albite glass were heated at 850° and 950°C for various periods to study the crystallization kinetics.

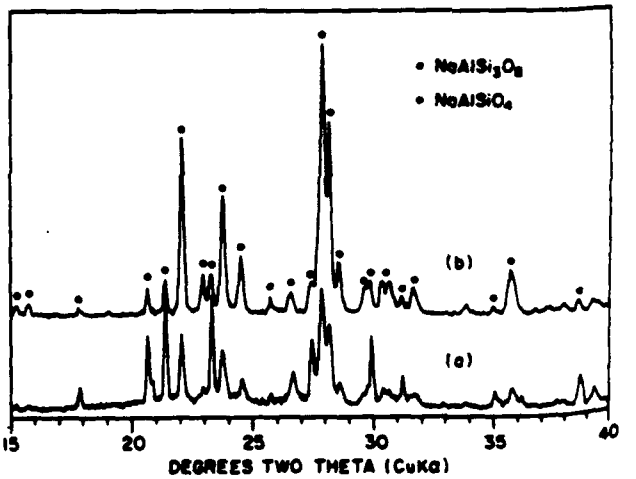

Fig. 5. Powder XRD patterns of albite glass seeded with (a) hexagonal anorthite and (b) fine, triclinic anorthite, and crystallized at 850°C for 4 days.

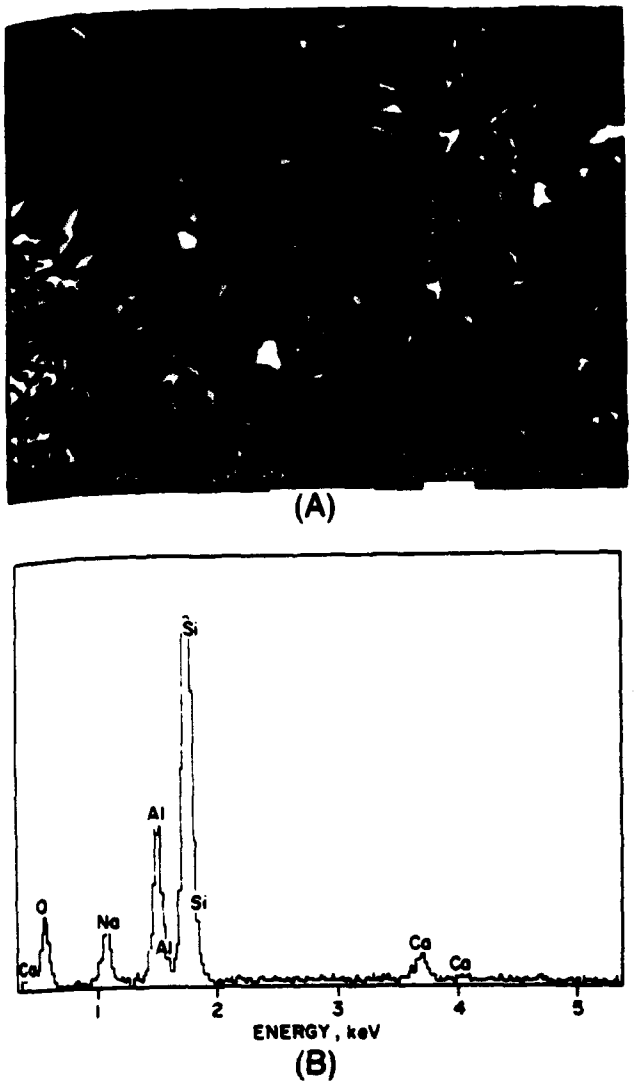

Fig. 6. A center crystalline region of albite glass seeded with hexagonal anorthite and partially crystallized at 850°C for 4 days: (A) SEM micrograph and (B) EDS plot.

Figure 1 shows the powder XRD patterns of the seeded samples after holding for different times at 950°C. The principal crystalline phase in these patterns is albite which may have incorporated some Ca from the seed forming an albite–anorthite solid solution. The composition of the solid solution, however, could not be determined by XRD. Small peaks of nepheline began to appear in the diffraction patterns after 1 to 2 days of heating. Figure 2 shows the results of quantitative XRD measurement of the amount of crystalline albite formed in these seeded samples. The relative intensity was obtained by comparing the integrated intensity of albite (002) and (040) peaks and that of the α-Al_2O_3 (012) peak. At 850°C, albite crystallization started after 1 day and reached a plateau after 2 days. At 950°C, the albite crystallization started after heating for 1 h and reached a plateau after 8 h. By a rough approximation, the activation energy Q_a was estimated by using the Arrhenius equation to be about 363 kJ/mol, and the preexponential constant, A_o, to be 1.14×10^{-12} s.

Based on the kinetic analysis above, a time period of 4 days was chosen to compare the effect of temperature on the crystallization of albite glass seeded with different phases. As shown in Fig. 3, no crystallization occurred below 800°C. The crystallization of albite increased to a maximum in the temperature region of 850–1000°C, and dropped to a minimum above 1100°C. The quantitative XRD measurements are consistent

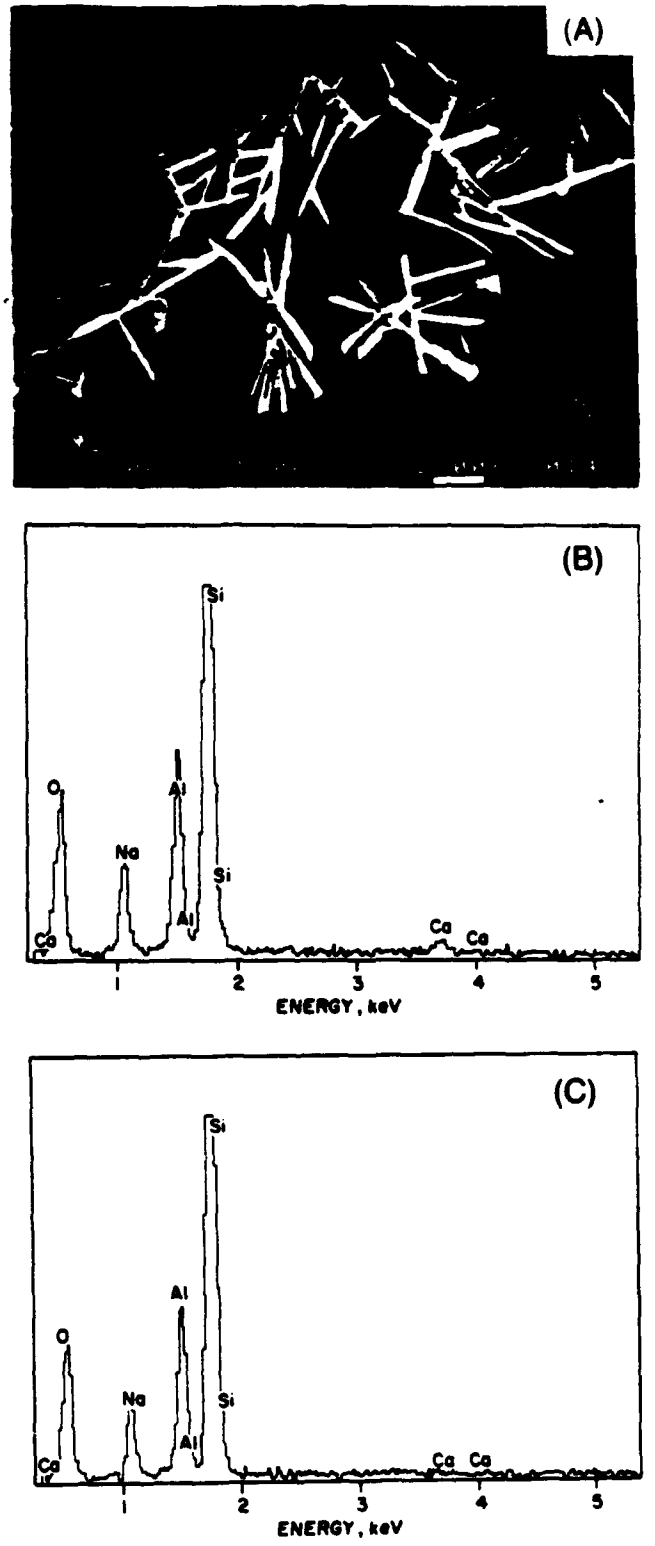

Fig. 7. A crystalline region at the edge of albite glass seeded with hexagonal anorthite and partially crystallized at 850°C for 4 days: (A) SEM micrograph, (B) EDS of upper crystalline region near the seed, and (C) EDS of lower region away from the seed.

with the SEM observations (see next section). There are variations in the amounts of albite crystallized around 850°C (Fig. 3) depending upon the type of seed. Fine, triclinic seeds are the most effective in crystallizing the albite glass. Coarse, triclinic anorthite seeds are less effective than their fine counterparts, as expected, because of the lower surface available in the former. The effect of seed size on the crystallization can be seen very

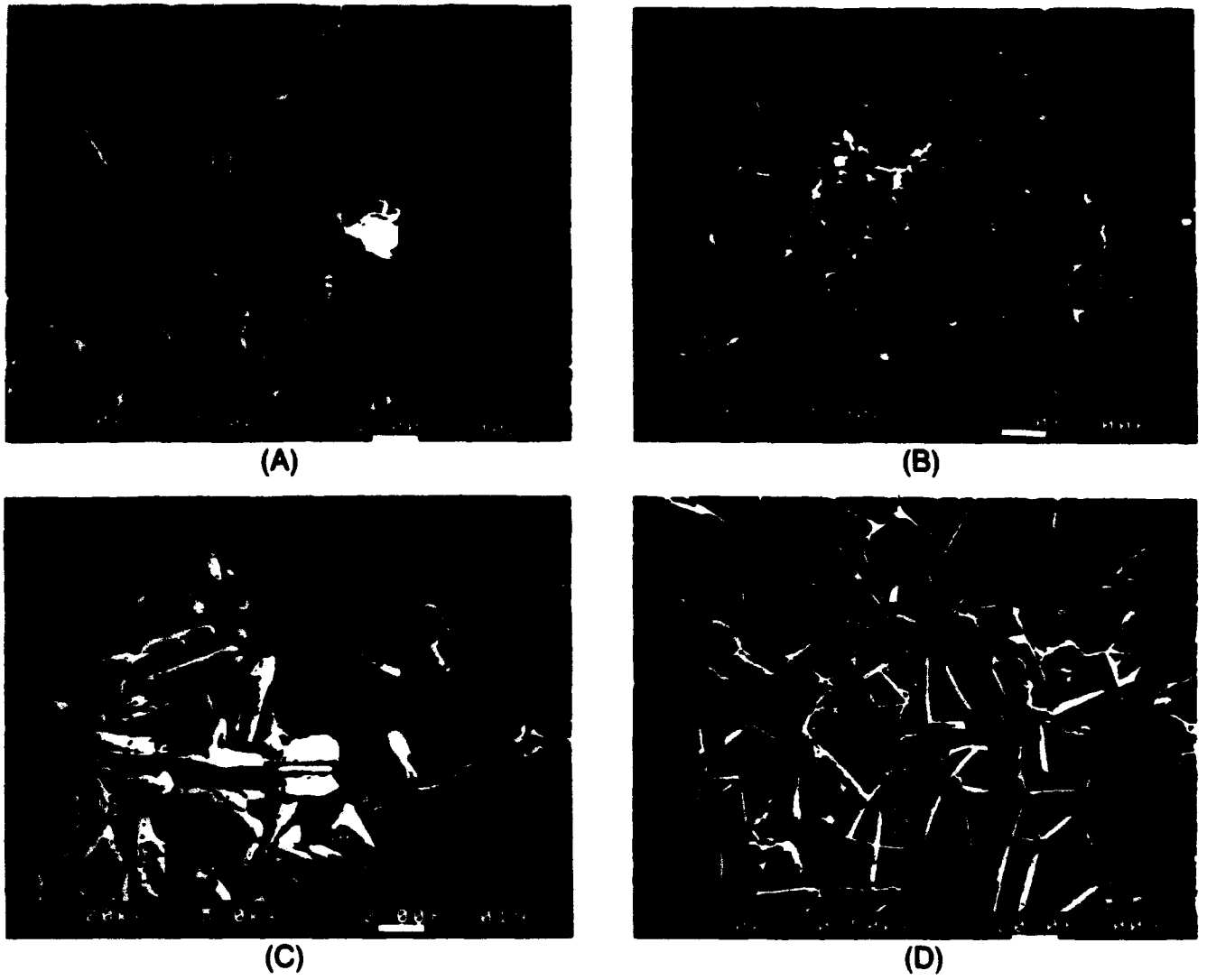

Fig. 8. SEM micrographs of albite glass seeded with fine, triclinic anorthite and reacted under different heat-treatment conditions: (A, B) 950°C, 48 h; (C) 900°C, 96 h; and (D) 1050°C, 96 h.

clearly in Fig. 4. The difference in crystallization could be measured only by using short treatment times in the temperature region of maximum crystallization (Fig. 3) when differently sized seeds were used. Although crystallization of albite glass occurred with all of the different types of seeds (Fig. 3), the use of hexagonal anorthite and xerogel of anorthite led to increased formation of nepheline compared to the other two seeds. Figure 5 shows the XRD patterns of albite glass seeded with fine triclinic or hexagonal anorthite and crystallized at 850°C for 4 days. Hexagonal anorthite led to increased crystallization of nepheline compared to the triclinic phase (Fig. 5). We reported earlier[15] the enhancement of nepheline crystallization in albite glass with ZrO_2 seeding. Thus, it appears, nepheline crystallization increases with nonisostructural seeding of albite glass.

(2) Microstructure Development

The microstructure of fine-anorthite-seeded albite glass is similar to that of crystalline-albite-seeded glass.[15] It can be described as elongated platelike crystals at the center of crystalline areas (Fig. 6) and needlelike small crystals near the interface between the crystalline phase and the glassy matrix (Fig. 7). The elongated shape of the crystal indicates high growth rate anisotropy, which results from the anisotropy of the surface energy. Mineralogists describe the morphology of feldspar crystal as habit.[17] The habits of feldspars depend mainly on crystallization temperature and to a lesser extent on chemical environments. An additional explanation by Uhlmann[18] is that the high growth anisotropy in albite and anorthite is due to the large entropies of fusion. He claimed that for materials with entropies of fusion $\Delta S_{fm} > 4R$, the most closely packed surfaces should be smooth, the less closely packed surfaces should be rough, and large anisotropy in the growth rate between such orientations should be observed.

Microstructural observation of partially crystallized albite glass seeded with hexagonal anorthite in Fig. 6(A) reveals 0.5-μm-thick and 3-μm-long platelike albite crystals in the center of a crystalline region. The region appears to be close to an anorthite seed, because high Ca content was detected by EDS (Fig. 6(B)). It is not clear whether the Ca diffused before, during, or after the crystallization, and whether the diffusion helped the crystallization due to the formation of the albite–anorthite solid solution. The epitaxial crystallization around the anorthite seeds is so fast and the first formed albite crystals are so small that no clear image of the early-stage solid-state epitaxy could be obtained. However, evidence for epitaxy has been demonstrated in anorthite-seeded albite gel[19] where the albite fibers grew directly from the anorthite but did not contain Ca. Figure 7(A) is an edge of the crystalline region where a small amount of Ca was detected in the upper left region (Fig. 7(B)), whereas no detectable Ca was found in the lower right region of the glassy phase (Fig. 7(C)). The upper left region apparently is close to the anorthite seed whereas the lower right region is away from the seed

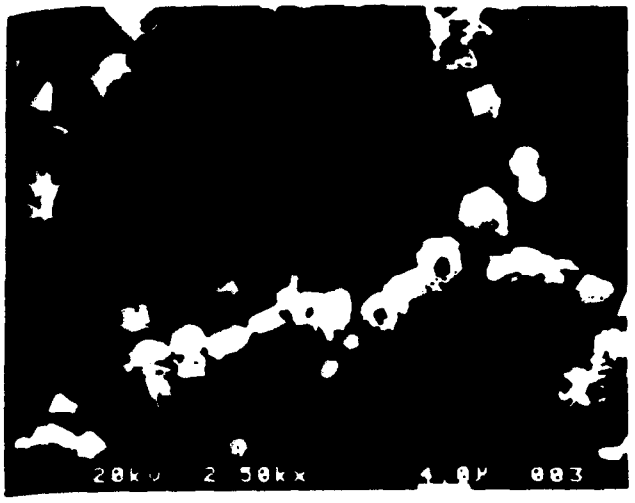

Fig. 9. SEM micrographs of nepheline crystals in albite glass sample seeded with hexagonal anorthite and treated at 850°C for 4 days.

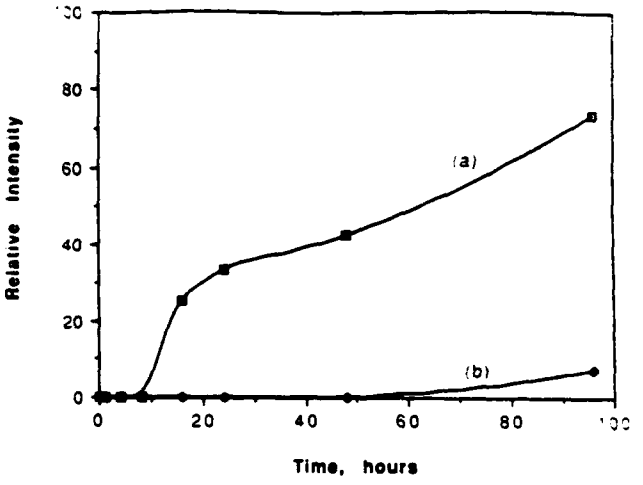

Fig. 11. Degree of devitrification in $Ab_{95}An_5$ glass vs holding time: (a) quantitative XRD analysis of sample heated at 950°C, and (b) quantitative XRD analysis of sample heated at 850°C.

In almost "fully" crystallized samples, it was difficult to find segregated regions with detectable Ca content. The crystals were distributed randomly and the original seed location could not be identified. Figure 8 shows SEM photographs of fine-triclinic-anorthite-seeded samples heated for different periods after heavy etching. The samples heated at 950°C for 8 to 48 h have microstructures similar to that in Fig. 8(A). Figure 8(B) shows the randomly oriented platelike crystals of the same area under a lower magnification. The particle size of the crystals remained stable up to 2 days of heating, and this is probably the best stage to form glass-ceramics. Significant grain growth occurred after heating for 4 days (Fig. 8(C)). The grain size and the inter-grain glassy phase increased after heating at higher temperatures (Fig. 8(D)).

Nepheline crystals were easily observed under SEM in the glassy region of hexagonal anorthite-seeded albite glass heated at 850°C for 4 days where about 10% of the phase was formed. As shown in Fig. 9, nepheline appeared in the glassy phase as hexagonal prisms which were not larger than 5 μm in all dimensions. A similar morphology was reported in earlier studies of Na_2O–Al_2O_3–SiO_2 glasses[4] and TiO_2-catalyzed nepheline glass-ceramics.[30] The EDS analysis did not show any Ca in nepheline, although up to 6 wt% of CaO could be added to a nepheline glass to form solid solution.[30] Note that in the region where nepheline formed, little or no albite crystals could be found. Thus nepheline cannot act as a nucleating agent for albite. It seems that nepheline crystals formed along a certain boundary which can be referred to as a grain boundary from the SEM pictures.

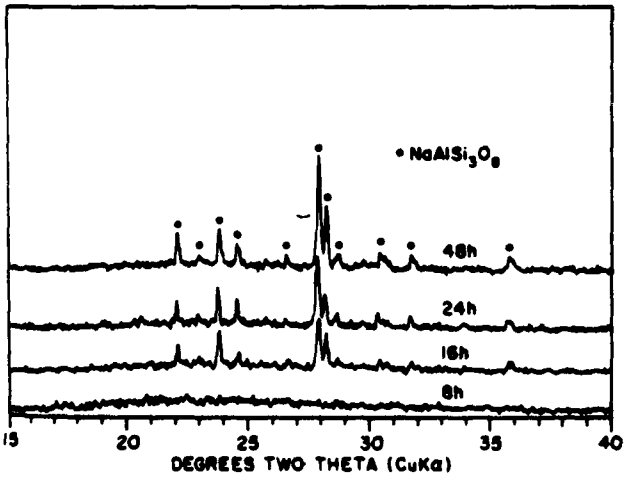

Fig. 10. Powder XRD patterns of $Ab_{95}An_5$ glass devitrified at 950°C for various holding times.

(3) Surface Devitrification in $Ab_{95}An_5$ Glass

Pellets of $Ab_{95}An_5$ were heat-treated together with anorthite-seeded and unseeded albite glasses. After heat treatment, the edges of the $Ab_{95}An_5$ samples were round and the surfaces were rough with many small holes which contained white crystals in the translucent glassy matrix. The anorthite-seeded samples were always opaque with sharp edges, and the unseeded albite glass samples were translucent with round edges. Figure 10 gives XRD patterns of $Ab_{95}An_5$ glass after heat treatment at 950°C. Compared with the patterns in Fig. 1, the two peaks around 2θ of 28° are sharper, and the peak at 2θ of 24° is always more intense than that at 2θ of 22°. This may be due to the bigger size and different composition of the crystals in $Ab_{95}An_5$. After polishing of the material at the surface, the peak intensities lowered significantly. Note in Fig. 10 there are no nepheline peaks. Figure 11 is the quantitative XRD of the powder from the whole sample. At 850°C, only a small number of crystals started to form at one surface of the sample after heating for 4 days. The crystals began to form after 16 h at 950°C. A rough approximation with the Arrhenius equation gives Q_s = 205 kJ/mol and $A_s = 1.05 \times 10^{-4}$. Compared with the A_e and Q_e values for epitaxial crystallization, the much higher A_s (1.0×10^8 times) and lower Q_s means much slower nucleation but a faster growth rate via surface nucleation. Figure 12 shows etched surfaces and vertical fracture cross sections of $Ab_{95}An_5$ glasses heated at 950°C for 1 and 4 days. Skeletal crystals formed after short-time heatings (Figs. 12(A) and (B)). Big dendritic crystal clusters and small crystal "flowers" were observed on the surface after prolonged heating (Fig. 12(C)), but only big clusters showed up in the cross section (Fig. 12(D)). The amounts of crystals in cross sections are not equal to those at the surfaces, and the crystals both in etched surfaces and in fracture cross sections are much less than those measured with quantitative XRD using the powders containing mostly the outerlayers of the sample. It was expected that the crystal morphology could be spherulitic or fibrillar at an undercooling greater than 100°C,[6] but no such crystals were found here with an undercooling of about 190°C.

IV. Summary

Albite glasses seeded with 5 wt% anorthite were crystallized with maximum crystallization in the temperature range of 850–1000°C. SEM studies indicated that after short-time holding at

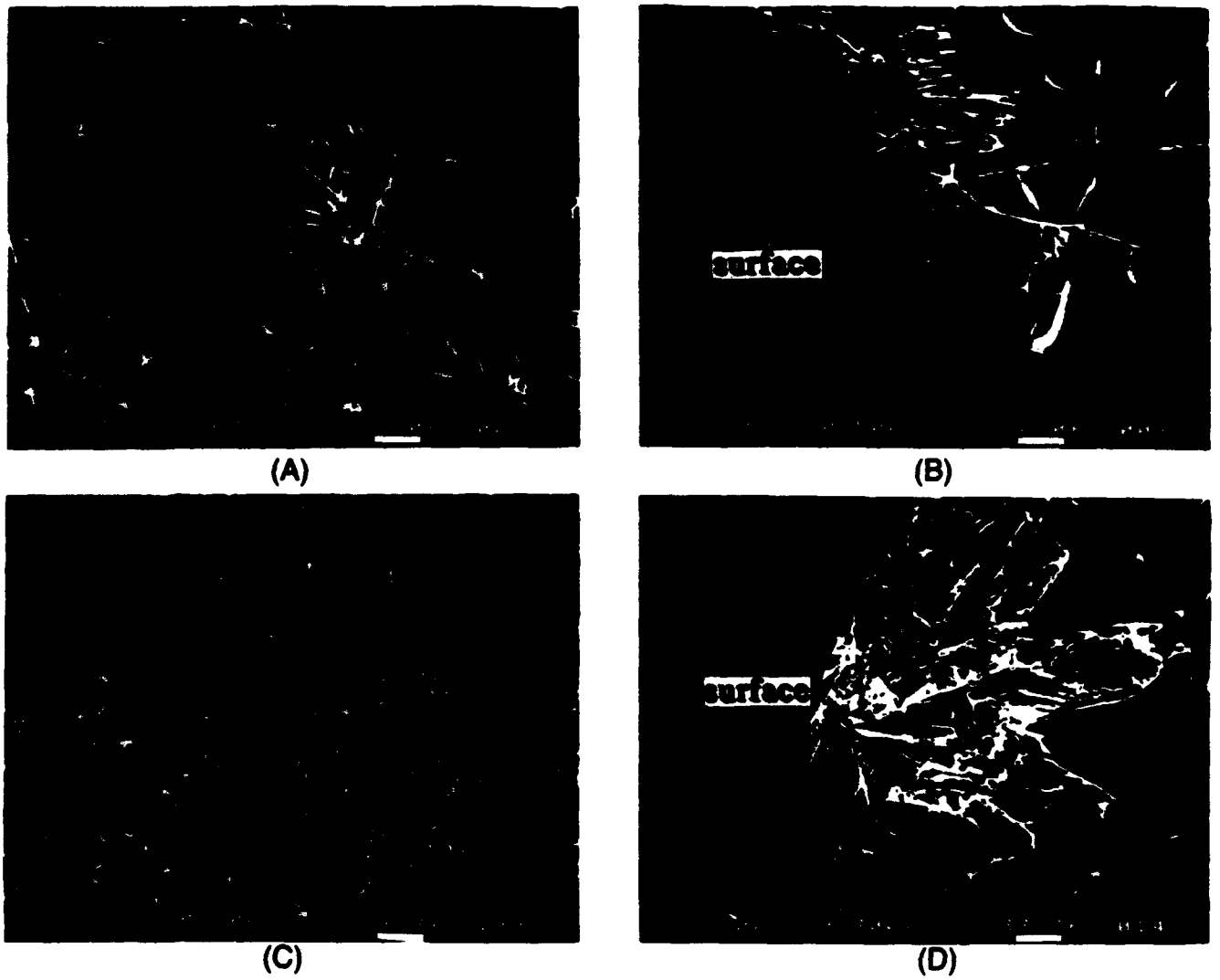

Fig. 12 SEM micrographs of $Ab_{95}An_5$ glass after various heat treatments: (A) a surface after 950°C, 24 h; (B) a cross section after 950°C, 24 h; (C) a surface after 950°C, 96 h; and (D) a cross section after 950°C, 96 h.

low temperatures, many small crystals nucleated from the seeds, suggesting an epitaxial growth mechanism, and ultimately grew to fine elongated needlelike and platelike crystals. Significant grain growth occurred in the sample heat-treated at 950°C for 4 days, and few but large crystals formed when the temperature was raised over 1000°C. The crystallization behavior of albite glass was affected by the nature and the size of anorthite seeds. The maximum crystallization was reached within 8 h at 950°C when fine seeds were used. Unlike the apparent epitaxial crystallization in 5-wt%-anorthite-seeded albite glass, the devitrification in $Ab_{95}An_5$ glass was via a surface nucleation mechanism, and the morphology and distribution of the crystals implied that this surface devitrification is useless for making glass-ceramics.

References

[1]P. W. McMillan, *Glass-Ceramics*. Academic Press, New York, 1979.

[2]D. M. Zirl and S. H. Garofalini, "Structure of Sodium Aluminosilicate Glasses," *J. Am. Ceram. Soc.*, **73**, 2848–56 (1990).

[3]M. Taylor and G. E. Brown, Jr., "Structure of Mineral Glasses—I. The Feldspar Glasses $NaAlSi_3O_8$, $KAlSi_3O_8$, $CaAl_2Si_2O_8$," *Geochim. Cosmochim. Acta*, **43**, 61–75 (1979).

[4]J. F. Schairer and N. L. Bowen, "The System Na_2O–Al_2O_3–SiO_2," *Am. J. Sci.*, **254**, 129–95 (1956).

[5]D. Cranmer and D. R. Uhlmann, "Viscosity of Liquid Albite, a Network Material," *J. Non-Cryst. Solids*, **45**, 283–88 (1981).

[6]R. J. Kirkpatrick, L. Klein, O. R. Uhlmann, and J. F. Hays, "Rates and Processes of Crystal Growth in the System Anorthite–Albite," *J. Geophys. Res.*, **84**, 3671–76 (1979).

[7]D. Cranmer and D. R. Uhlmann, "Viscosities in the System Anorthite–Albite," *J. Geophys. Res.*, **86**, 7951–56 (1981).

[8]T. J. Headley and R. E. Loehman, "Crystallization of a Glass-Ceramic by Epitaxial Growth," *J. Am. Ceram. Soc.*, **67**, 620–25 (1984).

[9]R. Roy, Y. Suwa, and S. Komarneni, "Nucleation and Epitaxial Growth in Diphasic (Crystalline + Amorphous) Gels"; pp. 247–58 in *Science of Ceramic Chemical Processing*. Edited by L. L. Hench and D. R. Ulrich. Wiley, New York, 1986.

[10]Y. Suwa, S. Komarneni, and R. Roy, "Solid State Epitaxy Demonstrated by Thermal Reactions of Structurally Diphasic Xerogels: The System Al_2O_3," *J. Mater. Sci. Lett.*, **5**, 21–24 (1986).

[11]Y. Suwa, R. Roy, and S. Komarneni, "Lowering Temperature by Seeding in Structurally Diphasic Al_2O_3–MgO Xerogels," *J. Am. Ceram. Soc.*, **68**, C-238–C-240 (1985).

[12]S. Komarneni, Y. Suwa, and R. Roy, "Enhancing Densification of 93% Al_2O_3–7% MgO Triphasic Xerogels with Crystalline α-Al_2O_3 and $MgAl_2O_4$ Seeds," *J. Mater. Sci. Lett.*, **6**, 525–27 (1987).

[13]G. Vilmin, S. Komarneni, and R. Roy, "Crystallization of $ThSiO_4$ from Structurally and/or Compositionally Diphasic Gels," *J. Mater. Sci.*, **2**, 489–93 (1987).

[14]G. Vilmin, S. Komarneni, and R. Roy, "Lowering Crystallization Temperature of Zircon by Nanoheterogeneous Sol-Gel Processing," *J. Mater. Sci.*, **22**, 3556–60 (1987).

[15]U. Selvaraj, C. L. Liu, S. Komarneni, and R. Roy, "Epitaxial Crystallization of Seeded Albite Glass," *J. Am. Ceram. Soc.*, **74**, 1378–81 (1991).

[16]E. M. Levin, C. R. Robbins, and H. F. McMurdie, *Phase Diagrams for Ceramists*. American Ceramic Society, Columbus, OH, 1964.

[17]J. V. Smith and W. L. Brown, *Feldspar Minerals*, 2nd ed.; Vol. 1. Springer-Verlag, Berlin, FRG, 1988.

[18]D. R. Uhlmann, "Crystal Growth in Glass Forming Systems: A Ten-Year Perspective"; pp. 80–124 in *Nucleation and Crystallization of Glasses*. American Ceramic Society, Columbus, OH, 1982.

[19]C. L. Liu, S. Komarneni, and R. Roy, "Crystallization of Anorthite Seeded Albite Xerogels by Solid State Epitaxy", unpublished results.

[20]D. R. Duke, J. F. MacDowell, and B. R. Karstetter, "Crystallization and Chemical Strengthening of Nepheline Glass-Ceramics," *J. Am. Ceram. Soc.*, **50**, 67–73 (1967).

Manuscript #1

HIGH TEMPERATURE STABILITY OF OXYCARBIDE GLASSES

HANXI ZHANG AND CARLO G. PANTANO
Department of Materials Science and Engineering, The Pennsylvania State University, University Park, Pa 16802

ABSTRACT

The stability of silicon oxycarbide glasses has been studied at temperatures up to 1500°C. The silicon oxycarbide glasses were synthesized using a sol/gel process. The pyrolysis treatment in argon influenced the structure and composition of the synthesized glasses, and in turn, their high temperature stability in oxidizing atmosphere. The oxycarbide glasses pyrolyzed at ≥ 1000°C had lower hydrogen concentration and a more polymerized network structure, and thereby were more resistant to oxidation and crystallization at higher temperatures.

I. INTRODUCTION

The thermochemical and thermomechanical stability of glasses has always been a critical issue in their high temperature applications. Ordinarily, oxide glasses crystallize and soften at elevated temperatures. There has been great interest in enhancing the stability of the glasses by incorporating carbon into glass structures[1-2]. The sol/gel process has made it practical to synthesize these glasses[3-5]. Carbon offers the possibility of 4 coordinate bonds to replace the oxygen anion which is only 2 coordinate, and this is expected to strengthen the molecular structure of the glasses. Chi[2], Zhang and Pantano[4], and Runland[5] have independently reported that there was limited crystallization of SiO_2 from the oxycarbide glasses. But these oxycarbide glasses were processed and evaluated in very different ways. Thus, the goal of this study was to systematically examine the relationships between processing and high temperature stability. The gels were synthesized using an established procedure and they were pyrolyzed to the glassy state in argon over the temperature range 800°C to 1400°C. Solid state Magic Angle Spinning ^{29}Si Nuclear Magnetic Resonance (MAS ^{29}Si NMR), ^{13}C NMR and chemical analysis were used to characterize these glasses. The decomposition and oxidation resistance was examined by thermogravimetric analysis (TGA). The role of glass structure and composition in the thermochemical stability will be discussed.

II. EXPERIMENTAL PROCEDURES

The oxycarbide glasses were synthesized by a sol/gel process[4]. Methyltrimethoxysilane was the starting material. 1 mole of $MeSi(OMe)_3$ was mixed with 4 moles of H_2O in a beaker, and the pH value of the solution was adjusted to 1 or 2 by adding 1M HCl solution. After 2 hours of stirring, the pH value of the solution was raised to 6.5 by addition of 2M NH_4OH. The solution gelled within about 24 hours. The gels were further dried in petri-dishes for 48 hours during which time the gels shrank by syneresis. The solid gels were dried at 65°C to 105°C for about a week. The dry gels were pyrolyzed to the glassy state in flowing argon at 800°C, 1000°C, 1200°C and 1400°C for 60 minutes. The oxycarbide glasses obtained were pulverized into 100 mesh powder for solid state ^{29}Si NMR+, TGA++ and chemical analysis+++. In the TGA analysis, the oxycarbide glasses were heated at 10°C/min up to 1500°C and held for 60 minutes. The powders studied in the TGA were subsequently examined by x-ray diffraction.

III. RESULTS AND DISCUSSION

The carbon and hydrogen contents of the oxycarbide glasses are shown in Figure 1. There is a big difference in composition between the glass heat treated at 800°C relative to those heat treated at ≥1000°C. The carbon content increases from 12.5% at 800°C to 14% at 1000°C and remains almost constant at higher temperatures. The hydrogen content

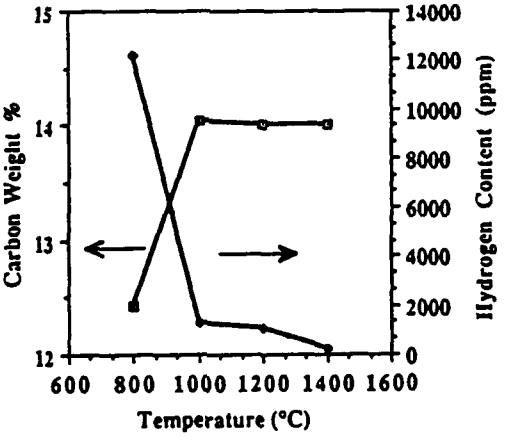

Figure 1. The variation of the carbon and hydrogen contents of the oxycarbide glasses with pyrolysis temperature.

+ Chemagnetic CMX-300A operating at 59.08MHZ

++Netzsch Simultanous Analyzer 429

+++Leco Chemical Analysis

decreases most drastically between 800°C and 1000°C and continues to decrease up to 1400°C.

Figure 2 is the Cross Polarization ^{13}C NMR of the glass pyrolyzed at 800°C. CP NMR depends upon the fast relaxation of H (to shorten the spectra acquisition time) and hence is only sensitive to those carbons that are bonded with or in the close proximity of, hydrogen. The glasses heat treated at higher than 1000°C exhibited weak spectra and this verified their low concentration of hydrogen. The strong signals in Figure 2 indicate that there is a large amount of elemental carbon and $\equiv SiCH_3$ in the structure of the oxycarbide glass pyrolyzed at 800°C.

The ^{29}Si NMR spectra of the oxycarbide glasses pyrolyzed at progressively higher temperatures are shown in Figure 3. The ^{29}Si NMR spectrum for the gel is also shown for comparison. The assignment of the peaks was made using standard compounds[6]. There are two species in the gel, $[O_3SiCH_3]$ and $[HOO_2SiCH_3]$[4]. The hydroxyl group left in the gel is the result of incomplete polymerization of the gel structure. The spectra for all the glasses show the presence of $[SiO_4]$, $[O_3SiC]$ and $[O_2SiC_2]$ species, but the amount of the oxycarbide species is quite different. With the increase of pyrolysis temperature, the relative concentration of $[O_3SiC]$ decreases. Above 1200°C, $[SiC_4]$ (~ -15 ppm) appears in the ^{29}Si NMR spectra. At 1400°C, most of the $[O_3SiC]$ species in the glass decompose and $[SiC_4]$ species increase in concentration.

It should be noted that the $[O_3SiC]$ peak shifts from -65ppm in the spectrum of the glass pyrolyzed at 800°C to ~ -75ppm in these higher temperature glasses. The broad $[O_3SiC]$ peak at -65 ppm in the spectrum of the 800°C glass probably represents a distribution of $[O_3SiCH_3]$ and $[OHO_2SiCH_3]$; these species are clearly resolved in the spectrum of the gel at -68 and -58 ppm, respectively. At ≥ 1000°C, the downfield shift of this broad peak denotes a relative loss of the terminal OH species (-58 ppm). This is consistent with the ^{29}Si NMR spectra of silicate minerals where polymerization of the silicate structure leads to a down field shift of the peaks[7]. Here the $[O_3SiC]$ peak shift from -65 ppm to -75 ppm corresponds to the removal of network terminating OH and CH_3 groups through polymerization of the network structure.

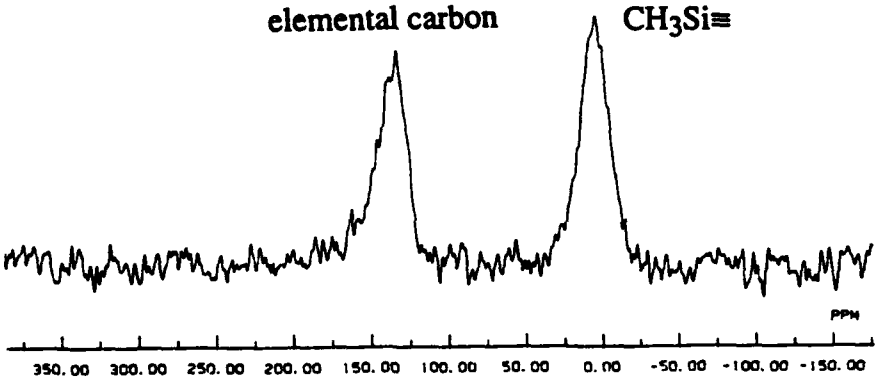

Figure 2. CP ^{13}C MAS NMR of the oxycarbide glass pyrolyzed at 800°C.

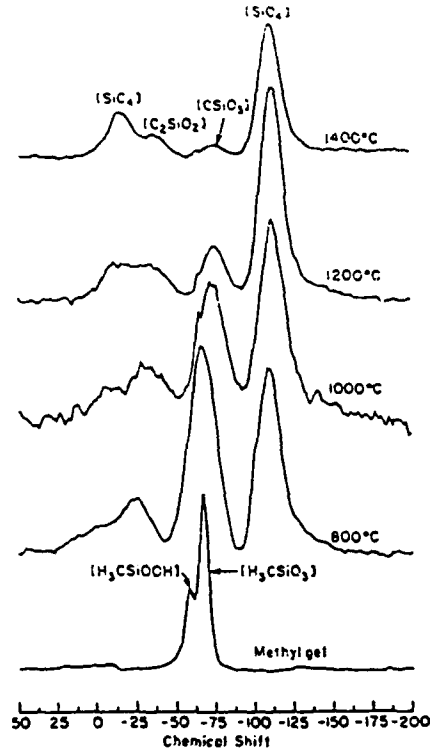

Figure 3. ^{29}Si MAS NMR spectra of the gel and the oxycarbide glasses pyrolyzed at various temperatures

Reactions which result in the polymerization of the glass structure can be shown as:

$$H_3CSiOH + HOSiCH_3 \rightarrow H_3CSi\text{-}O\text{-}SiCH_3 + H_2O \qquad 1)$$

$$\equiv SiCH_3 + H_3CSi\equiv \rightarrow \equiv Si\text{-}CH_2\text{-}Si\equiv + 2H_2 + C \text{ (free carbon)} \qquad 2)$$

The evolution of H_2O and H_2 accounts for the chemical analysis in Figure 1 where a relative increase in total carbon, and decrease in hydrogen, is revealed.

TGA of the glasses in oxygen up to 1500°C is shown in Figure 4. The weight change values are listed in Table I. The TGA results in Ar are included for reference.

Table I. Weight Change Behavior of the Oxycarbide Glasses up to 1500°C

Atmosphere	O_2	Ar
Pyrolysis Temperature(°C)		
800	-8%	-13%
1000	+2%	-11%
1200	+2%	-7%
1400	+2%	-6%

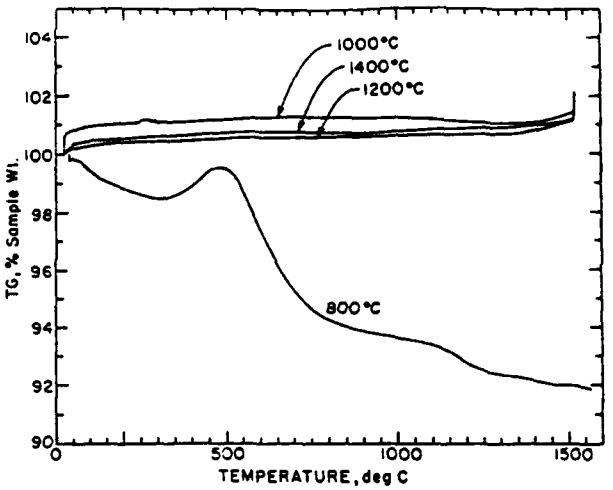

Figure 4. TGA of the oxycarbide glasses in Oxygen up to 1500°C

The behavior of the oxycarbide glass pyrolyzed at 800°C is very different from the other glasses. The glass loses weight up to 400°C and then gains weight between 400°C and 600°C. Above 600°C, the sample loses weight again. The residual material left after the TGA runs is almost white, and shows a strong peak of crystalline SiO_2 in the x-ray diffraction pattern. Conversely, the glasses heat treated in argon loses weight continuously in this temperature range.

Weight loss in O_2 has two possible sources:

1. Oxidation of the methyl group in the silicate network:

$$2 \equiv Si\text{-}CH_3 + 3O_2 \rightarrow 2 \equiv Si\text{-}O_{1/2} + 2CO\uparrow + 3H_2O\uparrow \qquad 3)$$

Weight loss is the result of the mass difference of CH_3 and $O_{1/2}$.

2. Oxidation of free (aromatic) carbon:

$$2C + O_2 \rightarrow 2CO\uparrow \qquad 4)$$

Since free carbon undoubtedly exists in the oxycarbide glasses, its oxidation contributes a weight loss.

Weight gain can be explained by replacement of network carbon by oxygen. One possible reaction is :

$$2 \equiv Si\text{-}CH_2\text{-}Si\equiv + 2O_2 \rightarrow 2\equiv Si\text{-}O\text{-}Si\equiv + 2CO\uparrow \qquad 5)$$

The sample gains weight from the mass difference of CH_2 and O.

Because of the terminal CH_3 and OH groups in the network of the glass pyrolyzed at 800°C, it has much less resistance to oxidation and crystallization. The terminal sites enhance the mobility of the network. The CH_3 is more readily oxidized than the network carbon that forms at high

pyrolysis temperature. The OH groups, which can condense to water at high temperatures, lower the viscosity and provide internal oxidants.

IV. CONCLUSION

It has been shown that there is a relationship between pyrolysis, structure/composition, and stability of oxycarbide glasses synthesized through the sol/gel process. Although the oxycarbide glass pyrolyzed at 800°C has abundant Si-C bonds in the glass structure, the network is terminated by $Si\text{-}CH_3$ and SiOH groups. These terminating groups increase the mobility and reactivity of the glass at high temperatures. Pyrolysis at ≥ 1000°C in argon is found to create a polymerized oxycarbide glass structure that is more stable upon further oxidation and decomposition at even higher temperatures.

ACKNOWLEDGEMENT:

The authors gratefully thank the Air Force Office of Scientific Research under grant No. AFOSR-89-0446 for their support of this research.

REFERENCES

1. T.H. Elmer and H.E. Meissner "Increase of Annealing point of 96% SiO_2 Glass on Incorporation of Carbon" J. *Amer.* Ceram. *Soc.*, 59(5-6), 206-09 (1976).
2. F.K. Chi, "Carbon-Containing Monolithic Glasses via Sol/gel Process" Ceram. Eng. Sci Proceedings, 4, 704-17 (1983).
3. Dennis N. Coon, "Effect of Silicon Carbide Additions on the Crystallization Behavior of a Magnesia-Lithia-Alumina-Silica Glass", J. *Amer. Ceram. Soc.*, 72(7), 1270-73 (1989).
4. Hanxi Zhang and C.G. Pantano "Synthesis and Characterization of Silicon Oxycarbide Glasses", J. *Amer. Ceram. Soc.*, 73(4), 958-963 (1990).
5. G. M. Runland, S.Prochazka and R. Doremus, "Silicon Oxycarbide Glasses: Part I. Preparation and Chemistry" *J. Materials Research.*, 6, (12) 2716-2722 (1991).
6. H. Marsman, NMR. Basic Principles and Progress, P. Diehl, E.fluck and R. Kosfeld, eds., New York, Springer-verlag, 65-235, (1981).
7. E. Lippman, M.Magi, A. Samoson, G. Engelhardt and A. R. Grimmer, "Structural Studies of Silicates by Solid-State High-Resolution ^{29}Si NMR", *J. Amer. Chem. Soc.* 102 (15), 4889-4893 (1980).

SOL-GEL FABRICATION OF $Pb(Zr_{0.52}Ti_{0.48})O_3$ THIN FILMS USING LEAD ACETYLACETONATE AS THE LEAD SOURCE

Ulagaraj Selvaraj,[+] Keith Brooks,[+] A.V. Prasadarao,[*] Sridhar Komarneni,[+#] R. Roy[+] and L.E. Cross[+]

FOR JOURNAL OF AMERICAN CERAMIC SOCIETY

KEY WORDS
PZT, Thin Film, Sol-Gel, Ferroelectric and Microstructure

Materials Research Laboratory,
The Pennsylvania State University,
University Park, PA 16802.

---

*Present Address: Andhra University, Visakhapatnam, India

#Also with the Department of Agronomy

+Member, American Ceramic Society.

SOL-GEL FABRICATION OF $Pb(Zr_{0.52}Ti_{0.48})O_3$ THIN FILMS USING LEAD ACETYLACETONATE AS THE LEAD SOURCE

Abstract

Lead zirconium titanate (PZT) thin films of the morphotropic phase boundary composition [$Pb(Zr_{0.52}Ti_{0.48})O_3$] were deposited on platinum coated silicon by a modified sol-gel process using lead acetylacetonate as the lead source. The precursor solution for spin-coating was prepared from lead acetylacetonate, zirconium n-butoxide and titanium isopropoxide. The use of lead acetylacetonate instead of the widely used lead acetate trihydrate provided more stability to the PZT precursor solution. Films annealed at 700°C for 12 min. formed well-crystallized perovskite phase of $Pb(Zr_{0.52}Ti_{0.48})O_3$. Microstructures of these films indicated the presence of submicron grains (0.1 to 0.2 μm). The dielectric constant and loss values of these films were approximately 1200 and 0.04, respectively, while the remanent polarization and coercive field were ~ 13 $\mu C/cm^2$ and ~ 35 kV/cm. Aging of the solution had almost no effects on the dielectric and ferroelectric properties of these films.

SOL-G.. FABRICATION OF $Pb(Zr_{0.52}Ti_{0.48})O_3$ THIN FILMS USING LEAD ACETYLACETONATE AS THE LEAD SOURCE

INTRODUCTION

The lead zirconate - lead titanate system [$Pb(Zr_{1-x}Ti_x)O_3$, x = 0 to 1 or PZT] forms perovskite type solid solutions over the entire compositional range[1]. PZT ceramic materials in various forms such as sintered bodies,[1-3] thin films,[4,5] fibers[6,7] and composites[8] have been extensively studied because of their excellent piezoelectric properties. Compositions close to the morphotropic phase boundary (x ≈ 0.52 to 55), exhibit high dielectric constants, and electromechanical coupling coefficients. PZT thin films have been prepared by various methods including rf-sputtering,[9] laser ablation,[10] metallo-organic decomposition[11] and sol-gel process.[4,5] The potential applications of these films include non-volatile memories, capacitors, pyroelectric sensors, surface acoustic wave substrates, micromechanical devices, switches, spatial light modulators, optical memories and displays, and frequency doublers for diode lasers.[12-15] Sol-gel processing of PZT thin films has gained much interest because of its (i) simplicity, (ii) low processing temperature, (iii) chemical homogeneity and stoichiometry control and (iv) the ability to produce uniform film over a large area.

PZT films have been prepared by sol-gel methods by using a variety of metal - organic precursors.[4,5,16-19] The widely used precursors for the preparation of PZT thin films include lead acetate trihydrate, titanium isopropoxide and zirconium isopropoxide or zirconium isobutoxide. Gurkovich and Blum[20] used lead acetate trihydrate and titanium isopropoxide dissolved in 2-methoxyethanol for the first time to synthesize monolithic lead titanate. This precursor method has been adopted by Budd, Day and Payne[16] to fabricate

lead titanate, lead zirconium titanate and lead lanthanum zirconium titanate films. We have followed this procedure to fabricate continuous lead titanate, PZT and modified PZT fibers.[6,7] It has been reported that the ferroelectric properties of PZT films degrade with aging of the precursor solution.[12] In addition, to obtain good properties complete dehydration of the lead acetate trihydrate is required. Multiple distillations of lead acetate dissolved in 2-methoxyethanol lead to the formation of $Pb(OOCCH_3)(OCH_2CH_2OCH_3).xH_2O$ ($x < 0.5$).[21] Other lead sources are also available to prepare PZT precursor solution. Chen et al.[17] and Hsueh and Mecartney[18] used lead 2-ethylhexanoate as the lead source for preparing PZT liquid precursors and thin films. Tohge, Takahashi and Minami[19] prepared $Pb(Zr_xTi_{1-x})O_3$ [x = 0 to 0.6] thin films from metal alkoxides such as lead ethoxide, zirconium n-butoxide and titanium n-butoxide stabilized with ethanol solution containing monoethanolamine and acetylacetone. Fukoshima et al.[22] deposited $Pb(Zr_{0.5}Ti_{0.5})O_3$ films from a complex precursor of lead 2-ethylhexanoate, zirconium acetylacetonate, titanium tetrabutoxide and butanol.

Modified metal chelate complexes with β-diketones, β-ketoesters, alkanolamines and diols are known to be more stable towards hydrolysis than the alkoxides of some metals such as Al, Ti and Zr.[23-26] These more stable chelated complexes have therefore been recognized as convenient starting materials for the preparation of homogeneous coating of Al_2O_3, TiO_2 and ZrO_2. We have used for the first time lead acetylacetonate complex as the source of lead in preparing a stable $Pb(Zr_{0.52}Ti_{0.48})O_3$ precursor solution. In this paper, the preparation of $Pb(Zr_{0.52}Ti_{0.48})O_3$ thin films using the new precursor solution, film microstructure, and dielectric and ferroelectric properties are discussed. Characterization of the sol-gel derived PZT powder by differential thermal analysis (DTA), thermogravimetric analysis (TGA) and X-ray diffraction (XRD) is also reported.

EXPERIMENTAL

The modified scheme for the preparation of $Pb(Zr_{0.52}Ti_{0.48})O_3$ precursor solution is outlined in Fig. 1. Lead acetylacetonate $[Pb(C_5H_7O_2)_2]$,[+] zirconium n-butoxide $[Zr(OBu)_4]$ 80% solution in 1-butanol[*] and titanium isopropoxide $[Ti(OPr^i)_4]$[*] were used as the starting materials. Lead acetylacetonate was dissolved in 2-methoxyethanol by refluxing the solution at 125°C for 12 h. To this solution, a stoichiometric amount of $Zr(OBu)_4$ was added and refluxed at 125°C for 6 h. $Ti(OPr^i)_4$ was then added to the Pb-Zr solution and again refluxed at 125°C for 6 h to form a 0.4 M PZT (acetylacetonate) precursor solution. Finally, 4 vol% formamide[*] was added to the solution in order to improve the drying behavior of the sol-gel.

PZT films were deposited onto platinum coated silicon substrates using a spin coater[♣] operated at 3000 rotations per minute for 20 s. Before coating, the precursor solution was passed through 0.2 μm nylon filters.[*] Rapid pyrolysis of PZT gel films was achieved by placing on a hot plate at 350°C for 5 min. Multilayer depositions (7 and 10 coatings) were performed to increase film thickness. These films were subsequently converted to crystalline $Pb(Zr_{0.52}Ti_{0.48})O_3$ by annealing between 600 and 700°C in air.

Crystallization behavior of the films was studied using a grazing angle X-ray diffractometer.[#] Film microstructure and thickness were evaluated using a scanning

---

[+]Alfa products, Ward Hill, MA.

[*]Aldrich Chemical Company, Milwaukee, WI

[♣]P-6000, Integrated Technologies, Achushnet, MA.

[#]Model DMICRO8, Scintag, Santa Clara, CA

electron microscope (SEM).[¥] Capacitance as a function of slowly varying bias voltage was measured with 10 mV signal at 10 kHz using an impedance analyzer.[♠] The dc bias voltage was stepped through 0.2 V increments from 0 to 10 V to -10 V and back to zero. Sputtered gold (~ 1000 Å) deposited through a shadow mask was used as the top contact electrode. The P-E hysteresis curves of these films were measured using a Sawyer - Tower circuit at 60 Hz. In addition, gel powder obtained from the coating solution was characterized using a differential thermal analyzer,[‡] a thermogravimetric analyzer[♣] and an X-ray diffractometer.[ł]

RESULTS AND DISCUSSION

SOLUTION STABILITY

The gelation time was taken as a measure of solution stability. At room temperature, when 9 moles of water was added to each mole of the PZT (acetylacetonate) solution, gelation occured in 4800 min. Under identical hydrolysis conditions, PZT (acetate) solution prepared using lead acetate trihydrate as the lead source gelled within 10 min. The procedure for preparing the PZT(acetate) solution is discussed in detail by Selvaraj et al.[6] Increased gelation time for the PZT (acetylacetonate) solution reflects its stability against hydrolysis and polycondensation reactions. Based on NMR results, Ramamurthi and Payne[21] interpreted the multiple distillation product of lead acetate trihydrate dissolved in 2-methoxyethanol as $Pb(OOCCH_3)(OCH_2CH_2OCH_3).xH_2O$ ($x < 0.5$). The increased chemical stability of PZT (acetylacetonate) solution as compared

[¥]ISI-DS 130, Akashi Beam Technology Corporation, Tokyo, Japan.
[♠]Model 4192A, Hewlett Packard, Cupertino, CA
[‡]Model DTA , 1700, Perkin-Elmer, Norwalk, CT.
[♣]Delta Series TGA7 , Perkin-Elmer.
[ł]Model DMC, 105, Scintag.

to PZT (acetate) solution can be attributed to the greater steric effects of the bidentate acetylacetonate ligands relative to acetate or 2-methoxyethoxide.[22-23]

GEL POWDER

XRD patterns of the gel powder heat treated at 500° and 600°C for 1 h are shown Fig. 2. A mixture of pyrochlore and perovskite phases were formed at 500°C, while complete perovskite phase resulted at 600°C. Fig. 3 shows the DTA and TGA curves for the gel powder pre-heated at 300°C for 2 days to remove the organics and residual carbon. From the TGA curve it can be seen that the gel exhibited approximately 4% weight loss in the temperature range of 50 to 700 °C due to the presence of adsorbed water and residual carbon. Removal of organics and the major amount of residual carbon from the gel powder by heat treating at 300°C provided unambiguous assignment of the DTA peaks at 480° and 585°C to pyrochlore phase formation and its transformation into perovskite, respectively.

THIN FILMS

Fig. 4 shows the grazing angle X-ray diffraction patterns of $Pb(Zr_{0.52}Ti_{0.48})O_3$ thin films on platinum coated silicon and heat treated at 500° and 700°C in air. These films formed pyrochlore phase at 500°C and complete perovskite phase at 700°C. Fig. 5 shows the SEM micrographs of 7 and 10 layer thick films of $Pb(Zr_{0.52}Ti_{0.48})O_3$ heat treated at 700°C for 12 min. The thicknesses of the 7 and 10 layer films as measured from SEM cross sections were 0.40 and 0.65 μm, respectively. These films exhibited fine grained microstructures with grain size ranging from 0.1 to 0.2 μm. Island-like regions 1 to 2 μm across were also observed. Compositional analysis by Energy Dispersive Spectroscopy (EDS) showed no variation between the island regions and the surrounding film.

Figs. 6a and 6b show the dielectric constant versus bias field for 0.40 and 0.65 μm thick films. The arrows are indicative of the sequence of data collection, for slowly varying bias field. The two peaks in Figs. 6a and 6b originate from the ferroelectric polarization reversal and domain switching.[5] The field separation between these two peaks correspond to coercive field values of 30 kV/cm and 27 kV/cm for films of 0.40 and 0.65 μm thickness, respectively. The dielectric constant (ε_r) of these films measured at zero bias was about 1200 whereas the dielectric loss value (tanδ) was about 0.04. Figs. 7a and 7b show the hysteresis loops of 0.40 and 0.65 μm thick films. The measured saturation and remanant polarizations (P_s and P_r) for the 0.40 μm thick film were 31 and 13 μC/cm^2, respectively. For the 0.65 μm thick film the saturation and remanant polarizations were 29 and 13 μC/cm^2. The coercive fields, E_c, calculated from the hysteresis loops were 36 and 33 kV/cm, respectively, for the 0.40 and 0.65 μm thick films. These values are slightly higher than those obtained from the C-V analysis described above.

To determine the aging effects of the PZT (acetylacetonate) solution on the dielectric and ferroelectric properties, thin films were formed using solution aged for 1 and 150 days. The dielectric and ferroelectric properties of these films (~ 0.4 μm thickness) deposited onto platinum coated silicon and annealed at 700°C for 12 min. are summarized in Table 1. Aging of the solution virtually had no effect on the dielectric and ferroelectric properties of these films. It can be attributed to the greater stability of PZT(acetylacetonate) solution relative to PZT(acetate) solution.[12]

CONCLUSIONS

A modified sol-gel process was developed to form $Pb(Zr_{0.52}Ti_{0.48})O_3$ thin films on platinum coated silicon. Lead acetylacetonate was used for the first time as the lead precursor instead of the widely used lead acetate trihydrate. A more stable PZT precursor solution resulted from the use of lead acetylacetonate. Thin film XRD results indicated that

the amorphous films formed well-crystallized PZT perovskite phase when annealed at 700°C for 12 min. The measured dielectric constant and loss values of these films were about 1200 and 0.04. Ferroelectric hysteresis with P_r of ~ 13 $\mu C/cm^2$ and E_c of ~ 35 kV/cm was demonstrated for $Pb(Zr_{0.52}Ti_{0.48})O_3$ films. Aging of the solution virtually had no effect on the dielectric and ferroelectric properties of these films. It has been shown from the present study that a stable PZT precursor solution can be prepared by using lead acetylacetonate as the lead source and this precursor can be used for the preparation of a variety of multicomponent thin films with lead as one of the constituents.

Acknowledgement

This research was supported by the United States Air Force Office of Scientific Research under grant No. AFOSR-89-0446.

REFERENCES

1. B. Jaffe, W.R. Cook, Jr. and H. Jaffe, "Piezoelectric Ceramics," pp. 135-83 Academic Press, New York, 1971.

2. L.E. Cross, "Future Prospects in Electroceramic Materials and Applications," Am. Ceram. Soc. Bull., 67[3] 578 (1988).

3. G. Haertling, "Piezoelectric and Elecro-optic Ceramics," pp. 139-226 in *Ceramic Materials for Electronics* Edited by R.C. Buchanan. Marcel Dekker, New York, 1986.

4. S.L. Swartz, S.J. Bright, J.R. Busch and T.R. Shrout, "Sol-gel Processing of Ferroelectric Thin Films," Ceramic Transactions, 14, 159-78 (1990).

5. L.E. Sanchez, S-Yau and I.K. Naik, "Observation of Ferroelectric Polarization Reversal in Sol-Gel Processed Very Thin Lead-Zirconate-Titanate Films," Appl. Phys. Lett., 56 [24] 2399-401 (1990).

6. U. Selvaraj, A.V. Prasadarao, S. Komarneni, K.G. Brooks and S.K. Kurtz, "Sol-Gel Processing of $PbTiO_3$ and $Pb(Zr_{0.52}Ti_{0.48})O_3$ Fibers," J. Mater. Res., 7[4] 992-96 1992.

7. U. Selvaraj, K.G. Brooks, S. Komarneni, S.K. Kurtz, D. Edie and P. Liu , " Fabrication of PZT and Modified PZT Fibers for Vibrational Damping," Pennsylvania State University Invention Disclosure No. 92-1121, University Park, 1992.

8. R.E. Newnham, "Composite Electroceramics," Ferroelectrics, 68, 1-32 (1986).

9. S.B. Krupanidhi and M. Sayer, "Radio Frequency Magnetron Sputtering of Multicomponent Ferroelectric Oxides," J. Vac. Sci. Technol. A 2[2], 303-306 (1989).

10. D. Roy, S.B. Krupanidhi and J. Dougherty, "Excimer Laser Ablated Lead Zirconate Titanate Thin Films," J. Appl. Phys., 69[11] 7930-32 (1992).

11. R. Vest, "Metallo-organic Decomposition (MOD) Processing of Ferroelectric and Electro-optic Films: A Review," Ferroelectrics, 102, 53-68 (1990).

12. L.M. Sheppard, "Advanced Processing of Ferroelectric Thin Films," Ceram. Bull. 71[1] 81-95 (1992).

13. B.P. Maderic, L.E. Sanchez and S.Y. Wu, "Ferroelectric Switching, Memory Retention and Endurance Properties of Very Thin PZT Thin Films, Ferroelectrics, 116, 65-77 (1991).

14. K. G. Brooks, K.R. Udayakumar, J. Chen, U. Selvaraj and L.E. Cross, "Smart Ferroelectric Films and Fibers; Applications in Micromechanics," Mater. Res. Soc. Symp. Proc. (1992).

15. G. H. Haertling, "Ferroelectric Thin Films for Electronic Applications," J. Vac. Sci. Technol. A 9[3] 414-420 (1991).

16. K.D. Budd, S.K. Dey and D.A. Payne, "Sol-Gel Processing of $PbTiO_3$, $PbZrO_3$, PZT and PLZT Thin Films," Brit. Ceram. Proc., 36, 107-121 (1985).

17. K.C. Chen, A. Janah and J.D. Mackenzie, pp.731- in *Better Ceramics Through Chemistry II.* Edited by C.J. Brinker, D.E. Clark and D.R. Ulrich, Pittsburgh, PA 1986.

18. C. Hsueh and M.L. Mecartney, "Microstructural Development and Electrical Properties of Sol-Gel Prepared Lead Zirconate-Titanate Thin Films," J. Mater. Res. 6[10] 2208-17 (1991).

19. N. Tohge, S. Takahashi and T. Minami, "Preparation of $PbZrO_3$-$PbTiO_3$ Ferroelectric Thin Films by the Sol-Gel Process," J. Am. Ceram. Soc., 74[1] 67-71 (1991).

20. S.R. Gurkovich and J.B. Blum, "Preparation of Monolithic Lead Titanate by a Sol-Gel Process," in *Ultrastructure Processing of Glasses, Ceramics, and Composites.* Edited by L.L. Hench and D.R. Ulrich. John Wiley and Sons, New York, 1984.

21. S.D. Ramamurthy and D.A. Payne, "Structural Investigations of Prehydrolyzed Precursors Used in the Sol-Gel Processing of Lead Titanate," 73[8] 2547-51 (1990).

22. J. Fukushima, K. Kodaira, T. Marsushita, "Preparation of Ferroelectric PZT Films by Thermal Decoposition of Organic Compounds," J. Mater. Sci., 19, 595-98 (1984).

23. W.C. LaCourse and S. Kim, "Use of Mixed Titanium Alkoxides for Sol-Gel Processing," pp. 304-10 in *Science of Ceramic Processing.* Edited by L.L. Hench and D.R. Ulrich. Wiley, New York, 1986.

24. H. Uchihashi, N. Tohge, and T. Minami, "Preparation of Amorphous Al_2O_3 Thin Films from Stabilized Al-Alkoxides by the Sol-Gel Method," J. Ceram. Soc. Jpn., 97, 396-99 (1989).

25. U. Selvaraj, S. Komarneni and R. Roy, Synthesis of Glass-Like Cordierite from Metal Alkoxides and Characterization by ^{27}Al and ^{29}Si MASNMR," J. Am. Ceram. Soc., 73[12] 3663-69 (1990).

26. U. Selvaraj, A.V. Prasadarao, S. Komarneni and R. Roy, "Sol-Gel $SrTiO_3$ Thin Films from Chemically Modified Alkoxide Precursors," Mater. Lett., 12, 306-10 (1991).

FIGURE CAPTIONS

Fig. 1 Scheme for the preparation of $Pb(Zr_{0.52}Ti_{0.48})O_3$ precursor solution using lead acetylacetonate as the lead source in a modified sol-gel process.

Fig. 2 DTA and TGA curves for the $Pb(Zr_{0.52}Ti_{0.48})O_3$ gel preheated to 300°C for 1 day.

Fig. 3 XRD patterns for the $Pb(Zr_{0.52}Ti_{0.48})O_3$ gel heat treated at 500° and 600°C for 1 h.

Fig. 4 Thin film XRD patterns of the $Pb(Zr_{0.52}Ti_{0.48})O_3$ gel films heat treated at 500° and 700°C.

Fig. 5 SEM micrographs of (a) 0.40 μm thick and (b) 0.65 μm thick $Pb(Zr_{0.52}Ti_{0.48})O_3$ films annealed at 700°C for 12 min.

Fig. 6 Dielectric constant versus bias field for: (a) 0.4 μm thick and (b) 0.65 μm thick $Pb(Zr_{0.52}Ti_{0.48})O_3$ films.

Fig. 7 Ferroelectric hysteresis loops for: (a) 0.4 μm thick and (b) 0.65 μm thick $Pb(Zr_{0.52}Ti_{0.48})O_3$ films.

Table 1

Dielectric and ferroelectric properties of 0.4 μm thick $Pb(Zr_{0.52}Ti_{0.48})O_3$ films with the precursor solution aging

Aging (days)	ε_r	$\tan\delta$	P_r ($\mu C/cm^2$)	P_s ($\mu C/cm^2$)	E_c (kV/cm)
1	1200	0.04	13.0	31	36
150	1210	0.04	13.1	30	34

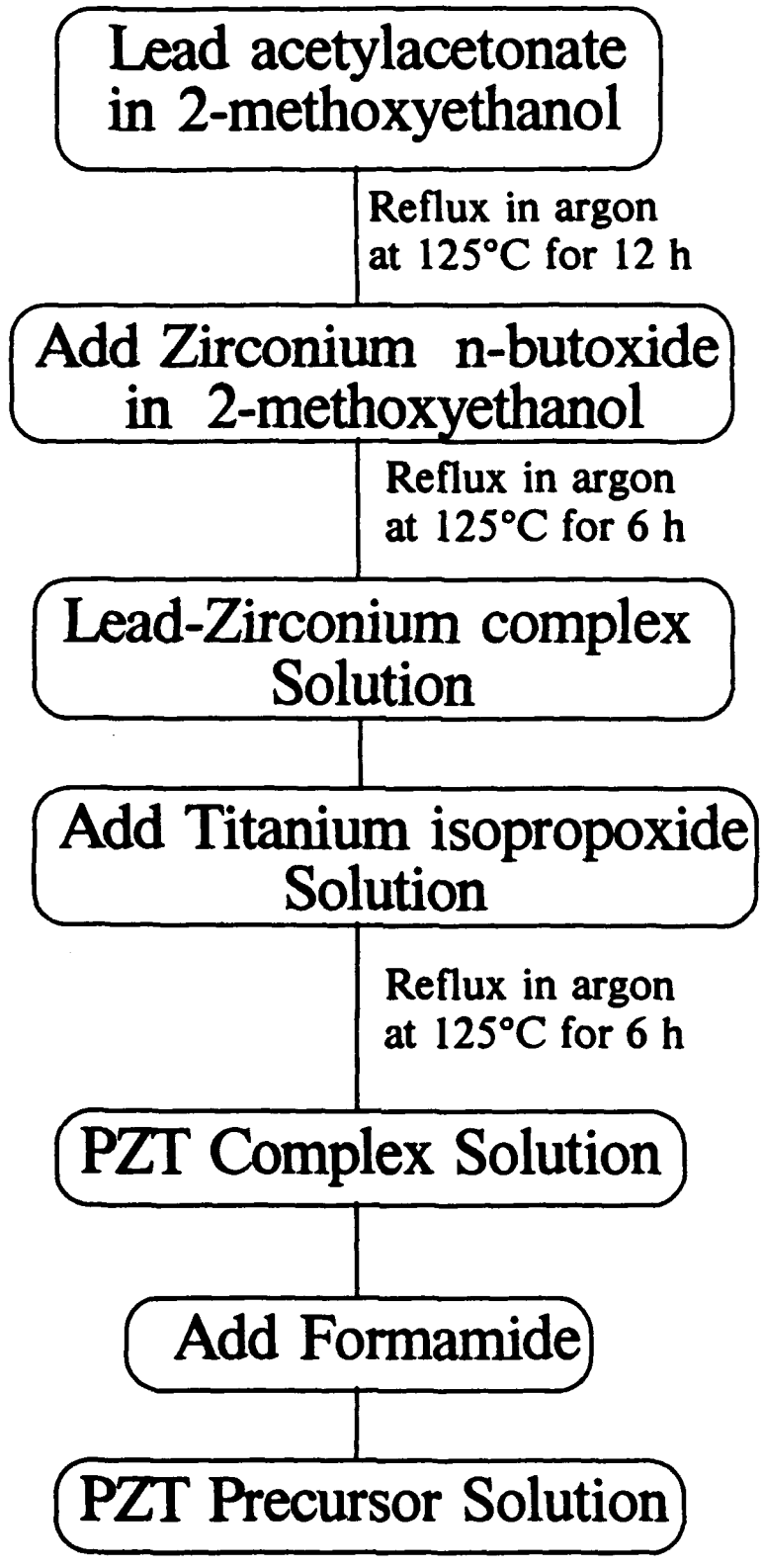

Fig. 1 Scheme for the preparation of PZT precursor solution using lead acetylacetonate as the lead source in a modified sol-gel process.

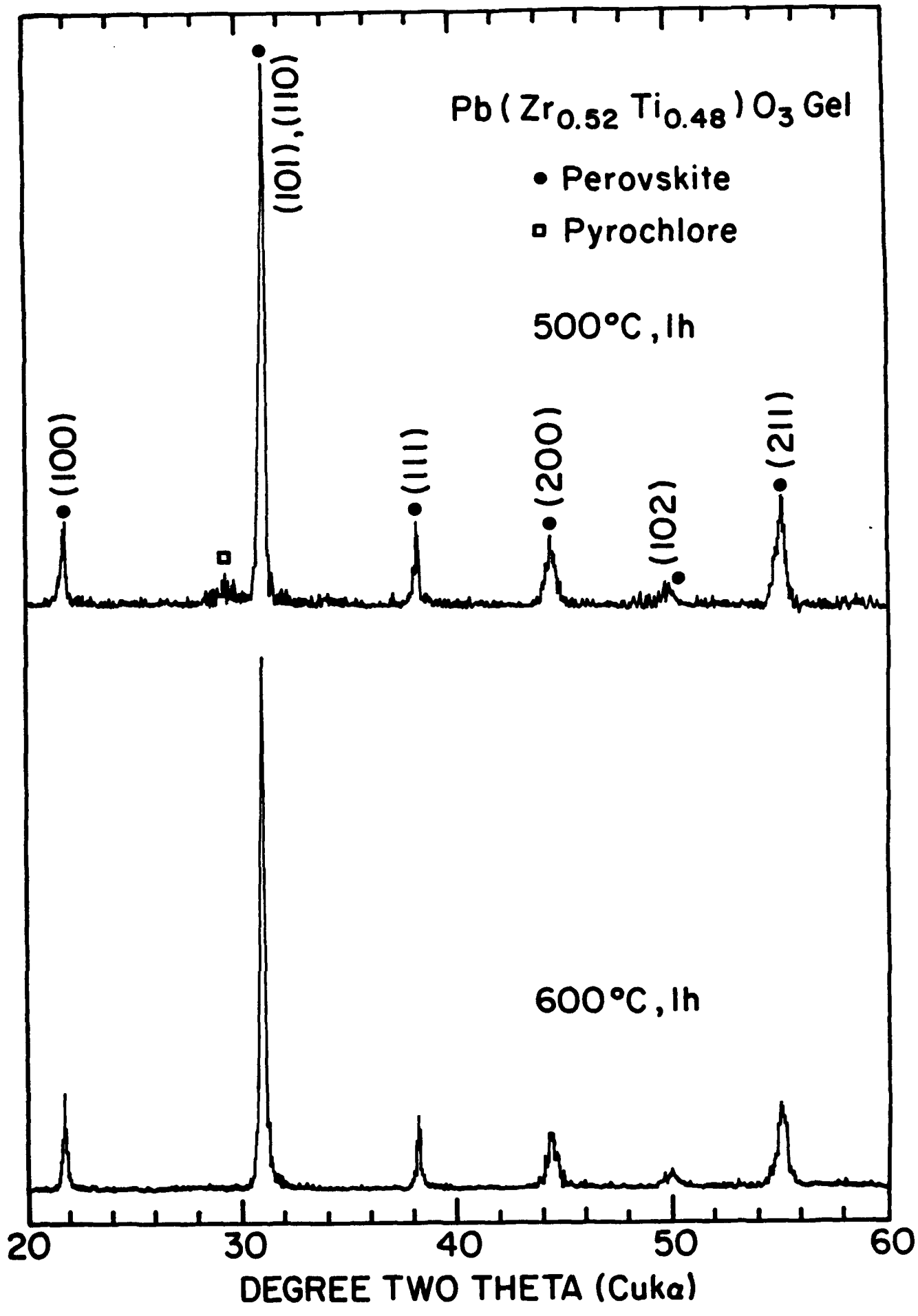
Pb (Zr0.52 Ti0.48) O3 Gel
• Perovskite
▫ Pyrochlore
500°C , 1h
600°C , 1h
(100)
(101),(110)
(111)
(200)
(102)
(211)
20
30
40
50
60
DEGREE TWO THETA (Cukα)

Fig. 2

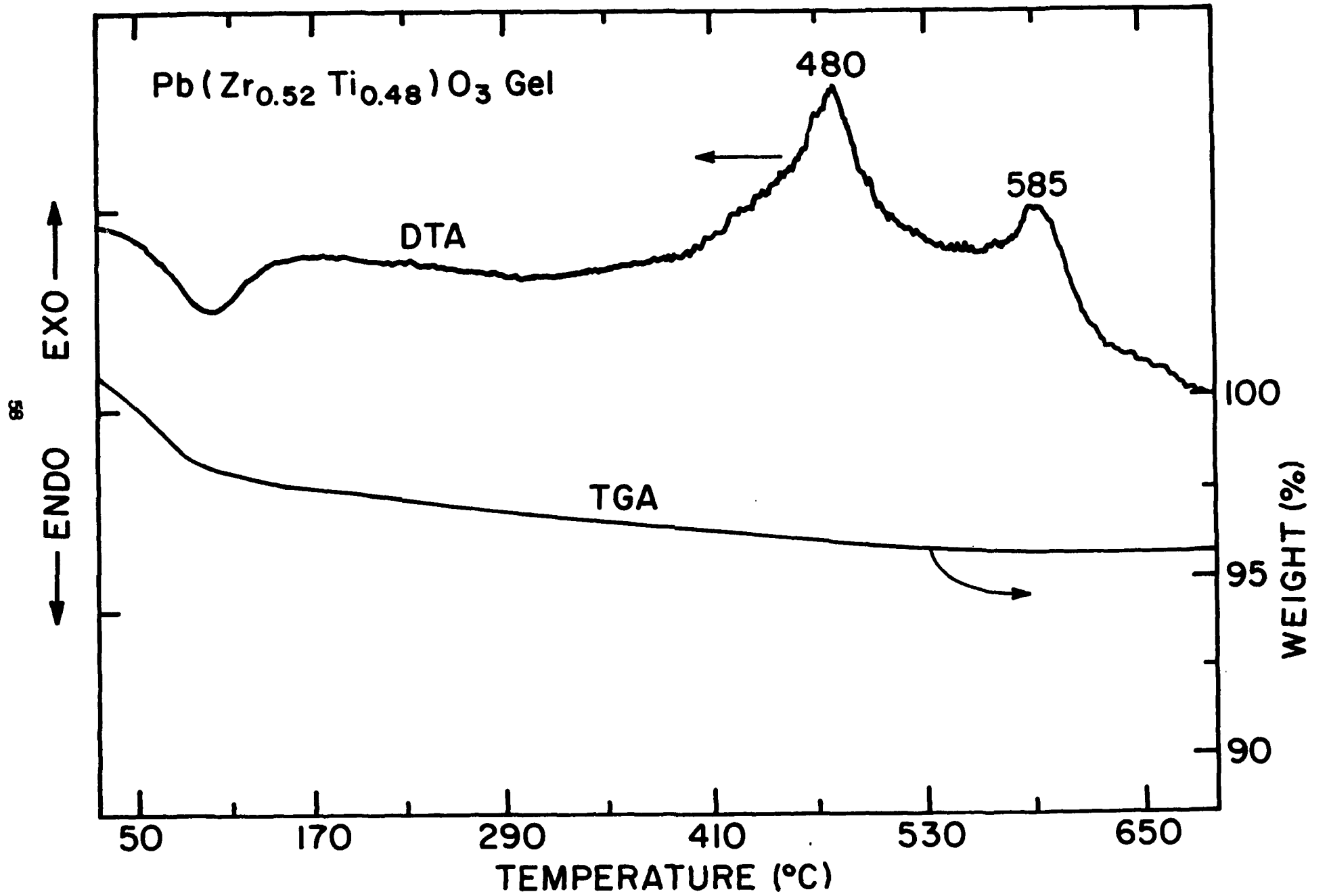
Pb(Zr0.52 Ti0.48)O3 Gel
480
585
DTA
TGA
EXO
ENDO
100
95
90
WEIGHT (%)
50
170
290
410
530
650
TEMPERATURE (°C)

Fig. 3

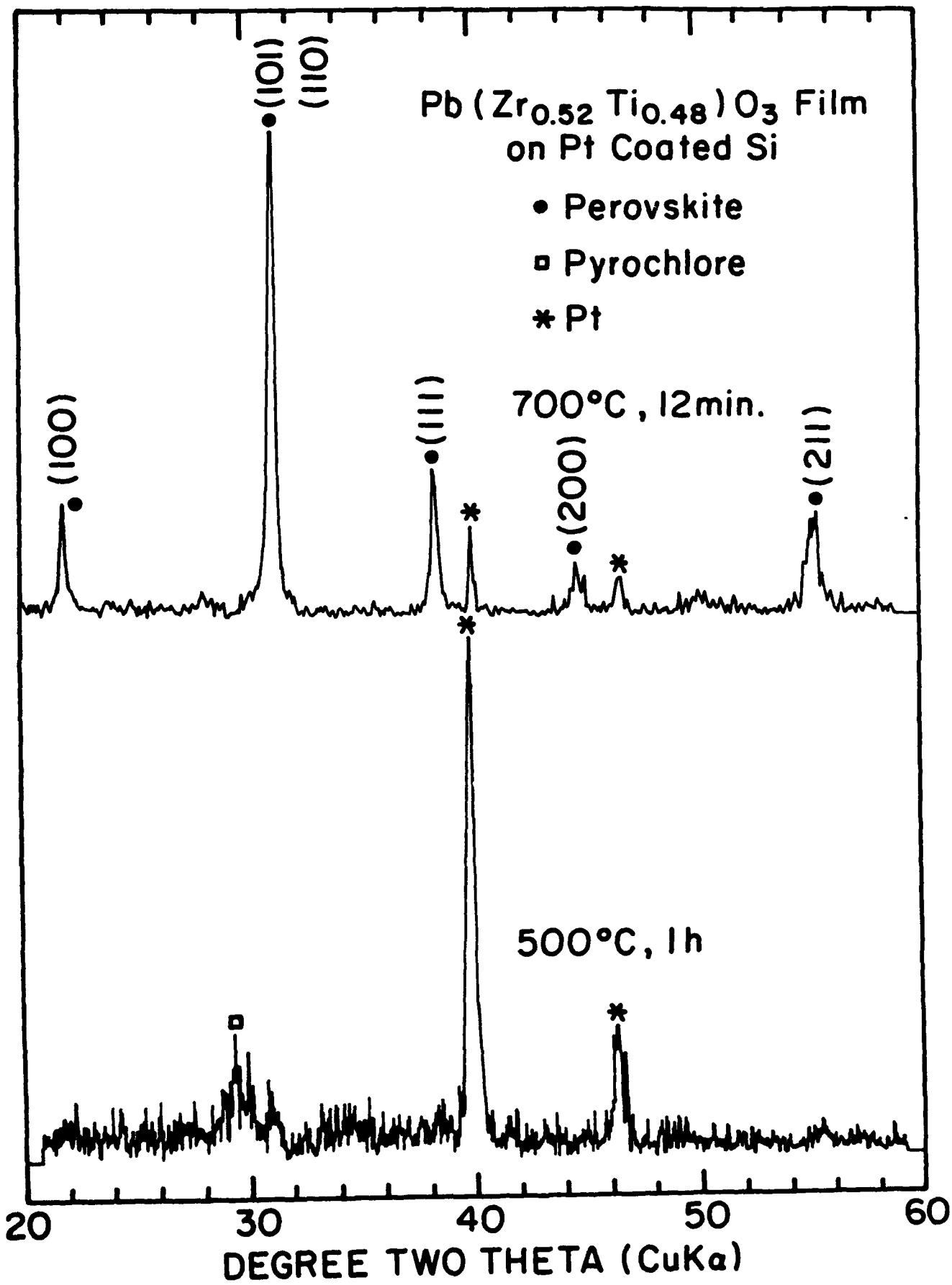
Pb (Zr0.52 Ti0.48) O3 Film
on Pt Coated Si
• Perovskite
▫ Pyrochlore
* Pt
(100)
(101)
(110)
(111)
(200)
(211)
700°C , 12min.
500°C , 1h
20
30
40
50
60
DEGREE TWO THETA (CuKα)

Fig. 4

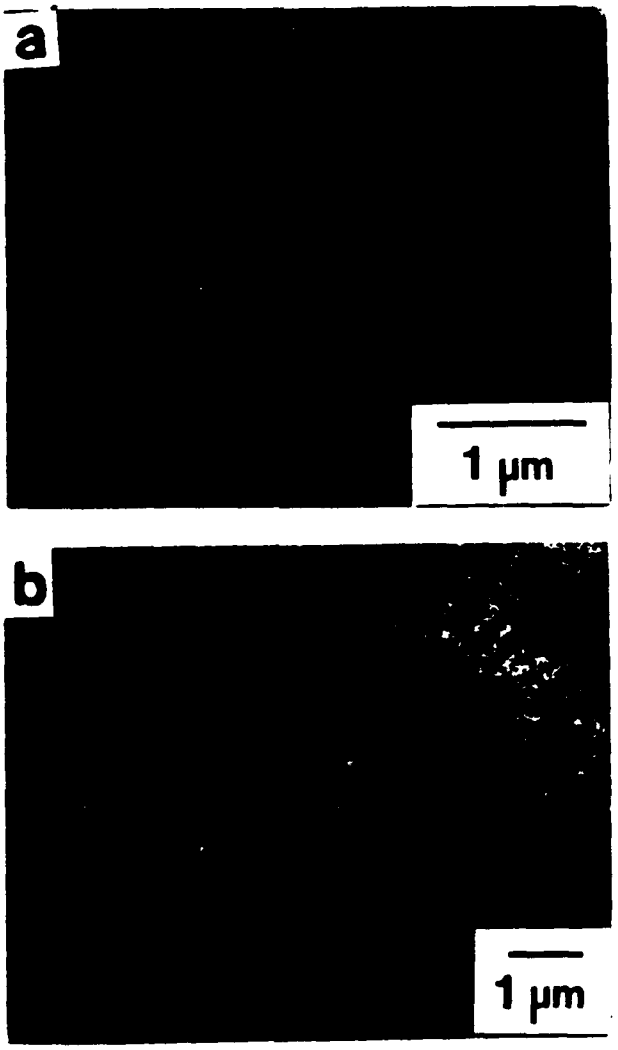

Fig. 5

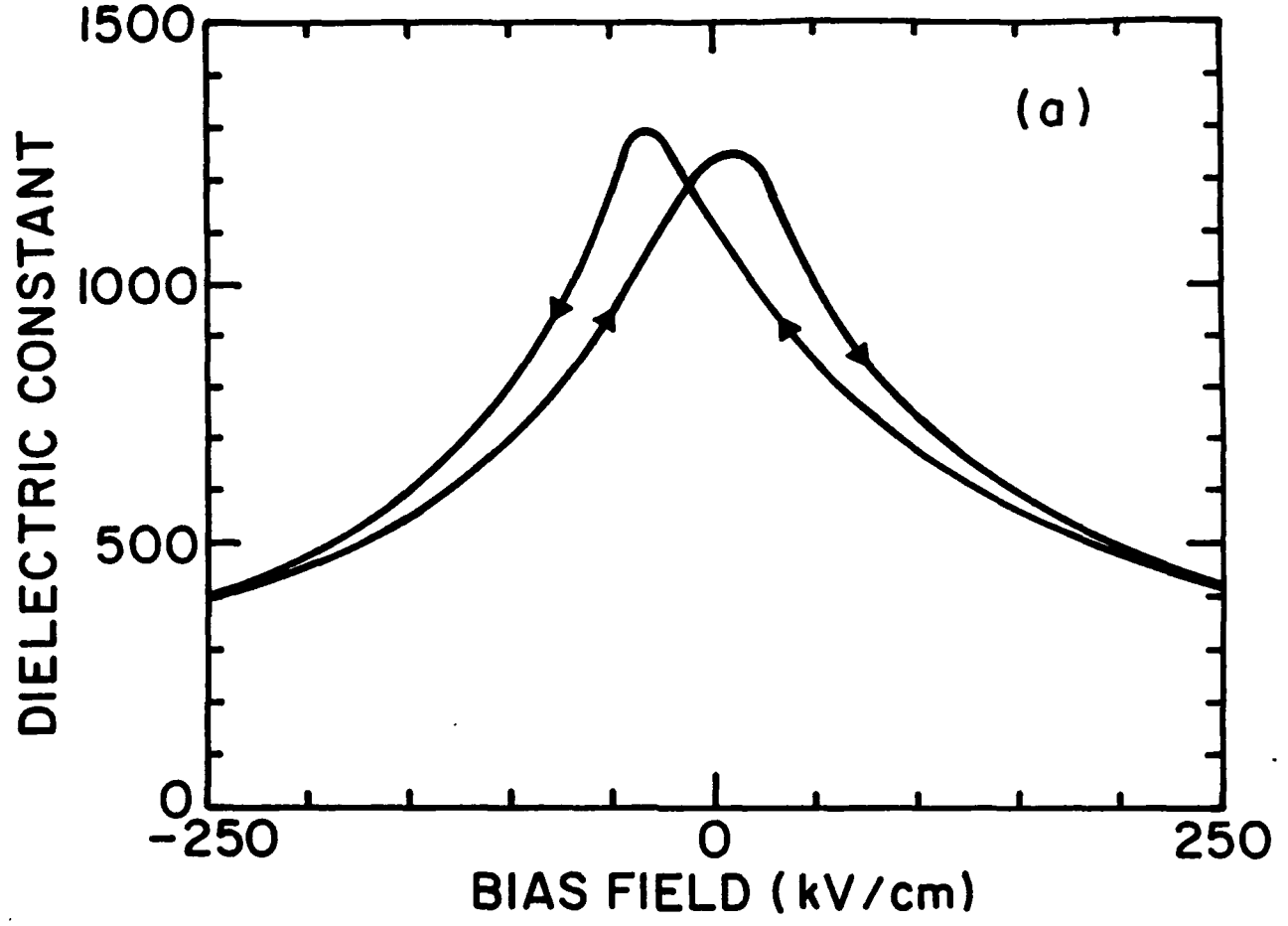
1500
1000
500
0
DIELECTRIC CONSTANT
(a)
-250
0
250
BIAS FIELD (kV/cm)

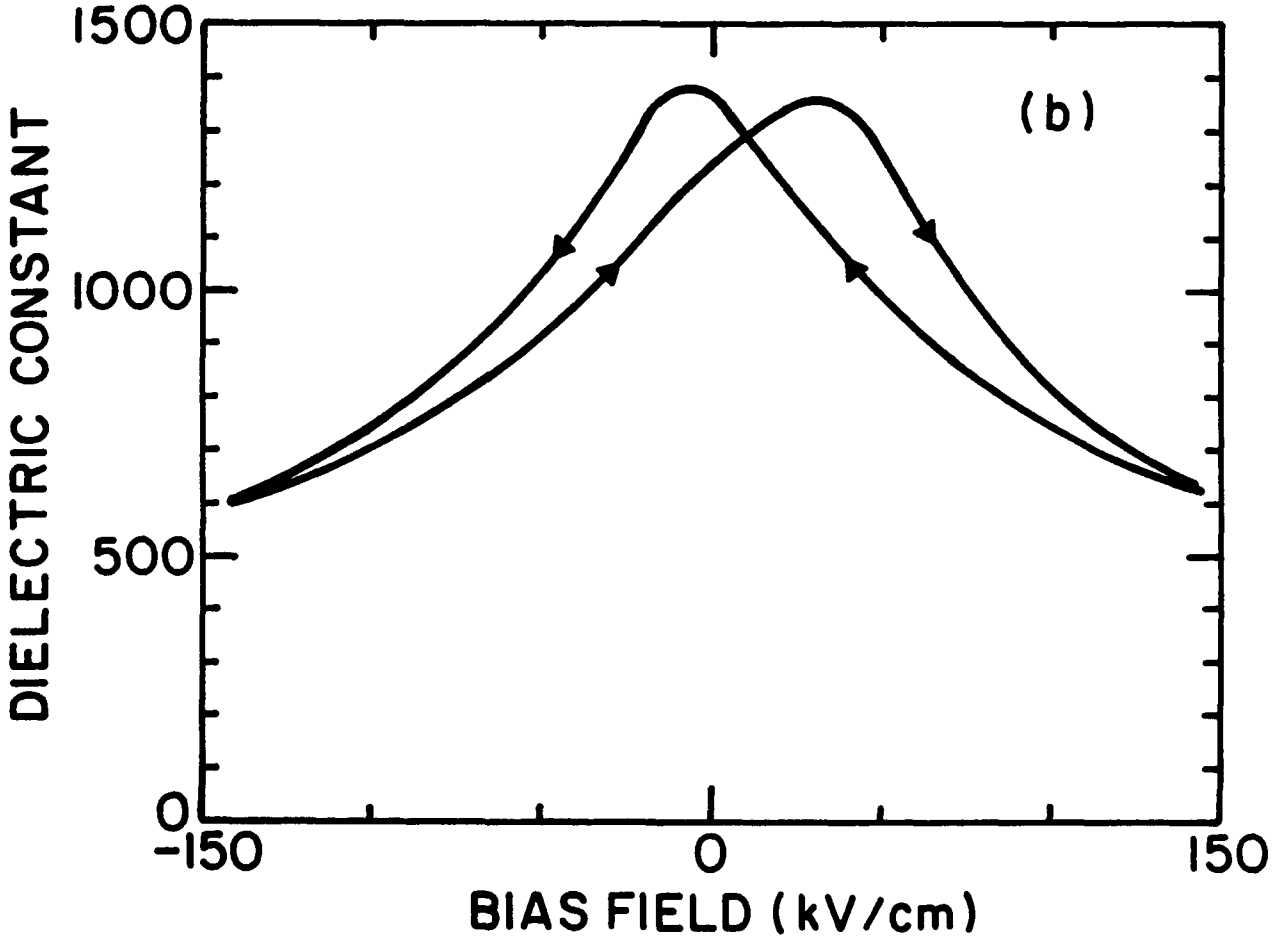
1500
1000
500
0
DIELECTRIC CONSTANT
(b)
-150
0
150
BIAS FIELD (kV/cm)

Fig. 6

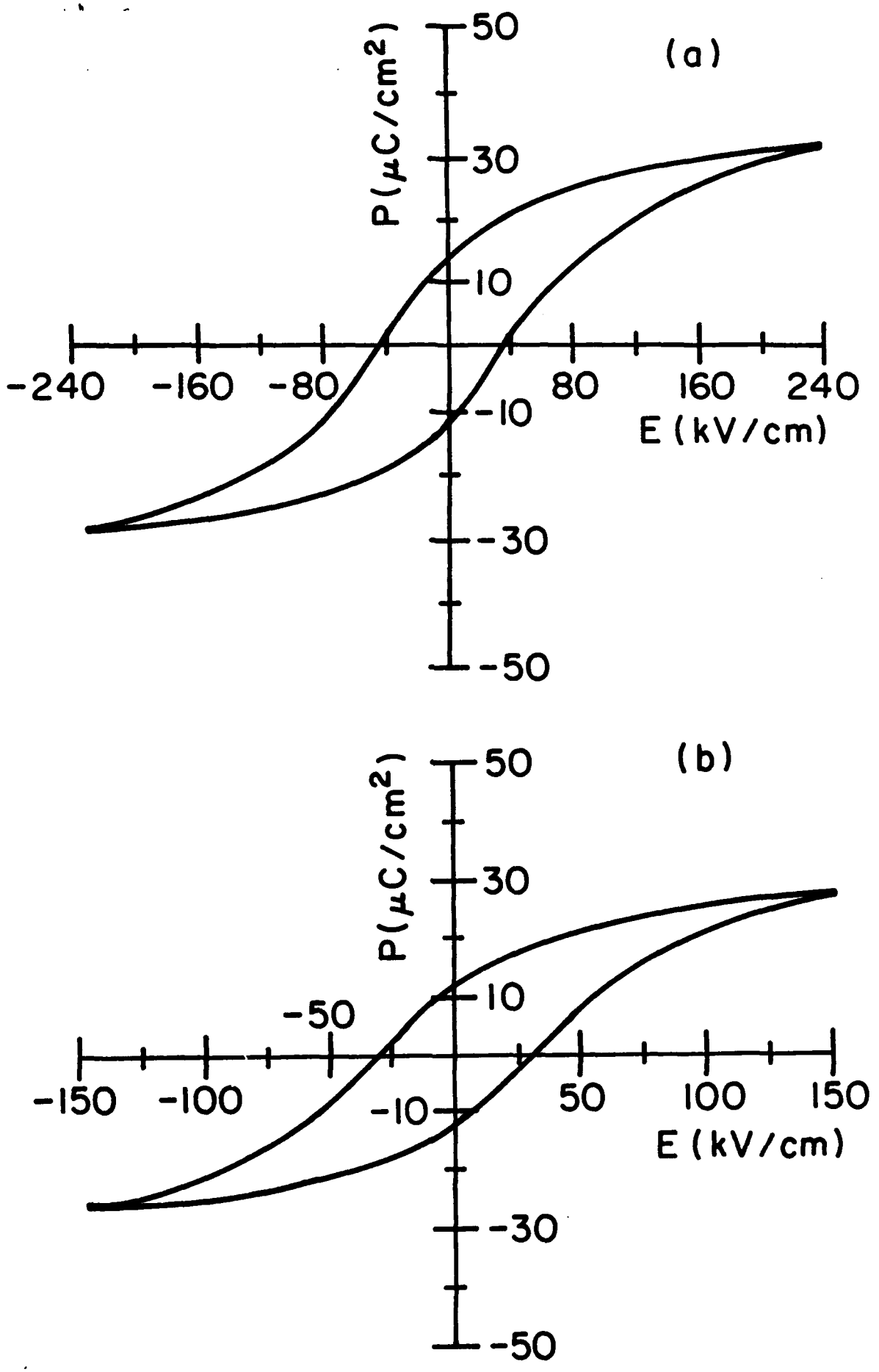
(a)
P(μC/cm²)
50
30
10
-10
-30
-50
-240
-160
-80
80
160
240
E (kV/cm)
(b)
P(μC/cm²)
50
30
10
-10
-30
-50
-150
-100
-50
50
100
150
E (kV/cm)

Fig. 7